PhD degree in Molecular Medicine (curriculum in Molecular Oncology)

European School of Molecular Medicine (SEMM),

University of Milan

The plasticity of miRNA pool: a novel approach to reveal mechanisms behind miRNA turnover

Francesco Ghini

Center for Genomic Science IIT@SEMM

Matricola n. R10316

Supervisor: Dr. Francesco Nicassio

Center for Genomic Science IIT@SEMM

Milan

Added Supervisor: Dr. Matteo J. Marzi

Center for Genomic Science IIT@SEMM

Milan

Anno accademico 2015-2016

A **Daniela**,

compagna nelle gioie e nelle difficoltà

di ieri, di oggi e per sempre.

LIST OF FIGURES

LIST OF TABLES

ABSTRACT

MicroRNAs (miRNAs) are a small (18-25nt long), evolutionary conserved, class of non-coding RNAs that appears as a major regulatory component of gene expression, implicated in virtually all known physiological and pathological processes. They act at post-transcriptional level by silencing the expression of a multitude of target mRNAs through various mechanisms, including target degradation and protein synthesis inhibition. As a result, the regulation of the miRNA pool is one of the critical events in the definition of cell identity and behavior both in physiology and disease.

Although large efforts have been put in understanding how miRNA transcription and biogenesis are regulated, to date very little is known on what happens to miRNAs once they exerted their repressive function, if they are recycled on other target molecules or degraded, and how fast they are turned over. Typically, miRNAs are thought to be stable molecules with long half-lives. Nevertheless, in last years it emerged that some miRNAs could be also turned over rapidly upon different cellular conditions.

To clarify how miRNAs decay in mammalian cells, we developed a new tailored approach based on in vivo RNA labeling (4sU pulse-chase) and high-throughput sequencing, which allows to investigate the modes and the mechanisms of miRNAs decay without perturbing global miRNA levels or miRNA processing. By this approach, we precisely measured miRNA decay rates in exponentially growing 3T9 mouse fibroblasts. Overall, miRNA turnover appeared heterogeneous; hence, miRNAs are not just stable molecules as previously thought. We could distinguish two pools of miRNA by decay: a group of miRNAs that are, indeed, very stable molecules (T1/2 >24h, ‘slow’); and another group composed of miRNAs quickly turned over in the cell (T1/2 <14h, ‘fast’). We further exploited RNA labeling by 4sU to quantitatively measure the biosynthetic rate (transcription) of miRNAs alongside. By integrating decay rates with biosynthesis, we developed a mathematical model to infer how different decays impact on miRNA regulation during cell transitions: fast miRNAs quickly reach a plateau of accumulation and are downregulated in few hours as compared to slow miRNAs.

These findings were recapitulated in a specific biological process, namely the regulation of miRNAs by serum stimulation of quiescent fibroblast, which is characterized by a consistent

change in gene and miRNA expression in absence of cell division (hence, miRNA cannot be diluted). Indeed, serum ‘up’ and ‘down’ regulated miRNAs were characterized by marked difference in turnover rate, compatible with the kinetic of their changes and often coupled with transcriptional regulation, pointing out how multiple mechanisms concomitantly control miRNAs and their activity in mammalian cells.

Mechanistically, our analyses suggested that the ratio between high affinity targets and miRNA abundance [which we termed target per miRNA (TPM) value] is a key determinant in the definition of the type of miRNA decay, supporting the ‘target-induced miRNA decay’ (TIMD) as a common mechanism that promotes miRNA degradation. This contention is also supported by a clear parallelism between decay-associated miRNA isoforms (trimmed and tailed sequence variants) and miRNA degradation dynamics, implying that i) the distribution of miRNA isoforms is reflecting the type of decay of miRNAs, and ii) specific enzymatic activities (i.e. nucleases, transferases) are in place and mediate miRNA degradation.

So far, no endogenous target has been directly linked to TIMD mechanism. Our analyses provided a list of potential targets involved in TIMD, which could be critical in clarifying the role played by such mechanism in physiology. Preliminary experiments were performed on one of such target, which is much expressed upon serum stimulation of quiescent fibroblasts and highly complementary to a miRNA suddenly downregulated. Exploiting CRISPR/cas9 based genome engineering, we specifically affected miRNA:target interaction, keeping transcript level and protein functionality unaltered, ensuing in a consequent effect on miRNA regulation (loss of downregulation upon serum stimulation), fully supporting TIMD as an endogenous mechanism in control of miRNA functions.

1. INTRODUCTION

1.1 The microRNA revolution

1.1.1 The non-conding RNA landscape

Since the discovery of the ribosomal RNA in 1950 and the definition of its central role in protein translation, non-coding RNAs have been gradually received more attention by the scientific community resulting in the characterization of one of the most important post-transcription control mechanism, the RNAi pathway, mediated by miRNAs (Cech and Steitz 2014). The existence of miRNAs as post-transcriptional regulator was firstly conjectured by Jacob and Monod in 1961, which hypothesized that the Lac repressor might be "an RNA fraction", but only in 1993 a short RNA was described as responsible in controlling the timing of development transition in *C.elengans (Lee et al. 1993)*. After that, other labs reported the existence of hundreds of short RNAs showing a length of 22 nt in worms, flies and mammals, which were called microRNAs (miRNAs) (Pasquinelli et al. 2000; Lagos-Quintana et al. 2001; Lau et al. 2001; Lee and Ambros 2001). Today, we know that miRNAs are a small (18-25nt long), evolutionary conserved, class of non-coding RNAs that appears as a major regulatory component of gene expression, implicated in virtually all known physiological and pathological processes. As mentioned above, miRNAs act at post-transcriptional level by silencing the expression of a multitude of target mRNAs through various mechanisms, including target degradation and protein synthesis inhibition (Eulalio et al. 2008; Bartel 2009; Jonas and Izaurralde 2015). Due to their widespread regulation activity, it has been predicted that miRNAs control the activity of 50% of all protein coding genes and are involved in almost all cellular processes such as development, proliferation, apoptosis, DNA damage (Krol et al. 2010b). Moreover, starting from the discovery of miR-15 and miR-16 genetic deletion in B-CLL (Calin et al. 2002), miRNAs have been associated to different human pathologies, including viral diseases, immune related diseases, neurodegenerative diseases and cancers (Li and Kowdley 2012).

1.1.2 MicroRNAs bind targets through “seed” interaction

MiRNAs function within the RNA induced silencing complex (RISC), loaded on Argonaute proteins (Ago). Target RNAs are recognized through base-pare interaction between the miRNA sequence and target sequence, the so-called "miRNA responsive elements" (MREs), usually located in the 3' untranslated region (3'UTR) of the target. MREs typically comprise a region of six nucleotides that is complementary to bases 2-7 of the miRNA (the "seed", which defines the pool of targets in a cell) (**Figure 1**). Since miRNAs discover, scientist put much efforts in understanding the binding rules that govern miRNA:target interaction. In particular, besides the seed matching, the pairing of a 7mer is essential for the exact definition of the canonical site of binding (Bartel 2009). In particular, two kinds of 7mer interaction have been described: i) a 7mer flanked by Adenosine in position 1 (7mer-A1site) or ii) a 7mer-A1 plus a nucleotide match at position 8 (7mer-m8 site). Of note, both of them increase the strength of miRNA:target binding. The last type of interaction appears as a seed match plus A1 and m8 sites that drastically increases target prediction specificity and thus, ability to bind the MRE (Lewis et al. 2005). As the complementarity between miRNAs and RNA targets is limited, hundreds or even thousands of RNAs could interact with a single miRNA.

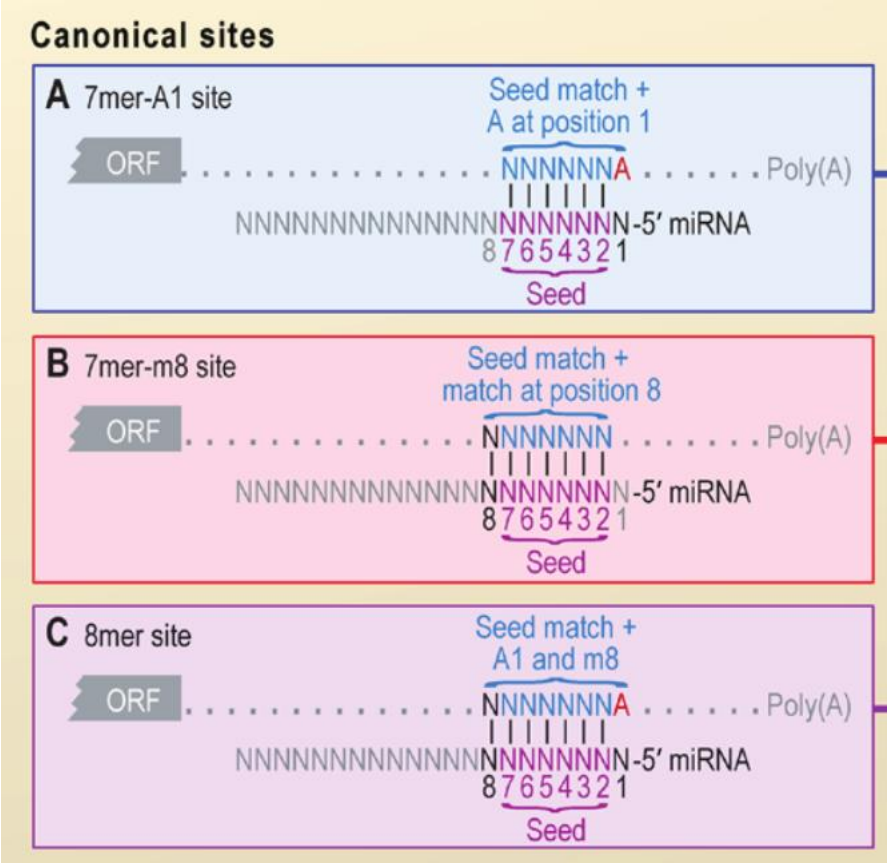

Figure 1. miRNAs bind target through seed interaction. Different types of miRNA:target interaction, from (Bartel 2009)

1.1.3. MiRNAs are conserved molecule and are specifically located in the genome

The last release of a well-known miRNAs database (miRBase21) account for 2588 miRNAs in human, although various species are not functionally defined, yet (Griffiths-Jones et al. 2008). From a development point of view, there are several miRNA loci that come from gene duplication during evolution: as a result, miRNAs which show identical seed are classified in the same "miRNA family" and should target the same molecules (Bartel 2009). Thirty-four miRNA families are conserved between *C.elegans* to Human, while 196 families are conserved across mammals. Interestingly, there are also examples of extended miRNA families deriving from a common evolutionary origin but that vary for a specific nucleotide in seed sequence. Examples include either the extended family of miR-141 and miR-200c (Kim et al. 2013) or the miR-16 and miR-503 (Rissland et al. 2011).

MiRNAs are furthermore classified depending on their genomic location (**Figure 2**). Indeed, miRNA genes can be encoded from introns or exons sequence of host genes, both coding and non-coding (collectively called "intragenic miRNAs"); on the other hand, miRNA transcribed regions have been found in genome areas which are far from transcribed genes ("intergenic miRNAs").

Finally, miRNA genes could be located alone in the genome (single loci) or in close proximity to other miRNAs, forming a cluster, a polycistronic transcript that must be processed in order to produce miRNAs (Ha and Kim 2014). In general, classification of miRNAs in clusters is based on the presence of a common promoter region. While intragenic miRNAs often share the promoter of the host gene, the definition of the promoter region for intergenic miRNAs has been problematic due to the complexity in defining transcription start sites (TSS) that might locate many kilobases far from miRNA gene. Moreover, each promoter could be tissue specific. Recently, a collection of Chip-seq data and nascent RNA-seq analysis has allowed the identification of most promoter regions and, furthermore, of the length of the precursor transcripts (Ozsolak et al. 2008; Chang et al. 2015; Marzi et al. 2016).

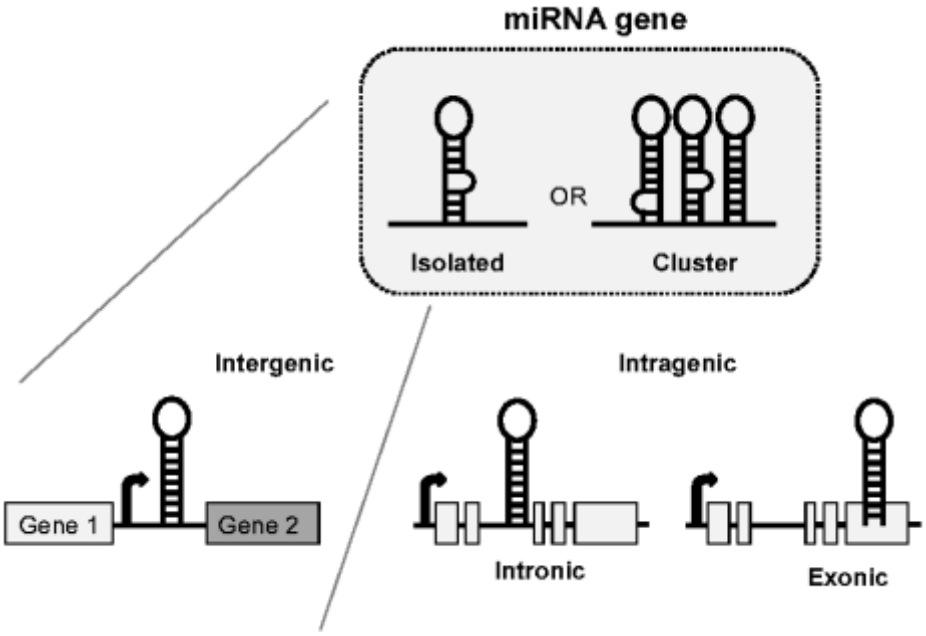

Figure 2. MiRNA genes location in the genome. miRNAs are differently classified depending on their location. (Role of non-coding in Cystic Fibrosis, Chapter 12 Varilh et al, book edited by Dennis Wat, 2015)

1.1.4. The mechanisms of miRNA biogenesis

MiRNAs biogenesis involves two main steps occurring in nucleus and cytoplasm, respectively (**Figure 3**). In the nucleus, miRNAs are usually transcribed by RNAP-II, leading to the production of primary transcripts (pri-miRNA). As protein coding genes, miRNAs transcription is controlled by transcription factors that modulate the expression of the locus. Indeed, publications showing transcription factors which coordinate miRNAs expression are many; in particular, it has been demonstrated that MYC, ZEB1 and ZEB2, MYOD1 and p53 modulate the expression of 17-92a (Chang et al. 2008), miR-200, miR-1 and miR-34 clusters, respectively (Kim et al. 2009). Moreover, miRNAs transcription is controlled by DNA methylation and histone modifications, which can promote or inhibit transcription factors recruitment on miRNA genes (Davis-Dusenbery and Hata 2010).

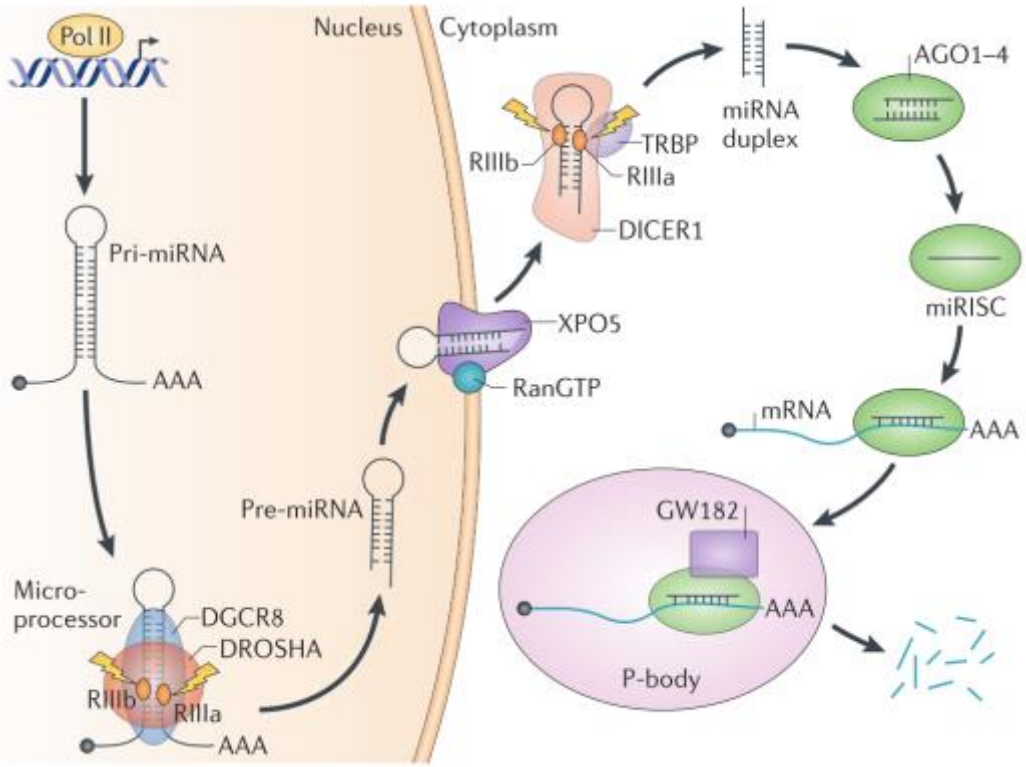

Figure 3. Scheme of miRNA biogenesis. Adapted from (Lin and Gregory 2015)

Pri-miRNA is a long transcript (typically 1kb) harboring stem-loops region (33-35 nt of length) in which miRNAs are embedded. To process this structure, pri-miRNAs require the association of Microprocessor complex, a 364 KDa complex which is composed by DROSHA, an RNase III-type endonucleases and two DGCR8 molecules which allow the correct binding of DROSHA to pri-

miRNA molecules ((Nguyen et al. 2015)**Figure 4**). Both DROSHA and DGCR8 knockout results in mouse lethality during embryogenesis, confirming their importance in miRNA biogenesis; moreover, Microprocessor activity is deeply conserved among animal species (Ha and Kim 2014). Recently, mechanisms by which the Microprocessor recognizes and process pri-miRNAs has been discovered, in particular scientists found consensus sequences both on pri-miRNA stem and loop. After recognizing and binding to the pri-miRNA, DROSHA acts as a ruler, by defining the length of the processed transcript; DGCR8 dimerization enhances processing efficiency and mediates the suppression of unproductive processing (Nguyen et al. 2015).

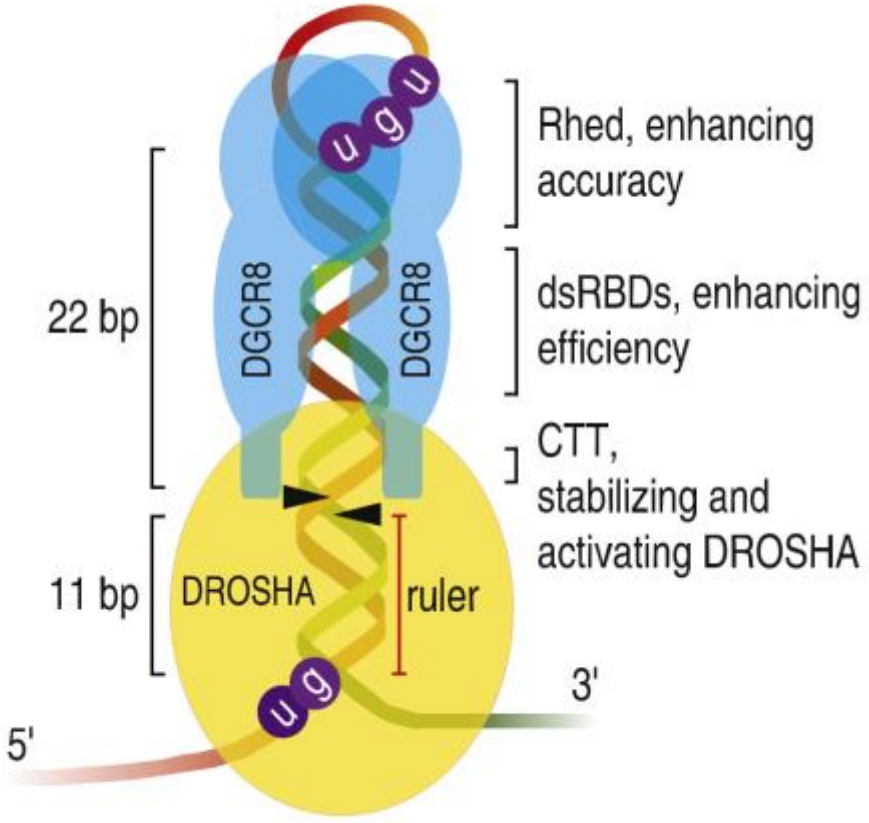

Figure 4. Scheme of binding to pri-miRNA by DROSHA and DGCR8. Adapted from *(Nguyen et al. 2015)*

Pri-miRNA maturation results in the production of precursor-miRNA (pre-miRNA, 60-100 nt long), a stem-loop RNA that is exported into the cytoplasm through EXP5 and RAN-GTP. In particular, EXP5 has the ability to recognize a dsRNA sequence >14bp with a 3' overhang sequence (i.e. the result of DROSHA cutting) (Lund et al. 2004). Once in the cytoplasm, pre-miRNA is sequestered by DICER, a 200 KDa RNase III-type endonuclease, which mediates the cleavage of the precursor to produce an 18-24 nt long RNA-duplex. DICER action is facilitated by TRBP, which modulates the efficiency of processing even if it seems not essential for loop

cleavage (Fukunaga et al. 2012). The small RNA duplex is subsequently loaded on AGO proteins to form the pre-RNA-induced silencing complex (pre-miRISC). At this time, the RNA duplex undergo the unwinding, a process by which only one molecule of the duplex is maintained. The strand that remains loaded on AGO is named "guide strand", while the discarded strand is defined as "passenger strand". One of the hypotheses behind miRNA unwinding come from the biochemical reaction that allow miRNA loading on AGO proteins. Indeed, this is an active process requiring ATP to open the binding pocket of AGOs. The accessory proteins, such as HSC70 and HSP90, mediate AGOs conformational opening, so that a stiff dsRNA can be bound (Iwasaki et al. 2010). The consequent release of AGO tension leads to miRNA ATP-independent unwinding of the passenger strand. The way by which guide and passenger are chosen depends on thermodynamic stability of the two ends of the RNA duplex: the guide strand usually presents an unstable 5'end and a Uridine at nucleotide position 1 (Schwarz et al. 2003; Hu et al. 2009). Interestingly, alternative selection (also defined "arm switching") has been observed from global studies that have determined miRNAs identity and expression levels in multiple tissues(Chiang et al. 2010).

The guide strand bound to AGO proteins associated to GW182 protein is called miRISC complex. In human four AGO proteins exist (AGO1-4) and are all capable of inducing translation repression, conversely, only AGO2 can cleave perfectly matched miRNA targets, triggering their degradation (Huntzinger and Izaurralde 2011). Of note, all AGO proteins can bind indistinguishably all human miRNAs (Dueck et al. 2012). From a structural point of view, AGO proteins present a bilobar structure with different domains that mediate the binding of miRNAs and the activity on targets (**Figure 5**). The MID-PIWI domains form one lobe and are essential for guide strand binding. Moreover, the PIWI domain mediates the slicing activity due to the presence of an active site similar to domains in the RNase H enzyme. The PAZ domain acts as pocket for the 3'end miRNA sequence, suggesting that its activity is essential for recognition and binding of the 3'complementary site to targets (Kim et al. 2009; Elkayam et al. 2012).

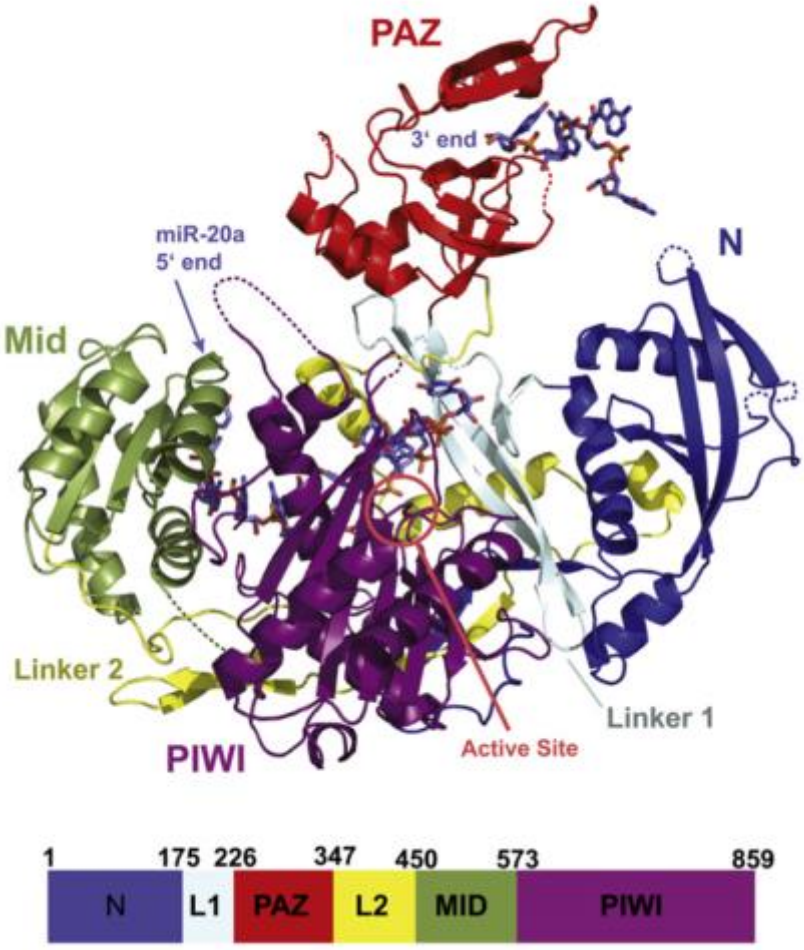

Figure 5. Protein structure of AGO2 complexed to a guide miRNA. Shown are different domains and miRNA chain. From (Elkayam et al. 2012)

Of note, an alternative pathway for the biogenesis of miRNAs exists in cells, which allow to bypass DROSHA step, leading to direct loading of a "pre-miRNA-like-structure" onto DICER. This is the case of the so-called Mirtron, a fraction of miRNAs inside intron sequences that are processed by mRNA splicing machinery. This activity results in an alternative stem-loop structure that is sequestered by DICER (Ha and Kim 2014). Other particular sequences are involved in alternative miRNA biogenesis, such as the endogenous short hairpin RNA (Chong et al. 2010), tRNAs like precursor (Babiarz et al. 2008) and small nucleolar RNAs (snoRNA), which generate alternative miRNAs because of a stem-loop structured that bind DICER and AGO2 (Ender et al. 2008).

1.2. The regulation of miRNA biogenesis

1.2.1 Regulation of Microprocessor complex

MiRNA maturation is a finely regulated process, where accessory proteins can promote or inhibit miRNA biogenesis. In particular, DROSHA efficiency and the maintenance of the homeostatic balance between DROSHA and its partner are pivotal. Interestingly, DROSHA and DGCR8 are controlled through an auto-regulated feedback loop. DGCR8 stabilizes DROSHA through protein interaction while DROSHA destabilizes DGCR8 mRNA through a cleavage activity on its mRNA (Kim et al. 2009). Moreover, DROSHA is regulated by post-transcriptional modifications [reviewed in (Ha and Kim 2014)] such as: i) phosphorylation, which is required for the nuclear localization; and ii) acetylation, that leads to protein stabilization. Moreover, DGCR8 increases its affinity to DROSHA upon phosphorylation by ERK and deacetylation by HDAC1. Pri-miRNA processing efficiency is indeed mediated by further proteins such as p68, p72, SMAD proteins, p53 and TDP43, which interact selectively with DROSHA and/or pri-miRNAs, resulting in increased activity and stability. Of interest, some proteins recognize specific pri-miRNA sequences, facilitating the processing of the molecule, as in the case of HNRNPA1 and KSRP (Guil and Caceres 2007; Trabucchi et al. 2009), or promoting degradation, such as for LIN28A and LIN28B with let-7 precursors (Viswanathan et al. 2008; Chang et al. 2013).

Pri-miRNA processing is also subjected to drastic dysregulation in multiple human cancers. In first instance, a considerable number of miRNAs are generated from fragile sites or DNA regions that are frequently amplified, deleted or translocated in cancer (Lin and Gregory 2015). As already mentioned, B-CLL samples frequently show a deletion of the chromosome 12q14, which contains the miR-15 and miR-16 locus, resulting in a loss of their expression by 70% (Calin et al. 2002). A second example is reported for pri-miR-128b, where a point mutation in the gene leads to a block in processing and decreased expression of the mature miRNA (Kotani et al. 2010). In addition to genomic alterations, miRNA transcription factors might have modified expression in cancers and, thus, play a role in miRNAs dysregulation. For example, cMYC amplification, frequently observed in cancer, lead to overexpression of the miR-17-92a cluster (the oncomiR-1) and global reduction of tumor suppressive miRNA(Chang et al. 2008); p53 mutations cause down-regulation of miR-34 family, a major cell-cycle regulator (Okada et al. 2014); in cancer, histone modifications and DNA

methylation act together to repress miRNAs in specific tumors (Guil and Esteller 2009). Also proteins of the Microprocessor can be differentially expressed in cancer: either DROSHA overexpression or downregulation were specifically observed in various type of cancer with different consequences on tumor maintenance (Lin and Gregory 2015). DGCR8 mutations are reported in Wilms tumor, resulting in cellular transformation and tumor growth (Kumar et al. 2007).

1.2.2. Regulation of DICER and AGO proteins

In human, DICER regulation is mediated by co-factors, which regulate processing efficiency. One of such proteins is TRBP that stabilizes DICER and, when phosphorylated, promotes accelerated processing of miRNAs (Paroo et al. 2009). Another regulator is KSRP that favors miRNAs processing upon binding to the pre-miRNA loop complexed to DICER (Trabucchi et al. 2009). A further mechanism, involving LIN28A/B will be discussed below (see section "Enzymes which mediate miRNAs degradation"). From a pathological point of view, DICER mutations have been mapped in different types of cancer and mainly facilitate tumor initiation, a particular situation called DICER syndrome. Patients with this disorder, have mutation on Dicer1 gene encoding for a shorter protein, which is unable to process pri-miRNA and result in increased cellular growth (Slade et al. 2011). Finally, AGO proteins undergo an extensive regulation which can modify their activity on targets. Post-transcriptional modification of AGO2 such as hydroxylation, increases AGO2 stability and promote localization in p-bodies, which are foci in the cytoplasm locating enzymes that mediate mRNA degradation (Ha and Kim 2014). MAPKAPK2 and AKT3 are responsible for AGO2 phosphorylation leading to localization to p-bodies or translational repression, respectively. On the contrary, phosphorylation of Tyr393 upon hypoxia results in the dissociation of DICER from RISC complex and inhibition of pre-miRNAs processing. It has been demonstrated that cellular stress or viral infection cause AGO poly(ADP-ribosyl)ation, inhibiting the activity on targets. In general, miRNA loading on AGO proteins appears to stabilize the complex, while empty AGO are destined to proteasome degradation, suggesting that miRNAs are direct regulator of AGOs stability (Ha and Kim 2014).

1.3. The turnover of microRNAs

Overall, levels of miRNAs are the result of integrated biosynthetic and decay processes. However, while the mechanisms controlling miRNA biogenesis have extensively studied, how miRNAs are degraded still remains obscure. For long time, miRNAs were though to behave as very stable molecules with long half-lives (greater than 24h), apparently downregulated through dilution by cell division. A few studies attempted to characterize globally the degradation rates of miRNAs using inhibitors of RNA transcription (actinomycin D or alpha-amanitin) or by block/loss of miRNA processing enzymes (i.e. Dicer) (Bail et al. 2010; Gantier et al. 2011; Guo et al. 2015).

In particular, Bail et al treated HEK-293 cells with actinomycin-D, which selectively binds to DNA at the transcription initiation complex preventing RNA-pol-II elongation (Sobell 1985). After 8 hours of treatment, authors analyzed the stability of miRNAs through microarray technology. Of note, they noticed that of all miRNA probes present on the chip, only 30% was detected with a stable expression level after actinomycin-D administration. They found only five miRNAs which significantly decrease their abundance after that time point, but no half-lives were calculated in this study. To this end, authors conclude that the majority of miRNAs decays very slowly.

As alternative approach, miRNA decay was studied upon DICER1 knock down (Gantier et al. 2011). By inhibiting DICER1, one of the major processing enzyme, pre-miRNAs are no longer transformed into mature forms. Thus, pre-existing miRNAs can be followed after functional loss of Dicer, measuring the degradation rate. In this study, authors estimated miRNAs half-life in MEFs exploiting an inducible system in which the addition of 4-OHT causes DICER1 know-down. In particular, miRNA decay rates were assessed at day 3-5 after OHT induction by exponential fitting, also keeping into account cell duplication (which dilutes miRNAs). Authors found that miRNAs have an average half-life of 5 days, with a range between 4 and 9 days for most miRNAs.

Finally, actinomycin-D treatment has been recently coupled to RNA sequencing in order to study miRNA decay (Guo et al. 2015). In this paper, authors confirmed that, in general, miRNAs decay slowly, but also discovered a specific subset of miRNAs presenting a rapid turnover. In particular, this "fast" class mainly contains passenger miRNAs.

These studies by-and-large agreed that many miRNAs behave as stable molecules, but failed in identifying miRNAs with fast turnover. On the contrary, a number of recent publications showed

that miRNA can undergo a fast decay depending on cell context. In the next paragraphs we will present different situations wherein miRNAs show rapid turnover.

1.3.1 miR-29b in mitotic arrested cells

In HeLa cells, miR-29b is finely regulated during cell cycle. In particular, it is co-transcribed with miR-29a, which differs for few nucleotides outside the seed sequence. Interestingly, while miR-29a show little changes during cell cycle, miR-29b significantly accumulates in mitotic cells and presents two different decay behaviors depending on cell cycle stage. By transfecting a miR-29b duplex in cell and doing a pulse-chase experiment, researcher have revealed that the half-life of miR-29b changes from 4h in cycling cell to >12 in mitotic arrested cells. Of note, the decay rate of miR-29a was not modified in the two cellular statuses. Further analysis revealed that the presence of Uracils at the position 9-11 of miR-29b is necessary, but not sufficient, for the fast decay behavior (Hwang et al. 2007).

1.3.2. miR-503 in G0-G1 transition

A similar example come from a study showing the regulation of miR-16 family members upon G0-G1 transition in NIH-3T3 murine cells (Rissland et al. 2011). Among the members of the extended miR-16 family, miR-503 was drastically downregulated during cell-cycle re-entry, as revealed by northern blot analysis. In parallel, pri-miR-503 showed a rapid decrease, suggesting that cells are not directly altering miR-503 decay, but just the transcription activity of the locus, while miR-503 is constitutively unstable with a measured half-life of 3hr. MiR-503 half-life was further validated independently from cell transition upon exogenous expression of miR-503 within G0 phase. However, mechanisms that mediate the fast turnover rate of miR-503 still remain undiscovered.

1.3.3 The miRNA-cluster miR-183/96/182 in mouse retina

Fast miRNAs turnover appears to be a common feature in neuronal cells (Krol et al. 2010a). In particular, in the mouse retina, it has been reported that miR-183/96/182 cluster is profoundly repressed when animals are moved from light to dark. MiRNA down-regulation is achieved by inhibiting transcriptional activity of the miR-183/96/182 locus. Thus these microRNAs, as miR-503 in G0-G1 transition, have an intrinsically low stability. Of note, other miRNAs in mouse retina show fast decay (let-7b, miR-29c, miR-15 and miR-16) but did not undergo transcriptional inhibition and their final levels remain unaltered. Moreover, scientists found that mouse non-

differentiated ES cells present miRNAs with a global slow turnover rate. Conversely, once cells differentiated to pyramidal neurons miRNAs turnover became faster. These data support the theory that miRNA decay might be regulated depending on cellular context.

1.4. Mechanisms behind microRNA turnover

From a mechanistic point of view, degradation of miRNAs might involve different levels of regulation, such as complementary target transcripts, enzymatic activities and/or competing endogenous RNAs. In the next paragraphs we are going to present such mechanisms which often present intertwined processes.

1.4.1 Target-induced miRNA degradation

According to target-induced miRNA decay mechanism (TIMD), the expression of high-complementary RNA targets could promote miRNAs degradation (Ameres et al. 2010; Baccarini et al. 2011; de la Mata et al. 2015). Such mechanism has been associated with two conditions: i) the extensive complementarity between the target and miRNA, which typically involves a region in addition to the seed which is complementary to the 3' end of miRNAs, and the induction of decay-associated miRNA isoforms (3'tailing and trimming isoforms which are reviewed below). Acceleration of miRNAs decay after interaction with a target has been observed both in vitro and in vivo. In the in vitro study, authors produced a recombinant AGO2 protein, which is able to bind, in solution, a guide miRNA forming a mature RISC complex. The artificial RISC complex is then associated to a chemical resin (De et al. 2013). Once a prefect-match target is added to the resin, the guide miRNA is quickly unloaded from AGO2, suggesting that the stability of the complex is function of target binding (**Figure 6**). Indeed, specific mismatches in the target sequence lead to inhibition of unloading ability. This study also confirmed the stability of the AGO2-miRNA complex; indeed, by adding a secondary guide RNAs, which were equally able to bind AGO2, only a fraction of pre-loaded miRNA (10%) has released to allow binding of secondary guide RNA (De et al. 2013).

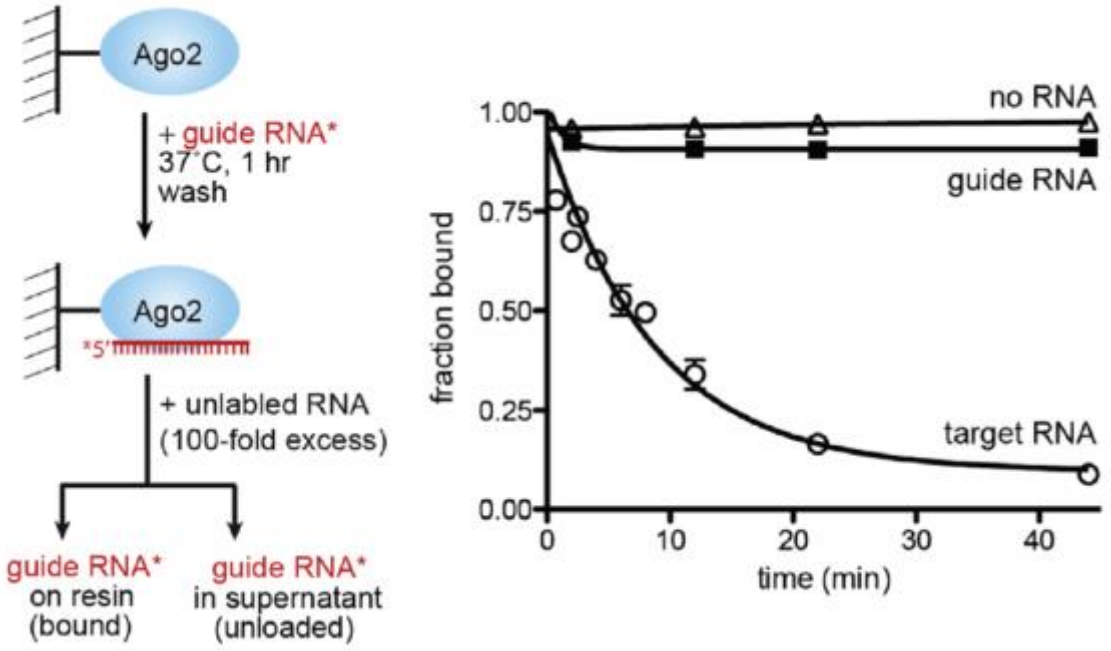

Figure 6. miRNA unlaoding from Ago2 upon addition of a perfect target From (De et al. 2013)

TIMD has been demonstrated also through the expression of an artificial miRNA reporter in vivo, bearing multiple perfectly complementary or bulged sites (Baccarini et al. 2011). In this experiment, a perfect target (PT), a bulged target (BT) and a target with low complementarity at the 5'end for miR-223 were selectively induced by Doxycycline treatment and miR-223 decay was monitored (**Figure 7**). An unrelated target (19aPT) has been used as negative control. Of note, all targets induced miRNA degradation, but only the perfect one results in a reduction >80% after 96 hours. Moreover, they found an extensive accumulation of tailed and trimmed miRNA variants, after target induction (for explanation of miRNA variants see paragraph "Determination and nomenclature of IsomiRs")

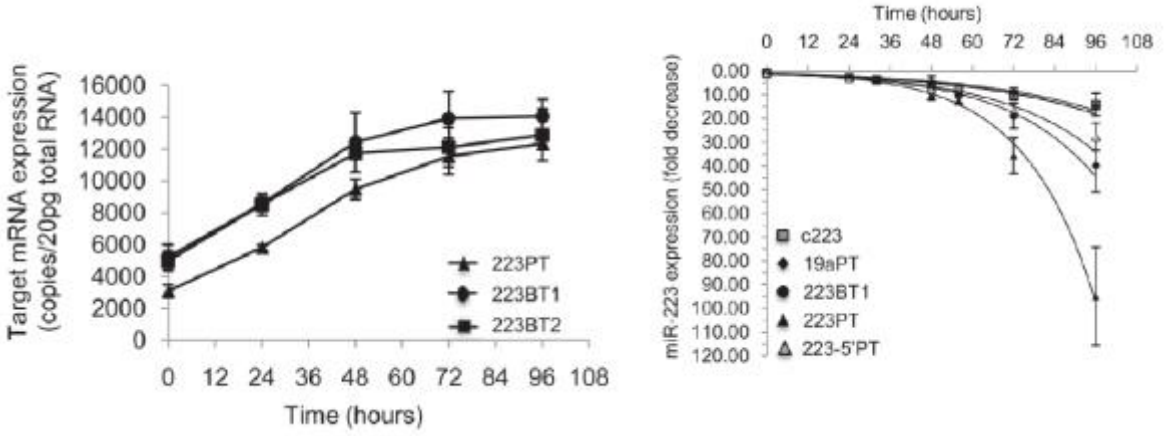

Figure 7. Exogenous targets overexpression lead to miRNA degradation. From (Baccarini et al. 2011)

Other studies, conducted in different model organisms (such as Drosophila M.), also reached similar conclusions (Ameres et al. 2010). Upon overexpression of an extensive complementary target to let-7 miRNA, authors observed active production of tailed and trimmed miRNA variants (**Figure 8**). Of note, they also found the degradation of the canonical mature form as in the study reported above. Moreover, they underlined the importance of the 3'-complementarity by demonstrating a lower accumulation of miRNA variants upon introduction of mismatches in the 3' end binding sequence of the target.

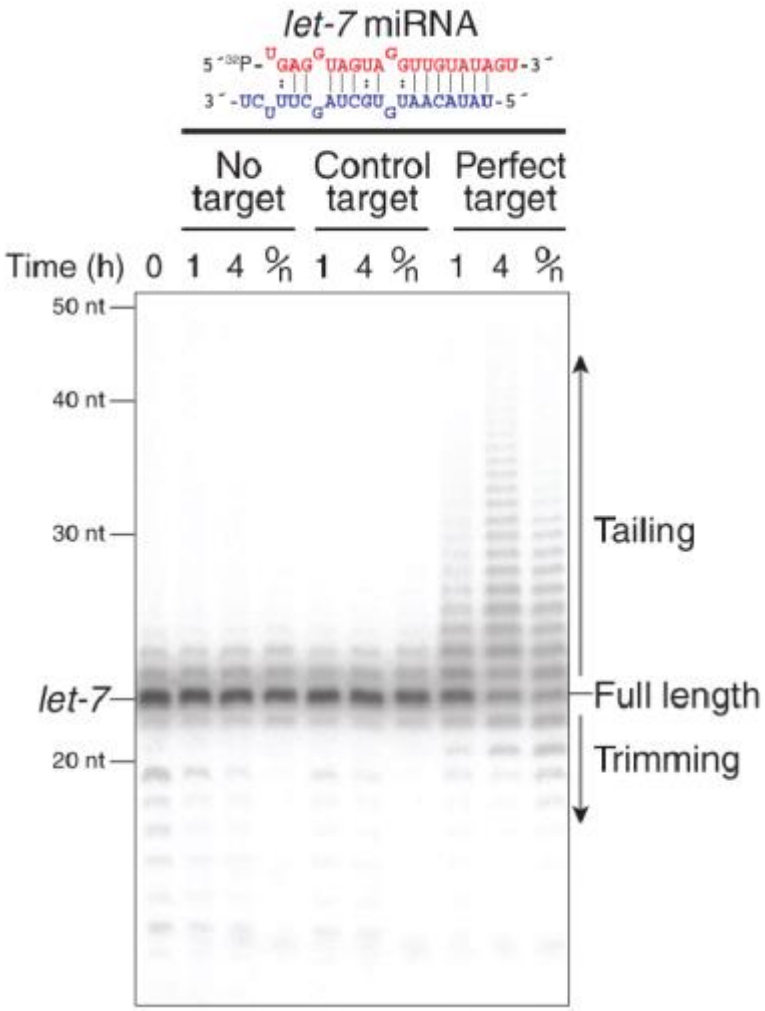

Figure 8. Overexpression of exogenous target leads to accumulation of miRNA variants. From (Ameres et al. 2010)

Finally, enzymes that might mediate miRNA variants production associated with TIMD were recently characterized (Haas et al. 2016). In particular, upon overexpression of a miR-27 perfect target in HeLa cells, AGO2 proteins co-immunoprecipitate with a nucleotide transferase and a specific exonuclease that are responsible for tailing and trimming of mature miRNAs, respectively. Beside these studies, in which miRNA degradation has been induced by overexpression of

exogenous targets, TIMD has been also reported to occur in vivo by endogenous targets. This was particularly shown upon the expression of a non-coding RNA, transcribed by *Herpesvirus saimiri* DNA, called HSUR. The interaction with miR-27 involved also in this case a 3' complementarity which was essential to trigger miR-27 degradation (Cazalla et al. 2010; Marcinowski et al. 2012).
In summary, TIMD has been widely observed for some specific miRNAs, both in vitro and in vivo. Anyway, the rules which exactly define target:miRNA stoichiometry still remain undiscovered. It has been demonstrated that TIMD is predicted to occur only when a miRNA interacts with a highly complementary target expressed over a certain concentration with respect to the miRNA and to the rest of the target pool bound by the miRNA (Denzler et al. 2014). Accordingly, the model predicts that TIMD should not occur when a very abundant miRNA interacts with low-affinity and/or low-expressed targets; conversely, TIMD is more likely when high-affinity and abundant targets interact with a miRNA expressed at low levels compared to the total target pool (Bosson et al. 2014). In conclusion, we still need a molecularly defined model for miRNA decay that takes into account miRNA:target interactions not just at a qualitative level (type of interaction, complementarity) but also at a quantitative level.

1.4.2. Enzymes which mediate miRNAs degradation

Degradation of miRNAs is supposed to involve enzymes which often have an activity in degrading mRNAs. So far, only exonuclease 3'-5' has been showed to have a role in miRNA degradation. These "miRNases" are expressed in specific organisms and act on defined miRNA substrates. In *Arabidopsis thaliana* miRNAs degradation is mediated by the small RNA degrading nucleases (SDNs, (Ramachandran and Chen 2008)); it has been reported that downregulation of all SDN proteins results in miRNA accumulation. SDN proteins have the ability to degrade ssRNA in the range of 17-27 nt giving back a degradation product of about 6-9 nt. Conversely, they showed no activity on pre-miRNAs. Besides SDNs, a second protein, HEN1, protects miRNAs from SDNs activity through O-methylation of miRNA residues, but the dynamic regulation between these proteins still remains unclear. In *C. elegans* XRN1 and XRN2 are two 5'-to-3' exoribonucleases which have been implicated in processing and/or degrading different RNA substrates, such as tRNA, snoRNA, rRNA, mRNA and, indeed, several miRNAs. Of note, they are quite conserved

across eukaryotes (Chatterjee and Grosshans 2009). In worms, XRN1 and XRN2 knock down lead to miRNAs accumulation confirming their role in promoting miRNA decay (Krol et al. 2010b). The presence of co-factors that modulate XRNs activity has been demonstrated in yeast and metazoan, but clues on their existence in other organisms are lacking. In humans, weak pieces of evidence reveal the implication of XRN1 knock down in upregulating only miR-382 level in HEK293T cell lines (Bail et al. 2010). In melanoma cells, polynucleotide phosphorylase (PNPase), an IFN-inducible 3'-to-5' exoribonucleases, is involved in the degradation of miR-221, miR-222 and miR-106b without affecting pri- and pre-miRNAs expression (Das et al. 2010). Upon ectopic expression of PNPase, miRNAs level significantly decreases. Indeed, this might contribute to the pattern of expression of miRNAs upon INF-β stimulation. Finally, a recent study pinpoints DIS3L2, a 3'-to-5' exoribonucleases, directly bound to AGO2 protein (Haas et al. 2016). In particular, authors reveal that impairment of DIS3L2 expression leads to reduced degradation of miRNAs, both in human and in mouse cells and show that TUT1, a terminal uridylyl transferase, co-immunoprecipitates with AGO2 and DIS3L2. These data suggest a role in TIMD mechanisms for terminal transferases, specific proteins that catalyze the addition of nucleotides at 3'end of RNA. A connection between 3' modifications and TIMD was already established in previous studies, both in human and in other organisms. Indeed, GLD-2 (a non-canonical cytoplasmic poly(A) polymerase) has been proved to mono-adenylate 3' end of miR-122 leading to miRNA stabilization (D'Ambrogio et al. 2012). Of interest, hHCV infection causes GLD-2 down-regulation and miR-122 degradation (Cazalla et al. 2010; Kim et al. 2016). TUTs proteins were already involved in uridylation of pre-let-7. In particular, TUT4 is selectively recruited by LIN28A, a protein that regulates biogenesis of let-7 family members (Viswanathan et al. 2008; Chang et al. 2013). More in detail, TUT4 transforms pre-let-7 molecules in a substrate for DIS3L2 degradation activity by adding uridine to the 3'end sequence.

1.4.3. Determination and nomenclature of IsomiRs

Typically, miRNAs have been mapped in short RNA sequencing experiment referring only to the canonical sequence annotated in miRNA databases, such as miRBASE. Conversely, accumulation of several lines of evidence confirmed that different miRNA sequences are originated by the same

miRNA precursor (Neilsen et al. 2012). These variants of the prototypical miRNA are defined IsomiRs. IsomiRs are associated to RISC complex and biologically active, confirming they can interact with RNA target (Cloonan et al. 2011). IsomiRs expression profile is usually conserved across different samples and animal species (Burroughs et al. 2011). Anyway, profound alterations in IsomiRs expression have been found in different development stages, suggesting that they can be dynamically regulated and might play a physiological role (Guo et al. 2011; Neilsen et al. 2012). Most IsomiRs differ from the canonical sequence for nucleotides addition or deletion either at the 3' or 5' end (Neilsen et al. 2012). 5' modifications change the seed of the miRNA ("seed-shifting") and consequently the target repertoire of the canonical miRNA is completely changed (Azuma-Mukai et al. 2008). Accordingly, this kind of modification is rarely observed, while 3'end modifications are much more abundant (Burroughs et al. 2011). 3' end modifications can be produced either during miRNAs biogenesis or when the miRNA loaded on the miRISC complex. In this latter respect, 3'end IsomiRs has been frequently associated with miRNA stability (Ameres et al. 2010; Baccarini et al. 2011; Lee et al. 2014; de la Mata et al. 2015). Adenine and Uridine additions are the most frequent modifications at the 3'end, but the specific enzymes that catalyze these reactions are just starting to emerge (see section "Enzymes which mediate miRNAs degradation"). IsomiRs nomenclature is still rather confusing; in this study, we classified the various forms as described in **Figure 9** and detailed below.

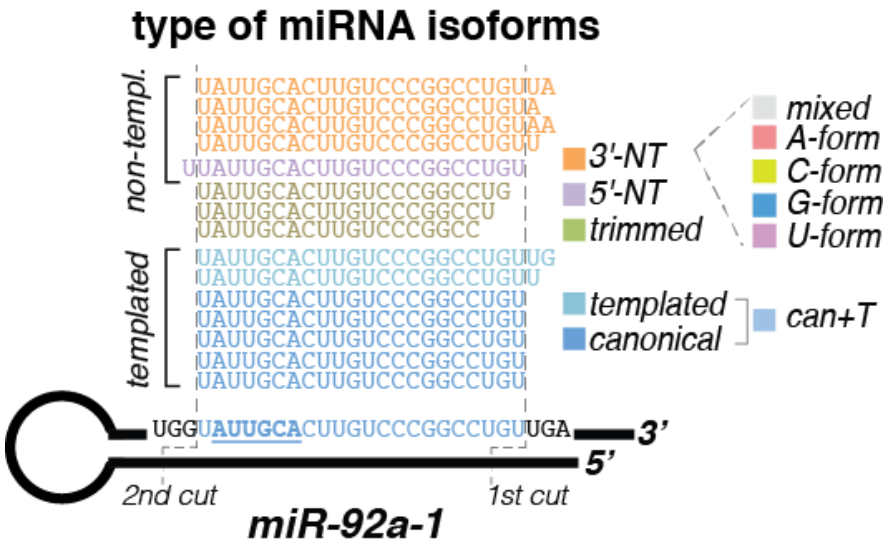

Figure 9. Types of miRNA isoforms

- **Canonical forms** are arbitrary defined as the mature sequences deposited in the miRBase database and, usually, are the most abundant form as defined by short RNA sequencing

data. Of note, the majority of qPCR assay for miRNA detection are designed to recognize only this type of form.

- **Templated forms** are miRNAs that perfectly aligns to pre-miRNA sequence, but differ from the canonical miRNA for addition of nucleotides at either the 5' or 3'end. They originate either from an imprecise cut by DROSHA (for 3p arm) or DICER (for 5p). Of note it is formally impossible to distinguish "templated" forms produced by imperfect processing from identical sequences originated by enzymatic activity (i.e. tailing or trimming) on a canonical miRNA.
- **5'-Non-Templated forms (5'-NT)** are considered all those miRNAs that present nucleotides addition at the 5'end, which do not align to the pre-miRNA sequence, meaning that active tailing occurred to the canonical form.
- **3'-Non-Templated forms (3'-NT)** are considered all those miRNAs that present nucleotide addition at the 3'end, which do not align to the pre-miRNA sequence. All four nucleotides might be added: we decided for simplicity to group together mono-, di- and tri-addition of the same nucleotide and defined them as A-, U-, C- and G-forms (Muller et al. 2014). Finally, we defined as "mixed" forms all those isomiRs that have multiple additions of different nucleotides.
- **Trimmed forms** are microRNAs that present trimmed nucleotide(s) at the 5' or 3'end. Trimming might be the result either of exonucleases activity or imprecise cut of DROSHA and DICER. While a single missing base is probably due to DICER and DROSHA inaccuracy, the presence of multiple (two or more) trimmed bases are more likely to be the product of exonucleases action.

1.4.4. Competing endogenous RNA

The competing endogenous RNA (ceRNA) hypothesis has been raised few years ago, based on the possibility that an endogenous target can compete with other transcripts for the binding to a shared miRNA (Salmena et al. 2011). In other words, the transcript sequesters the activity of the bound miRNA, leading to de-repression of other targets. A single target that interfere with another target is called "ceRNA", while a group of different molecules that influence each other form a ceRNA

network (ceRNet). The ceRNA view attributes a novel role to miRNA targets, which can communicate to each other through miRNAs titration (Salmena et al. 2011) (Figure 10). In particular, the presence of miRNA responding elements (MRE) in the 3'UTR of a target is responsible for the regulation of cognate targets that share similar MREs. Hence, a ceRNA is actually a physiological counterpart of a "miRNA sponge".

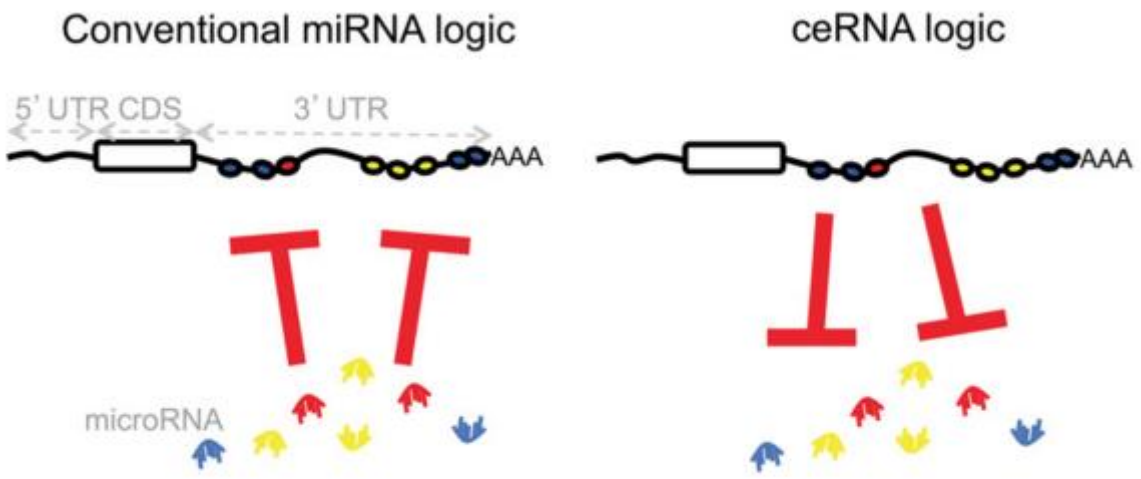

Figure 10. Scheme of the the ceRNA hypothesis. From (Salmena et al. 2011)

So far, many different types of RNAs have been identified to act as ceRNAs, such as pseudogenes (Karreth et al. 2015), protein-coding (Cesana et al. 2011) or lncRNAs [reviewed in (Thomson and Dinger 2016)]. Besides binary ceRNA interactions, computational studies exploited vast datasets (such as The Cancer Genome Atlas, TCGA) to isolate broad networks of interactions, usually including several miRNAs and mRNAs (Sumazin et al. 2011), whose dysregulation can also display profound biological effects, including tumorigenesis (Karreth et al. 2015). Nonetheless, the entire ceRNA hypothesis is still under debate, with many individual targets being expressed at too low concentrations to efficiently compete for active miRNAs (Denzler et al. 2014). On the other hand, approaches used to validate ceRNA mechanism are based on the evidence that target RNA possesses biological functions that are independent to the protein-coding region (Poliseno et al. 2010; Jeyapalan et al. 2011) . However, most of these approaches rely on overexpression systems (such as 3'UTR overexpression) or models that affect miRNA activity (such as miRNA reporters, Dicer knockout cell lines). Thus, the level of exogenous over-expression is particularly critical to understand the physiological relevance of the ceRNA interaction. Anyway, a recent publication demonstrated that the pathological NMYC gene amplification, occurring in patients with

neuroblastoma, confers ceRNA properties to NMYC mRNA (Powers et al. 2016). In fact, although the amplified transcript leads to protein overexpression, it also exerts a role in sponging let-7 family members due to the high level of expression it reached. Of note, the threshold of NMYC expression for inhibiting let-7 is completely in line to that requested by stoichiometric studies on miRNA:target interaction (Bosson et al. 2014; Denzler et al. 2014).

1.5. The 4-Thio-Uridine approach to study global RNA dynamics

Since 1978 the application of thiol-group containing nucleotides has been used to label the RNA for studying its regulation. In particular, 4-thio-uridine (4sU, Figure 11), a naturally occurring analogue of uridine, has been developed for its application in eukaryotic cells, where it enters into the nucleoside salvage pathway. There, 4sU is phosphorylated by UCK1/2 enzymes and can be incorporated into nascent RNA (Melvin et al. 1978). Because of the absence of thiol-group in the endogenous nucleotides, 4sU-RNA can be separated through thiol-specific biotinylation and then purified with streptavidin-coated magnetics beads (Cleary et al. 2005).

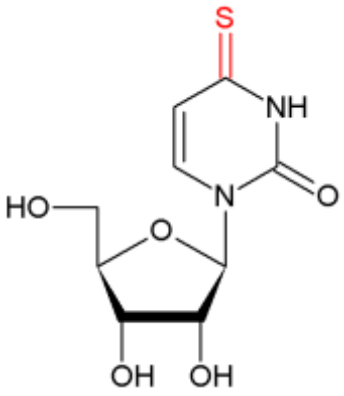

Figure 11. Chemical structure of 4-Thio-Uridine (From Sigma Aldrich)

Of interest, 4sU can be applied to a vast number of human and mouse cell lines with minimal adverse effects on cell viability and metabolism (Melvin et al. 1978; Dolken et al. 2008). Since its discover, 4sU has been used in the study of RNA synthesis and decay dynamics, mainly mRNAs, representing a good alternative to drugs based method, as discussed above (see paragraph "The turnover of the microRNAs"). In a first paper, 4sU has been administrated to NIH-3T3 cells to study the dynamics of mRNAs incorporation at steady state conditions (Dolken et al. 2008).

Authors performed a 4sU pulse experiment in which 4 time points (15-30-45-60') were generated. After 1 hours of 4sU administration, RNA labeling reached the 6-8% on total RNA. After extraction, 4sU-RNA has been analyzed through microarray technology to study dynamics of incorporation. Indeed, authors showed that the 4sU-RNA incorporation rate is a direct read out of the stability of a molecule. This hypothesis was based on the simple theory that, at cellular equilibrium and defined labeling time, an mRNA that presents a fast turnover incorporates more 4sU as compared to an mRNA with a slow one. The concept was transformed in a mathematical formula for the calculation of mRNAs half-life, which is, thus, based on incorporation rate (R) and duration of labeling (Tl), $T_{1/2} = -Tl * \ln(2)/\ln(1-R)$.

Indeed, the shorter is the 4sU-pulse, the more precise is the measure of RNA labeling and, thus, the determination of half-lives.

Therefore, as second approach, Rabani et al applied a shorter pulse of 4sU (10') coupled to RNA sequencing to globally study temporal RNA regulation in dendritic cells either in steady state condition or upon LPS treatment (Rabani et al. 2011). By combining such approaches, they found that 4sU short pulse enriched for unstable species and immature form of mRNA (unspliced transcripts). Interestingly, upon 10' of labeling, introns represent the 50% of all sequenced transcripts. On the contrary, total RNA-sequencing enriched, as expected, for mature form and unspliced transcripts account only for the 8.7% (**Figure 12**).

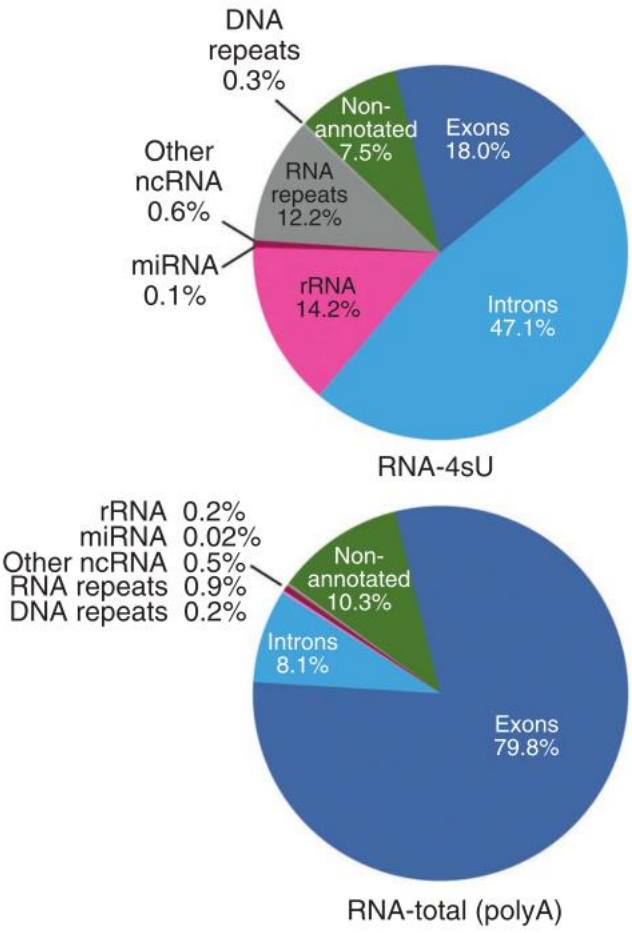

Figure 12. 4sU short pulse allows the enrichment of unspliced species. (From (Rabani et al. 2011))

By exploiting short 4sU pulse, authors studied the dynamics of mRNA regulation of dendritic cells both at steady-state condition and during stimulation with LPS. They measured half-life of mRNAs and found that degradation rate varies significantly between genes. Moreover, they measured mRNA transcription rates finding that temporal changes in mRNAs abundance were mainly due to transcription as compared to decay rate. In other words, they suggested that mRNA regulation is mainly driven by transcription while degradation dynamics do not affect considerably the modes of mRNA turnover. Concluding, this study allows the global determination of mRNA half-lives and consequent assessment of mRNA dynamics without affecting cell physiology. By combing short 4sU labeling and NGS techniques, authors provide a new tool for evaluating the different modes by which a transcript is regulated in cells at specific condition.

2. MATERIALS AND METHODS

2.1 Cell treatments and procedures

Mouse parental 3T9 fibroblasts were cultured in DMEM (Dulbecco's modified Eagle's medium) supplemented with 10% fetal bovine serum (FBS), 100 U/ml penicillin and 100 μg/ml streptomycin. hTERT immortalized human BJ fibroblasts were culture in MEM supplemented with 10% FBS, NEAA, hygromycin. HeLa cells were grown in Eagle's minimum essential medium supplemented with 10% FBS. 3T9 cells were induced to quiescence in a serum-deprived medium for 3 days. Cell cycle re-entry was stimulated by adding fresh medium with 10% FBS. For cell cycle analysis, cells were treated with 33 μM BrdU for 30 min, harvested by trypsinization and ethanol-fixed. Staining was performed with anti-BrdU primary antibody (1:5 in PBS 1% BSA, BD Biosciences) and anti-mouse Cy5-conjugated secondary antibody (Jackson Immunoresearch). DNA was stained with O.N. incubation with 2.5 μg/ml Propidium Iodide (Sigma). Samples were acquired on FACS-CALIBUR (BD Biosciences) flow cytometer and analyzed using FlowJo 10 software. For immunofluorescence analysis cells were plated on coverslips and after treatment with 4sU (300 μM, 3 hours) were fixed with Paraformaldehyde. Nucleoli were stained with anti-nucleolin (1:800, Abcam Cat. Num.ab50279) plus anti-rabbit FITC conjugated secondary antibody (1:500, Jackson Immunoresearch). Nuclei were stained with DAPI. Visual inspection of Nucleolar stress was performed under a fluorescent microscope (Olympus AX70; 40x and 100x objective lens).

2.2 4-Thiouridine labeling and isolation protocol

4-Thiouridine, (4sU - Sigma cat.no T4509), was added to culture medium at a final concentration of 300 μM. Cells were pulsed for 3 hours and subsequently chased with 1 mM Uridine (Sigma cat.no U3003). For continuous labeling experiments, 4sU treatment (300 μM) was performed with increasing time (15', 30', 45', 60', 120', 180'). Total RNA was extracted at each time points by miRNeasy Mini Kit (Qiagen cat no. 217004), according to the manufacturer's instructions including the recommended DNase I digestion. Separation of 4sU-incorporated (newly synthesized RNA) from non-incorporating (pre-existing RNA) was performed as previously described (Rabani et al. 2011) with minor modifications. Briefly, starting from 40 μg of total RNA diluted in 100 μl

of RNase-free water, 100µl of biotinylation buffer (2.5× stock: 25mM Tris pH:7.4, 2.5mM EDTA) and 50 µl of EZ-link biotin-HPDP (1 mg ml−1 in DMF; Pierce/Thermo Scientific 21341) were added and incubated for 3h at RT. Unbound biotin-HPDP was removed by adding chloroform/isoamylalcohol (24:1) and purifying the mix using MaXtract high-density tubes (Qiagen). RNA was precipitated by adding NaCl (5M) at 1/10 volume and isopropanol at equal volume. Biotinylated RNA was resuspended in water (55°C, 5'), quantified with a Nanodrop 1000 spectrophotometer (to keep track of the yield after the first phase of the procedure) and, then, purified using 50µl of Dynabeads MyOne Streptavidin T1 (Invitrogen). Before mixing with RNA, beads were washed twice in Wash Buffer A (100mM NaOH, 50mM NaCl) and once in Wash Buffer B (100mM NaCl), then resuspended in 100 µl of Buffer C (2M NaCl, 10mM Tris-pH:7.5, 1mM EDTA, 0.1% Tween-20) to a final concentration of 5µg/µl. RNA was added in an equal volume and rotated at RT for 15min. Beads were washed 3 times with Wash buffer D (1M NaCl, 5mM Tris pH7.5, 0.5mM EDTA, 0.05% Tween-20). RNA was eluted from the beads in 100µl of 10 M EDTA in 95% formamide (65°C, 10 min). Eluted fraction was diluted in TRIzol® LS Reagent *(*Life Technologies; cat.no. 10296-028*)* and RNA extracted with miRNeasy Micro Kit (Qiagen; cat.no. 217084) and finally eluted in 14 µl of RNAse free water. 4sU-RNA quantification was conducted with Qubit® (Life Technologies).

2.3 Determination of miRNA half-lives

For mRNA and pri-miRNAs, half-life (T1/2) were calculated indirectly measuring the ratio (R) between newly-transcribed (labeled) over total RNA (Dolken et al. 2008), according to the following equation: $\mathrm{T1/2}\ (h) = Labeling\ Time(h) \times \frac{\ln(2)}{\ln(1-R)}$. For miRNAs, half life (T1/2) were

calculated by pulse-chase, measuring the decay of labeled RNA species during the chasing time. For genome-wide analysis of miRNA half-life, three independent pulse-chase experiments were used (decay dataset). The decay dataset (normalized and background subtracted, **see paragraph 4.2.2.1**) was imported in GraphPad Prism 6 and half-lives were modeled by a one-phase exponential decay, with a plateau fixed to a constant value of 0 and a fitting method based on least squares. In the fitting the replicate values at each time-point (N=3) were averaged. The simple one-

phase decay was compared to a two-phase decay, which would imply the existence of different miRNA pools with specific decay rates (e.g. miRNA unloaded and loaded on Ago2). The Extra sum-of-squares F-test was used to select the best model. We preferred the simpler model unless the P-value was < 0.05. 'Fast' and 'Slow' classes were defined as follows: 'fast', $T1/2_{ave}$<14hrs with $T1/2_{max}$<20 hrs; 'slow', $T1/2_{ave}$>24hrs with $T1/2_{min}$>15hrs. Half-lives and confidence intervals are reported in in **Table 1**.

2.4 Statistical Analysis

Analyses (Oneway, Scatter Plot, Contingency) and statistics were produced using JMP 10 (SAS) software. Microsoft Excel was used to generate bar graphs with average and st.dev of repeated experiments. The number of replicates and the statistical test used are indicated in Figure Legends. Heatmaps were generated by Java TreeView software (http://jtreeview.sourceforge.net) for Mac OSX.

2.5 Small RNA sequencing and data analysis

Total RNA, including small species, was isolated through the miRNeasy Mini (Qiagen). When the expected yield was <1µg miRNeasy Micro kit (Qiagen) was used. Small RNA sequencing libraries were prepared using 300 ng of 4sU-RNA (decay dataset) or 1000 ng of total RNA (serum-stimulation dataset) with the Illumina TruSeq™ Small RNA kit, following manufacturer's instructions. We additionally sequenced RNA from growing cells (not labeled without isolation – UNT), total RNA pulsed with 4sU (labeled without isolation – 4sU) and 4sU RNA from non labeled cells (non labeled with isolation, negative control – NEG). Sequencing was performed on an Illumina HiSeq 2000 at 50 bp single-read mode and 20 million read depth (8x). Data analysis was performed with the *IsomiRage* workflow, as previously described (Muller et al. 2014). Raw data together with detailed description of the procedures are available in GEO database.

2.6 Normalization of Small RNA sequencing data

Data normalization was performed after reads mapping, assignment and filtering. In the "decay dataset", data were normalized using miR-92a-3p reads (i.e. canonical miRNA and other templated reads), a highly expressed and stable miRNAs (T1/2 >24hours by RT-qPCR, Figure 28). Other normalization approaches, employing abundantly expressed and stable miRNA species (e.g. miR-25-3p) or by library size, yielded to similar results as they were moderately or highly correlated

during the time course (Figure 29). After data normalization, the background level (reads in the negative control - 4sU-RNA extracted from unlabeled total RNA) was subtracted from each sample. The negative control (NEG) library had an average number of reads that was < 3% respect to the labeled sample, suggesting that 4sU libraries had purity >97%.

In the "serum-stimulation dataset", normalization was performed with the library size (reads-per-million) and, then, further corrected for serum-induced RNA amplification. Briefly, the RNA content of the cells was measured at each time-point (repeated analysis of yield of RNA extraction from the same number of cells, i.e. one million). The content ranged from 7.78 pg in quiescence cells to 11.9 pg in growing cells. Accordingly, a log2 scaling factors was calculated: 0h=0; 1h=0.1; 2h=0.194; 4h=0.199; 6h=0.313; 8h=0.433; 10h=0.513; 12h=0.455. Serum-regulated miRNAs were then identified by normalizing single-cell-RPM values over the 0 hours sample and selecting those miRNAs that were regulated of ±0.5 log2FC (12hrs).

MiRNAs precursor (pri-miRNA) and mRNA RTqPCR expression analysis

Primary transcripts of miRNAs (pri-miRNAs) were evaluated by quantitative PCR on 4sU or total RNA. RT-qPCR was performed on equal volumes of 4sU samples by using SuperScript® VILO cDNA Synthesis Kit (Life Technologies cat.no. 11754050) and Fast SYBR green master mix (Life Technologies). When total RNA was used, 25 ng of cDNA were used as input for the detection of pri-miRNAs and 5 ng for the detection of mRNAs. Primer pairs were designed through computer assisted primer design software (Primer3) preferentially within 500 bp upstream the sequence of the mature miRNA according to UCSC genome. The complete list of primers used in this study is shown in below.

	FORWARD	**REVERSE**
PRI-miR-100-let7a	TGCCACAAACCCGTAGATCC	AGGGCAGGAGAAGGTGTACT
PRI-let7b-let7c2	TGGGGCATAGCGATGAAAAC	TGTGAGCACAGGTCTGATATGG
PRI-miR-155	AAGGCCTGTTACTAGCACTCAC	AGGGTGACTCTTGGACTTGTC
PRI-miR-15a-16	GGCTTTGAAAGATGTGCTGCTC	CGAGAAAAGCAAGTCATTTTCCC
PRI-miR-34a	AGGACTTCGGAAGCTCTTCTG	AACTTCTCCCAGCCAAAAGC
PRI-miR-503	AAGTTTCGGTTAGCCTGCAG	AAGTGAGGCGCTAACAACAC
PRI-miR-9_1	CGCTTGGTTTCAGCCTAGATTC	ATCACGACGAGACCTCAGAAAG
PRI-miR-26a_1	TTTGCCTGTAGCCAAGCTTG	CCTGCTTTGCTCATAACACTCG
PRI-mir-182	TCGACCTCTTCTCGGTGAAAAG	AAGCTTAGGATTCCCACCATCC
PRI-miR-92a_1	TCTATTGCTTTCGTTGGTGTG	CTAAATCCAGCGAGCAAACA
PRI-miR-30b-30d	ATCACCATGCCCAGCTAAAG	TTCTGAATCAAAATATTGGTATCATCT

PRI-miR-335	TCATGGGTTATAGCCAGTCGAG	GTCTGGGAAAGAACAACAAGCC
PRI-miR-24_1	TGCCTTGAGCAGTGAGAATG	CACCTCACAATCCTGGGTCT
dNGFR	CGTGCTGGCTATGAGGTCTT	CCGTTGGATTACACGGTCCA
c-MYC	TTTTTGTCTATTTGGGGACA	CATCGTCGTGGCCTGTCTG
CCNE2	AACCCAGATAATTCAGGCCAAG	CAGTACAGGTGGCCAACAATTC
GAPDH	CGTATTGGGCGCCTGGTCAC	ATGATGACCCTTTTGGCTCC
RRP0	TTCATTGTGGGAGCAGAC	CAGCAGTTTCTCCAGAGC
FOSB	CGACTTCAGGCGGAAACTGAT	TTTTGCAGCTCGGCGATCT
URFH1	GGCAGGCATCCATGGCCGGAGC	AGAGGCAACGGGGGCTGGAGAGG
MCM6	CCACAATCTCTGCACGAGCC	CCCCACGAAGAGAGGTTCC
SERPINE1 (gene body)	CAGAGAGGGAAAGGGGCT	CTCACATACAGCAGCCGGAA
SERPINE1 (MRE seq.)	AAATGGTGGCCCAATAGCGA	AAGCAAGCTGTGTCAAGGG
GFP	GAGCAAAGACCCCAACGAG	ATCATCCTGCTCCTCCACCT
Serpine1 primers for microdeletion detection	GGAGGGCACAACACTTTCAT	AGTGCTTCTTCTCCCCAACA

Determination of pri-miRNA synthesis rate by Inspect

The R/Bioconductor software INSPEcT was used to infer synthesis rates based on RNA- and 4sU-seq data (de Pretis et al. 2015). RNA-seq data coming from the two experimental conditions (Growing 3T9 fibroblasts – GW, and Serum Stimulation of quiescent 3T9 fibroblasts) were used. In growing conditions (GW), data are from biological triplicates (both the 4sU labeled and total RNA), while for Serum Stimulation (SS), a time-course was performed including 10 different time points. In the analysis step, the "degDuringPulse" option has not been used, since the length of the 4sU pulse used to label newly synthesized transcripts is shorter than the median half-life of transcripts calculated by similar studies where 4sU-tagging were used (10 minutes vs. 30 minutes (Rabani et al. 2011) . Read counts from Total RNA-seq experiments were inter-sample normalized using "glm analysis" of edgeR R/Bioconductor package. Read counts from 4sU-seq experiments were scaled within the INSPEcT package, following an optimization process that takes into account the calculation of the processing rates genome wide. RPKMs were calculated from RNA-seq and 4sU-seq experiments by dividing read counts by the length of the feature they are assigned to (expressed in KB) and by a pseudo-library size (expressed in Mb) that represents the average coverage of the RNA- or 4sU-seq experiment in all experimental conditions. Pseudo-library size is used instead of the real library size to maintain the normalization strategy implemented by the "glm fit" of edgeR, as previously described (de Pretis et al. 2015). Pseudo-library sizes used are the

following: 4sU-seq - GW = 52394638; RNA-seq - GW = 67071416; 4sU-seq - SS = 70754530; RNA-seq - SS = 80094546.

2.7 miRNA targets analysis

MiRNA targets were downloaded from TargetScan 6.2. High confidence targets were selected according to previously identified criteria (Marzi et al. 2012) and outlined in Figure 51. Mouse predictions referring to 8mers and 7mer-m8 with a context score (CS) <-0.2 were considered, while the other predictions were filtered out. Both the Conserved (CS) and Nonconserved (NCS) sites were used. Out of the different mRNA isoforms present for the same gene, only the longest was considered. These seed-containing targets were referred as 'seed' target genes (TG_seed). Targets were also classified according to the 3'-end pairing contribution, a feature that measures the presence of additional binding sites (in addition to the seed region) located at the 3'end of the miRNA. These targets containing 3'end compensatory regions were referred to as '3C' target genes (TG_3C). For '3C' target genes, predictions with context score >-0.1 were excluded. These targets were further distinguished according to strength of 3'-end pairing in: a) targets with 3C binding <-0.03 (3C.03), and b) targets with 3C binding <-0.05 (3C.05). Examples are shown in Figure 51. To select only those targets expressed in 3T9 mouse fibroblasts, the target lists ('seed', '3C.03' and '3C.05') were crossed with RNA-seq dataset (growing cells and serum-stimulated cells). Genes with FPKM values < 1 were considered as 'not expressed' and, thus, excluded. To calculate Target:miRNA ratios (TPM) FPKM values were converted into Copies per cell (CPC) with the same strategy used for Primary miRNA transcripts, which relies on absolute quantification of gene expression by digital PCR (ddPCR).

2.8 Droplet digital PCR (ddPCR)

Droplet digital PCR was performed using the QX200 Droplet Digital PCR system (Bio-Rad), with the QX200 EvaGreen ddPCR supermix. Mature miRNA detection by ddPCR was tested both with miScript system (Qiagen) and the miRCURY LNA system (Exiqon), with only the latter producing a specific digital response. As further controls, we measured a miRNA (miR-34a, LNA PCR primer set: 204486) low expressed in wild type 3T9 cells as a) endogenous molecules, b) molecules induced upon doxycycline inducible expression (pSLIK-miR-34a). We evaluated the absolute copy number of miR-34a performing a linearity curve, using different amount of cDNA

(0.2/0.1/0.05/0.025 ng) as input for the ddPCR. We estimated 231±42 copies/ng (2.74 copies per cell, CPC) in wild-type cells and 12568±734 copies/ng (149.5 CPC) in the case of the exogenous expression upon doxycycline treatment. Comparing miR-34a expression by small-RNA sequencing with ddPCR data, we derived a normalization factor to convert small-RNA seq reads per million (RPM) into copies per cells (CPC), which is CPC= RPM/10.85.

Detection of miRNA precursor (pri-miRNAs) is described in Figure 44**.** Digital PCR was performed with different amount of input RNA (0.25 and 2 ng of 4sU RNA; 1.25 and 10ng of total RNA), obtaining highly linear results from all the doses used as input. Copies/ng were converted into copies/cell by estimating the RNA content per cell from multiple experiments (11.9 pg for GW cells; 7.78 pg for SD cells) and the 4sU content per cell (6.3 fg for GW cells; 2.18 fg for SD cells). Comparing pri-miRNA expression by RNA sequencing with ddPCR data, we derived a normalization factor to convert RNA-seq reads (FPKM) into copies per cells (CPC), which is CPC= FPKM/7.36.

2.9 Ago2 RNA immunoprecipitation (AGO-RIP)

Ago2-RIP experiment was conducted with the Imprint RNA Immunoprecipitation Kit (Sigma-Aldrich), according to manufacturer's instructions. Briefly, cells are grown to ~80% confluency. A total of 10 million cells were used for each RIP experiment. Cells were trypsinized, collected in a tube and washed twice with ice cold PBS. Cells were resuspended in 200 µl of lysis buffer (Mild Lysis + Protease Inhibitor Cocktail (PIC) + Ribonuclease Inhibitor) and incubated on ice 15'. Cell debris were removed by centrifugation at 16,000g, 10 min at 4C. A fraction (5%) surnatant was collected as 'input' and stored on ice or flash frozen, while the remainder was used for immunoprecipitation. For each RIP, 20µl of Magnetic Beads with Protein A were pre-cleared with 200µl of Wash Buffer on magnetic stand and, then, mixed with 2.5 µg of control antibody (rabbit Anti-Rat IgG) or Anti-AGO2 antibody (mouse monoclonal 2A8 clone by Sigma Aldrich - Cat. Num. SAB4800048) at RT with rotation for 30 min. 2.5 ug rat IgG or monoclonal Anti-AGO2 antibody were added to magnetic beads. Samples were washed twice with 0.5 mL of wash buffer, then, cell lysates (surnatant) was added and incubated at 4°C with rotation over-night. Samples were then separated through magnetic stand, washed five times (0.5ml wash buffer, each time) and, finally, resuspended in 0.2ml of wash buffer. RNA extractions from RIP samples was performed

with 0.6 ml (1:3 ratio) of TRIzol LS (Life Technologies; Cat. Num 10296-028). A fraction (1/5) of the Ago2 associated RNA and 1/5 of the input RNA (around 100.000 cells) were analyzed by small RNA sequencing. To calculate the fraction of miRNAs loaded on Ago2, raw reads were normalized by the ratio of cells used to isolate the input and to perform the Ago2-IP (i.e. 95:5). For Western blot analysis, a fraction (5%, 10 μl) of Ago-RIP samples were resolved on SDS-PAGE (7.5% precast gel, Biorad), transferred on nitrocellulose membrane with Biorad Trans-Blot turbo and stained with Anti Ago-2 Ab (mouse monoclonal 2A8 clone).

2.10 Inducible Expression (Tet-ON) of miRNAs

Inducible expression of miRNA was achieved using pSLIK-Neo system (Addgene, plasmid #25735). Primary transcript sequences miRNAs (i.e. mmu-miR-34a, mmu-miR-182 and mmu-miR-9) were sub-cloned from Lenti-miR microRNA precursors clones (System Biosciences) into pSLIK-Neo. Constructs were sequence verified and used for lentiviral production and stable infection of 3T9 mouse fibroblast, as previously described (Follenzi and Naldini 2002). Briefly, 293T cells were seeded approximately 24 hours before transfection in a 15cm plate and incubated at 37°C with 5% CO2. The following day, the cells were transfected with a third generation packaging system (pVSV, pMDLg/pRRE, pRSV-REV, pADV) and the appropriate transfer plasmid using calcium phosphate. The media was changed 14 hours later, and 30 hours later the cell supernatant containing the vector was passed through a 0.22 μm filter, mixed to Polybrene (8 μg/mL, Sigma 107689) and used for 3T9 infection The day after the infection, fibroblasts were put on Neomycin selection (750 ng/ml) for one week and, then, treated with Doxycycline at different concentrations to induce miRNA expression. Several doses of doxycycline were tested, from 1 ng/mL (ineffective) to 1 μg/mL (not shown).

pri-miR-9 in pSLIK vector (5'→3')

TGGAGCCTTTCCACTAGCACCGGCGGAACCCTGCTTCTGCACGGAGGAGGGAGTGGGA
AATGGGCGGTCAGGCTTGGGGCCGCTTGGTTTCAGCCTAGATTCCCGACCTCAGAACC
GTCGGCGGTAGCATCTTTTCCTCGCCTTTCTGAGGTCTCGTCGTGATAGTGCGTGAGGT
CCTGGATCCCATCTTTTCGCCTCCACACCACGCGCGTCCCCCATCCGCCGTCGAGCGAC
TCGAGACTACGGAGGTCCAGGCGGTGGCCGGGAGGCTGCGTGGAAGAGGAGGAGGCG
GCCAGGAGGCGGGGTTGGTTGTTATCTTTGGTTATCTAGCTGTATGAGTGGTGTGGAGT
CTTCATAAAGCTAGATAACCGAAAGTAAAAATAACCCCATACACTGCGCAGAGGGCC
TGGAACGCTGGTAGTGGCCGAGCTGCAGGAGGGAGAGCCGTGCCAGGCGTGCCTGGA
GGCTGGAGGGCTGGGGGGAGGGGGACTCGTCGCCTTCAAAGGTTGCTCAGCCCGAGC
CACCTCGCGATCCCCACCCGCAACCTGCTCACCTGGGAAGAAAGCAA

pri-miR-182 in pSLIK vector (5'→3')
CTCGAGACTAGTGAATTCGGGAGGTGGTCGTGGGGTGGGGGGGAGGTGGCTGGAGGG
CAGGCAGGGCTTGAGGAGGTTTTACACTGGAACAGGACCATACAGGCCGAAGGACCA
TAGTCTGGACCTTGTGTTAACTGTGGGAAGAGCGCCCTCCTAAAACCACCCTAACTGC
TTCTTCTTCAGCATAGGCTTACTGGTCTGGCTGCTGGAGGCCTCCCACCATTTTTGGCA
ATGGTAGAACTCACACCGGTAAGGTAATGGGACCCGGTGGTTCTAGACTTGCCAACTA
TGGTGTAAGTGCTGAGCTGCTGAAGGTCTGCACCGTGCCGGAACCTGCCGATCACCAG
GAAGGAGAGGGGACTCCTGTCTCCAGACCACCAGGCAGTGGCAGAGGGTGGGCGCAG
CTGGAAGTGACCCTTAATGTTTCCCTGCGCCCCCCTGAGGTCACAAGTCATGAAGTCG
ACCTCTTCTCGGTGAAAAGGACTTGGGATCCGCGGCCGCACGCGTTTAATTAAGAATT
C

pri-miR-34a in pSLIK vector (5'→3')
GCCCTTATGGAGTCTTGCTAGTTGCCTGGGCTGGTCTTGAACTCCTGGCCTGAAGCGAT
CCTCCCACCTCGGCCTCCTGCATCCTTTCTTTCCTCCCCACATTTCCTTCTTATCAACAG
GTGCTGGGGAGAGGCAGGACAGGCCTGTCCCCCGAGTCCCCTCCGGATGCCGTGGACC
GGCCAGCTGTGAGTGTTTCTTTGGCAGTGTCTTAGCTGGTTGTTGTGAGCAATAGTAAG
GAAGCAATCAGCAAGTATACTGCCCTAGAAGTGCTGCACGTTGTGGGGCCCAAGAGG
GAAGATGAAGCGAGAGATGCCCAGACCAGTGGGAGACGCCAGGACTTCGGAAGCTCT
TCTGCGCCACGGTGGGTGGTGAGGGCGGCTGGGAAAGTGAGCTCCAGGGCCCCAGGA
GCAGCCTGCTCGTGGGTGCGGAAGGAAAAAGGCACAGGGGCTTGGTGTGGGCGGCTT
TTGGCTGGGAGAAGTTTGCACGTA

2.11 Reporter for miRNA activity (miR-sensor)

Sequences harbouring four highly complementary repeats for miRNA (i.e. miR-9) were purchased from TwinHelix and cloned into the 3'-UTR of a destabilized GFP (dGFP) in a bidirectional lentiviral vector (BdLV), that also expresses ΔNGFR (schematized in Figure 58). The vector was kindly provided by Luigi Naldini and his collaborators. Transduced cells were analyzed by FACS to isolate populations with similar NGFR expression as previously (Brown et al. 2006).

3'UTR sequence harboring 4x repeats of miR-9 or miR-181a binding site was subcloned by XbaI-XmaI digestion. The cloned sequences are reported below

miR-9 sensor:
TCTAGATAATCATACAGCTAGATAACCAAAGACGATTCATACAGCTAGATAACCAAAG
AACGCGTGTCGACTCATACAGCTAGATAACCAAAGATCACTCATACAGCTAGATAACC
AAAGACCCGGG

2.12 CRISPR/Cas9 mediated deletion protocol

Four sgRNAs flanking the miR-30 MRE were designed at position 573-580 of ENST00000223095.4, as shown in Figure 84 using the CRISPR Design Tool (Ran et al. 2013). SgRNAs were subsequently cloned in PX458 vector (Ran et al. 2013) and sequence-verified. 3T9 fibroblasts were co-transfected with two PX458 vectors (sgRNA_1 and sgRNA_2) harboring single sgRNAs sequence (5 μg each construct). Transfection reagent (Lipofectamine 3000) results in

transfection efficiency of 30%. 24h-48h post transfection, cells were harvested for FACS sorting. Top 2-3% of GFP+ cells were isolated at single cell level into 96-well plates. Five 96-well plates were produced for each condition tested. After 2 weeks, 96-well plates were duplicated and microdeletions of clonal cells were detected by PCR by using specific primer which mediate amplification one or two bands if mono-allelic or bi-allelic deletions were produced, respectively. Positive clones were analyzed and confirmed by DNA sequencing. The protocol efficiency was about 10% for mono-allelic and >1% for bi-allelic deletions.

SgRNA_1 caccgCAGGGAGAAGGCTCGCTATT

SgRNA_2 caccgACCCACAAACTTTTTTCATT

SgRNA_3 caccgGCAGGGAGAAGGCTCGCTAT

SgRNA_4 caccgTCTCCCAGTGGGGGGGCCCT

3.RATIONALE

Although large efforts have been put in understanding how miRNA transcription and biogenesis are regulated, to date we almost completely ignore what happens to miRNAs while they are functioning on RISC. In particular, we do not know if they could be recycled on other target molecules or are degraded, and if target RNAs are involved in the life/death of miRNAs. As miRNAs exert key regulatory functions in development and disease, it is critical to understand how cells globally coordinate miRNA lifespan and which are the key factors behind miRNA turnover.

Typically, miRNAs are thought to be stable molecules with long half-lives [greater than 24 hours, as observed for the mir-122 and mir-208 (Krol et al. 2010b; Ruegger and Grosshans 2012). Nevertheless, it has been also reported that some miRNAs could be rapidly turned over, such as for mir-503 (Rissland et al. 2011) and mir-182 (Krol et al. 2010a). Strikingly, the stability of miRNAs could be dependent on specific cellular conditions. For instance, in the mouse retina the turnover of mir-182 could vary upon dark adaptation or light exposure (Krol et al. 2010a). These data suggest that miRNA half-life could be physiologically regulated in defined context, depending on the need of the cell. Few studies have attempted to measure globally the degradation rates of miRNAs. In these studies, the general approach was to interfere with the generation of new miRNAs by using inhibitors of transcription (actinomycin D or alpha-amanitin) or by blocking miRNA processing [targeting processing enzymes (i.e. Dicer)]. The results suggested that almost all miRNAs possess slow degradation rates, with few exceptions (Bail et al. 2010; Gantier et al. 2011). However, such approaches introduce also non-specific effects at the level of the whole transcriptome and, thus, represent non-physiological conditions under which it could be reasonably hard to accurately measure how miRNAs are turned over.

To overcome this limitation, we developed a global approach to measure the turnover of miRNAs in cultured cells, without perturbing neither the transcription nor the biogenesis of the miRNAs (and other RNA species). By this approach we sought to verify whether all miRNAs have, indeed, a slow decay, to understand which are the transcriptional and post-transcriptional mechanisms that influence (or are influenced by) miRNA decay, and finally if miRNA degradation could be actively modulated upon specific cellular conditions.

4.RESULTS

4.1.Development of an optimized RNA labeling pulse-chase methodology to determine miRNA degradation rates in mammalian cells

4.1.1 4-Thio-Uridine incorporation into microRNAs

Previous approaches to describe miRNA degradation dynamics were based on measuring the decrease in miRNA levels while the generation of new molecules was blocked. This could be achieved through the administration of drugs, which block transcription (i.e. actinomycin-D or alpha-amanitin –(Bail et al. 2010)) or inhibiting those enzymes (e.g. Dicer) that are essential in the maturation of miRNAs(Gantier et al. 2011; Guo et al. 2015)). A major drawback of both approaches is the limited time window of analysis and the introduction of unwanted secondary effects (apoptosis and senescence), which greatly perturb cell physiology. We decided to develop a novel approach to measure miRNA degradation dynamics, by exploiting RNA labeling, in order to maintain transcription and maturation of miRNAs at their physiological rate. We took advantage of 4-thiouridine (4sU), a natural occurring analogue of uridine, typically present in mammalian cells at a low concentration (<1%). The molecular structure of 4sU, with a sulfhydryl group in position "4" of uridine nucleotide, does not interfere either with the incorporation in RNA chains during transcription (Melvin et al. 1978) and at the same time provides a mean for a thiol-specific biotinylation of the labeled RNA. Once biotinylated, the RNA could be selectively pulled-down from total RNA through streptavidin beads.

Nonetheless, high concentration or continuous administration of 4sU to cultured cells can lead to metabolic stress and to various extents, to RNA degradation (Burger et al. 2013). To this end, it is critical to verify whether 4sU administration display any toxic effect in the model system that is selected for the measurement of miRNA decay.

As model system, we decided to use NIH-3T9 cells, a murine fibroblast cell line. This choice has been motivated by several reasons: *i)* it is a genetically normal model, the lack of gene deletion or amplification allow an unbiased measurement of transcription and degradation dynamics; *ii)* 4sU has been already successfully applied to such cells, (200 uM, 1hour) to analyze transcriptional response upon IFNγ treatment (Dolken et al. 2008) and to measure transcription rate of MYC target

genes (Sabo et al. 2014), providing RNA sequencing data of 4sU short pulse and transcription dynamics, available as a resource for further studies (e.g. transcription rate of miRNA genes, see paragraph 4.3.3).

For our purposes, we needed to get 4sU incorporated into miRNAs, in conditions that minimize unwanted effects on cell physiology (Dolken et al. 2008; Burger et al. 2013). At first, we examined the incorporation dynamics of continuous 4sU labeling. We administrated to subconfluent growing 3T9 cells a dose of 300 μM 4sU for different times (15'-30'-45'-60'-120'-180') and collected total RNA (**Figure 13-PANEL LEFT**). Upon administration, 4sU passively reaches cytoplasm where UCK1 and UCK2 kinases catalyze its phosphorylation as 4sUTP. As a consequence of that, RNApol2 could incorporate 4sUTP into newly synthesized RNA chains (van Kuilenburg and Meinsma 2016). 4sU labeled RNA can be purified from total RNA through a biotinylation reaction followed by streptavidin-based pull down. A detailed protocol is included in Material and Method section.

Then, we measured 4sU yield and we found it increased linearly over time reaching a maximum of incorporation at 2 hours (5-6% labeled fraction on total RNA, **Figure 13-PANEL RIGHT**). After this time, RNA is no more labeled. This is probably due to the limited stability of 4sU available in the medium (which is about 2-3 hours), and to a negative feedback induced by high levels of nucleotides, which leads to the transcriptional block of UCK1/2 gene (van Kuilenburg and Meinsma 2016). It is also reported that high concentration of nucleotide analogues in the media could block the *de novo* pyrimidine pathway (Karle et al. 1984).

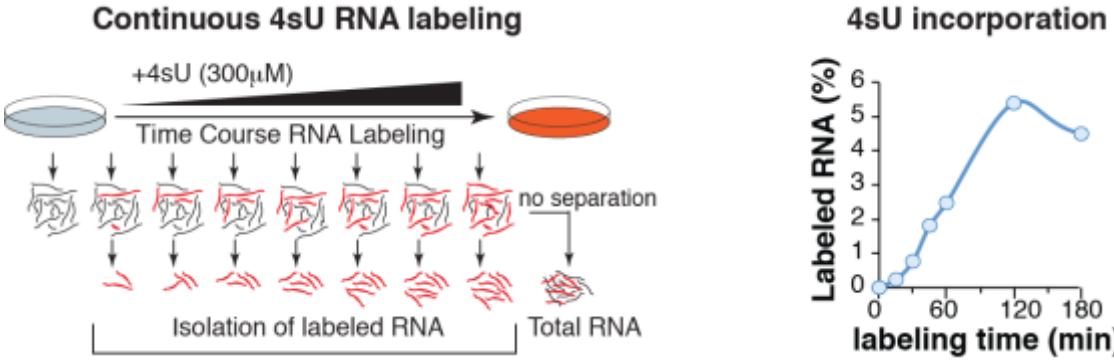

Figure 13 Setting and yields of 4sU pulse experiment. **LEFT PANEL** A scheme illustrates the experimental strategy of continuous RNA labeling by 4sU. 4sU (300μM) is added into the medium and RNA samples are collected at different time points (15'-30'-45'-60'-120'-180'). 4sU incorporated into newly synthetized RNA is isolated by thiol-specific biotinylation followed by pull-down with streptavidin beads. Unlabeled RNA (0') is used as reference. **RIGHT PANEL** The plot reports the yield of 4sU RNA isolation along the time course, expressed as percentage of labeled RNA over total RNA (4sU/Tot). The incorporation linearly increases up to 2 hours, when it reaches a maximum.

We then moved to analyze the dynamics of 4sU incorporation for long and short RNAs during pulse experiments by RT-qPCR. First, as validation of the approach, we measured the incorporation rate (4sU-labeled/Total RNA) of different mRNA species, including mRNAs with fast turnover (*myc* and *ccne2*) and mRNAs with slower turnover (*gapdh* and *rpp0*). As expected, the incorporation rate correlated with the different stability of RNA species, with unstable mRNAs (*myc* and *ccne2*) incorporating 4sU faster than more stable mRNAs (*gapdh* and *rpp0*, **Figure 14-LEFT PANEL**). Next, we monitored miRNA primary transcripts (pri-miRNAs), which are very short-lived, since are immediately processed by the microprocessor complex (Du et al. 2015). Indeed, we found they were efficiently labeled even at early time points (15'-30'), reaching maximal incorporation rate after 1-2 hours (**Figure 14-MIDDLE PANEL**). In most cases, we could get even a complete incorporation of pri-miRNAs (almost 100%), suggesting that 4sU incorporation works very efficiently. Finally, we measured labeling of mature miRNAs, including those miRNAs coming from the previously-mentioned primary transcripts plus other species. Overall, mature miRNAs were poorly labeled, in particular if compared to mRNA and pri-miRNAs, which is in line with previous observations claiming that miRNAs are much stable RNA species compared to mRNAs. The maximum rate of incorporation (<8%, **-Figure 14-RIGHT PANEL**) is reached at 2-3 hours of 4sU pulse. Although limited, such labeling rate could be sufficient to chase labeled species over time and measure miRNA degradation dynamics.

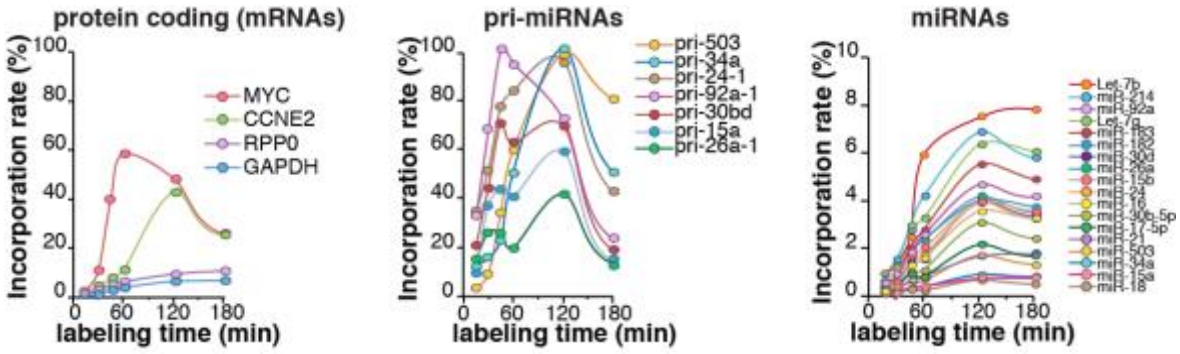

Figure 14. The labeling of different RNA species along the continuous 4sU pulse. Results are shown as 4sU incorporation rate and calculated as 4sU labeled over total RNA. Accordingly, RT-qPCR qPCR results were normalized by the yield of 4sU labeled RNA at each time point. **LEFT PANEL**. The plot shows incorporation dynamics of protein coding genes (mRNAs), including two unstable (ccne2 and myc) and two relatively stable genes (rpp0 and gapdh). **MIDDLE PANEL**. Incorporation rate of miRNA primary transcripts (pri-miRNAs- a list of complete primes could be found in material and method). **RIGHT PANEL**. Incorporation rate of mature miRNAs (miRNAs), as quantified by miScript Primer Assays (Qiagen). MiRNAs in the legend are ordered according to their labeling rate.

We sought to verify that 3 hours are compatible with the entire process of miRNA maturation, which requires of primary transcripts (pri-miRNAs, which are quickly labeled) to be processed by

the microprocessor (DROSHA/DGCR8) to produce the precursor hairpin molecule (PRE-miRNA), exported to the cytoplasm, further processed by DICER/TRBP complex and finally loaded on ARGONAUTE proteins (Ago), forming the miRISC complex. Indeed, it is unclear how much time is required for the entire process to happen in mammalian cells. Thus, we set up an experiment to verify if 3 hours could be enough to complete all the miRNA biogenetic steps, from transcription to loading onto the RISC complex. We exploited a lentiviral inducible expression system (pSLIK-Neo-TGmiR.Gβ2 **Figure 15-UPPER PANEL**), to induce the expression of two miRNAs, namely miR-34a, which had a low incorporation rate, and miR-182, which had a high incorporation rate and expected to be rapidly turned over, as previously shown (Krol et al. 2010a). We infected 3T9 cells with pSLIK-Neo-pri-miR34a and pSLIK-Neo-pri-miR182, respectively, and measured primary transcripts and mature miRNAs at three different time points (3-8-11 hours) after doxycycline treatment. A significant increase in miRNA levels started to be detected early for both miRNAs, already at 3 hours post induction (**Figure 15-LOWER PANEL**).

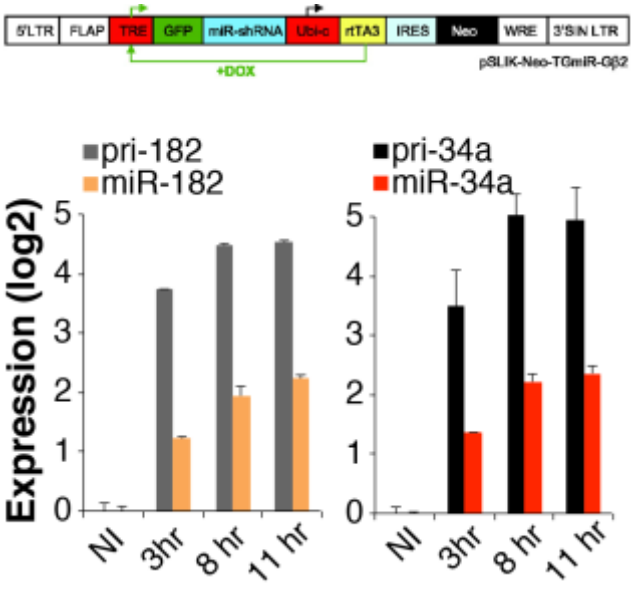

Figure 15. Pri-miRNA inducible vectors for exogenous expression of miR-34a and miR-182. **UPPER PANEL**- A lentiviral Tet-inducible expression system (pSLIK-neo) has been used to exogenously induce miRNA expression. After infection and selection with neomycin (750 μg/mL), miRNA expression has been induced for 3, 8, 11 hours with doxycycline (doxy, 2 μg/ml). **LOWER PANEL**- Levels of miR-182 and miR-34a precursors and mature miRNAs were evaluated by RT-qPCR. The plot shows log2 fold changes (average and st.dev. of two independent experiments) calculated over not-induced cells (NI)

To be sure that the newly produced miRNAs are effectively loaded on AGO complex, we performed AGO2 RNA Immunoprecipitation (AGO-RIP - **Figure 16)**. The isolation of AGO2 was checked by western blot, resulting in specific pull-down of the protein of interest **(Figure 17 –**

LEFT PANEL). Next, we extracted total RNA from AGO2 pull-down and measured the expression of miR-34a by quantitative PCR in control cells and at 3h upon miR-34a. We observed a 1-fold increase in miR-34a loading, an amount that mirrors precisely the increment of mature miRNAs (1-fold) due to exogenous pri-miRs vector expression (**Figure 17 – MIDDLE PANEL**). Importantly, the efficiency of Ago2-RIP was the same in control and induced cells, as no differences in loading were observed for unrelated microRNA (miR-21 and let-7b, **Figure 17 – RIGHT PANEL**). Based on the above-mentioned results, we established that 3 hours of 4sU treatment was sufficient to label mature miRNA molecules and compatible with the entire biogenesis of miRNAs.

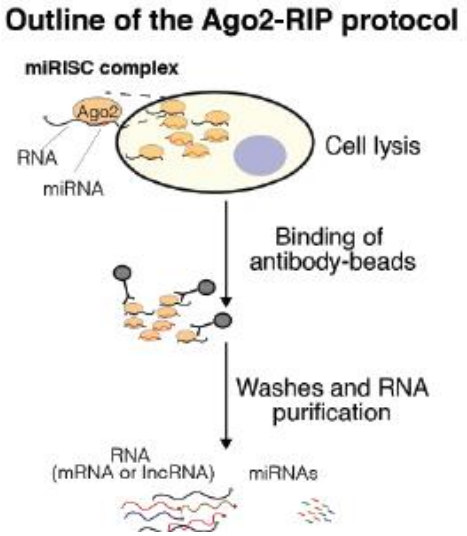

Figure 16. Scheme of AGO2 RNA immunoprecipitation. AGO2 was immunoprecipitated upon lysis of 10^6 3T9 cells. RNA extracted from from AGO2 pull-down was analyzed to RT-qPCR to measure miRNAs loading on AGO2.

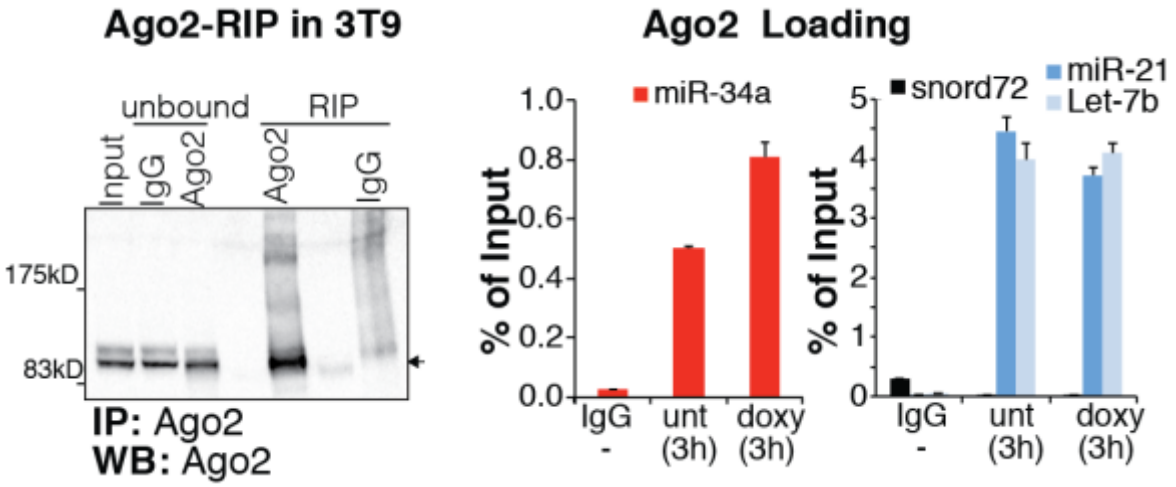

Figure 17.AGO2-RIP reveals miRNAs are loaded after 3 hour of pri-miRNA induction. **LEFT PANEL**. The specificity of the RIP has been evaluated by western blot using anti-Ago2 (Sigma Aldrich, SAB4800048) antibody. Ago2 protein is visible just in the RIP performed using Ago2 antibody and not with the unrelated (IgG) antibody. **MIDDLE PANEL**. Increase in total miR-34a and Ago2 loaded miR-34a was observed, meaning that after 3 hours newly synthetized

miRNAs are efficiently loaded on the Ago. **PANEL RIGHT**. MiR-21 and let-7b were used as positive controls, while snord72 served as negative control for the RIP.

4.1.2. 4sU-incorporation and cell viability

Having set the time and the dose necessary for miRNA labeling, we decided to verify whether our conditions are compatible with the cell phisiology. Indeed, high levels of 4sU nucleotide could induce transcriptional stress and RNA degradation and, as a secondary effects reduced proliferation (Dolken et al. 2008); (Burger et al. 2013). Therefore, we tested the possibility of 4sU toxicity at the dose set for miRNA labeling (300 uM for 3 hours). We initially measured cell proliferation rate upon 4sU treatment by counting cell numbers (in triplicates) both at 24hr and 32hr after seeding, measuring cell doubling time. We did not found any differences in cells proliferation by comparing treated to not-treated cells (Figure 18- **UPPER PANEL**). We also verified that 4sU did not alter the distribution of cell population in different cell-cycle phases. To investigate this aspect, we performed a Propidium Iodide (PI) profiling in cells with or without 4sU treatment (same as above). We did not find any significant differences in FACS-sorted cell population across different cell cycle stages (Figure 18-**LOWER PANEL**).

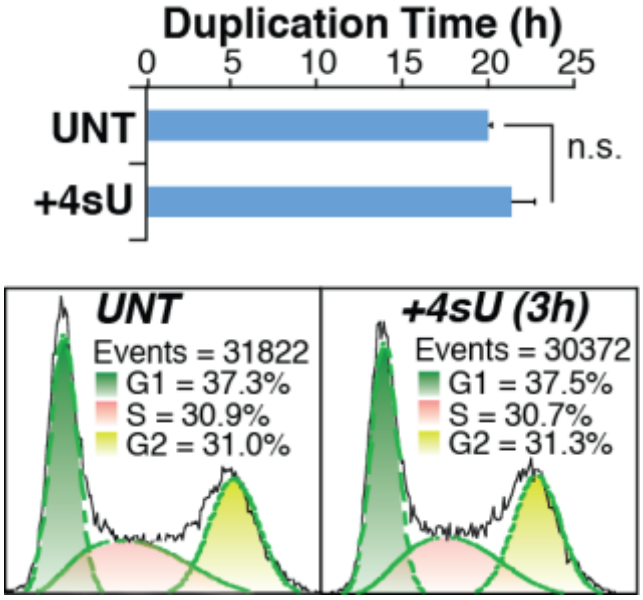

Figure 18 Effect of 4sU incorporation on cell cycle - Cell proliferation has been evaluated by calculating the duplication time (upper panel) and cell cycle profile (lower panel) of 3T9 cells upon 4sU treatment. **UPPER PANEL** Cell duplication time has been measured by counting cells at different time points (0-8-24 hours). Shown is the average with the s.e.m. of three experiments. **LOWER PANEL** - The cell cycle profile of control (Untreated – UNT) and 4sU treated (4sU) cells has been analyzed by FACS (MACSQuant Analyser-Miltenyi) using Propidium Iodide (PI) staining. Shown is the distribution in the G1, S and G2/M phase of the cell cycle in one representative experiment. No significant differences were observed.

We next move to check for 4sU induced transcriptional stress. An hallmark of such effect is the massive destabilization of nucleolar structure, which leads to incomplete transcription and degradation of ribosomal RNA (Burger et al. 2013). Therefore, we looked at the nucleoli structure and the integrity of rRNA in 3T9 cells upon treatment. Immunostaining with nucleolar marker (anti-Nucleolin Ab) revealed unaltered nucleolar structure with no spread signals (**Figure 19 - UPPER PANEL**). Accordingly, electrophoresis analysis of total RNA extracted from cells that were either i) treated with 4sU, or ii) treated and chased for 8 hours, revealed no signs of degradation in ribosomal RNA (rRNA) (**Figure 19 - LOWER PANEL**).

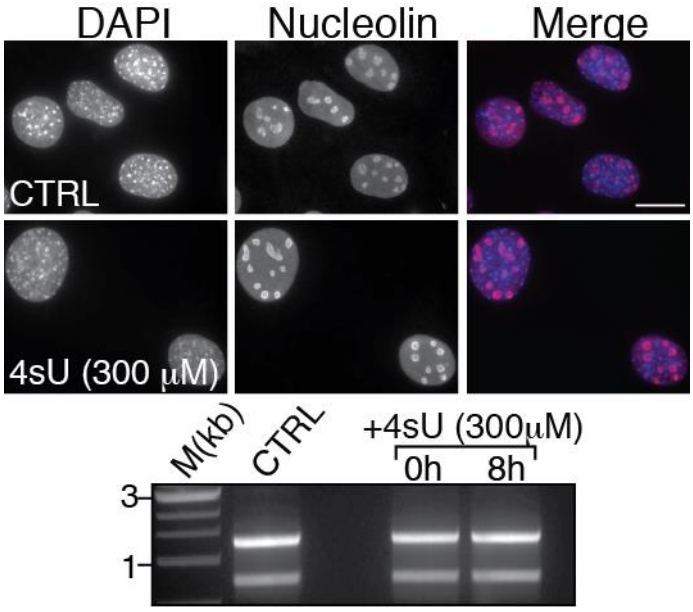

Figure 19. Effect of 4sU treatment on RNA metabolism. Effects of 4sU treatment have been evaluated directly analyzing the morphology of nucleoli by immunofluorescence with anti-Nucleolin staining (Abcam, ab50279), a marker of nucleoli. The integrity of ribosomal RNA (rRNA) after 3hrs of treatment of with 4sU (0h) and 8 hours upon wash out (8h) has been also verified by gel electrophoresis. No differences were observed in treated samples as compared with untreated controls.

4.1.3. 4sU-isolation technical variability

A relevant technical issue is to assess the reproducibility of 4sU extraction protocol and evaluate the impact on yield and purity of samples. Hence, we replicated four times the isolation of 4sU RNA using independent samples, all treated with same 4sU concentration for 3h. As shown in **Figure 20**, no major differences were found between replicates. A final issue regards the purity of the 4sU RNA we extracted, which impact on miRNA half-life measurement (in fact it determines

the background level that should be subtracted to each sample signal). To test the purity, we performed 4sU extraction from a negative control (i.e. a sample not treated with 4sU), which allowed us to set the background level and calculate the sample purity (>97%).

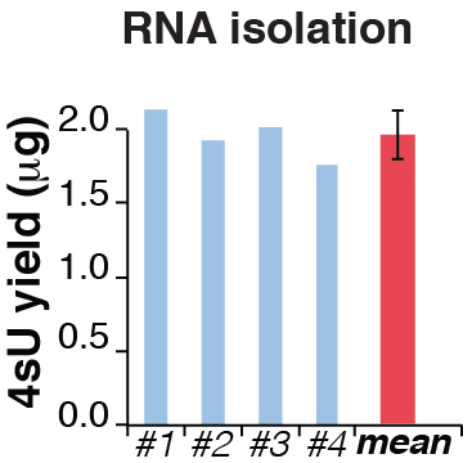

Figure 20. Reproducibility of 4sU extraction. The isolation of 4sU RNA has been repeated four times starting from the same RNA (40 ug, from cells with 3hrs of labeling) to evaluate the technical variability of the procedure. A red bar shows the mean with the s.e.m.

4.1.4 Differences of using HDPD-Biotin or MST-Biotin-XX chemistry for biotinylation reaction

It has been recently reported by Matthew Simon's group that pull down of short 4sU labeled RNA by HDPD-Biotin could be poorly efficient (Duffy et al. 2015). Authors claimed that biotinylation of the sulfhydryl group with a different chemistry, namely MST-Biotin-XX, is more efficient. This contention has some consequences for our purpose, implying that with HDPD-chemistry we had i) a longer biotinylation time (3 hours for HDPD-Biotin, 30' for MST-Biotin-XX); ii) very inefficient pull down of miRNAs harboring few uridines; and iii) a globally low 4sU yield.

We sought to verify this in exponentially growing 3T9 cells, directly comparing the two chemistries. We performed parallel extractions with the two methods using as input total RNA from the same samples (PULSE – 300uM at different time points). As showed in **Figure 21**, MST-Biotin XX provides an apparent increase of the yield in terms of purified 4sU-RNA, but negative control (4sU untreated) revealed that, at least in part, this was due to a reduced purity. Overall, the purity of HDPD method was >10 times better than MTS-biotin. Hence, the increase in yield is limited.

TOTAL EXTRACTION YIELD

Time	HDPD-Biotin (ng)	MST-Biotin-XX (ng)
15'	756	7980
30'	3374	8736
45'	5768	11900
60'	10640	12236
90'	11270	10164
NEG	148	4200

Figure 21. Extraction yield of MST-Biotin-XX and HDPD-Biotin methods. Exposed are the different yield of 4sU extraction based on the two methods. Yield are expressed as total ng. NEG shows yield of negative samples not treated with 4sU.

Next, we addressed the ability of recovering labeled miRNAs with various uridine numbers in their sequence. Overall, the two extraction methods provided comparable results in terms of miRNA enrichments (**Figure 22**). Focusing on uridine content, we did not observe any specific bias in miRNA recovery. As an extreme case, miR-214 which harbor just one uridine is efficiently extracted by both methods. As expected, the 4sU incorporation percentage results higher for MST-Biotin XX compared to HDPD-Biotin. This is due to the increased general yield observed for MST-Biotin (and related background) and do not reflect a better performance of the isolation method. Taken together, these data suggest that both methods are reliable, with different overall performance, and could be used for the efficient isolation of labeled miRNAs.

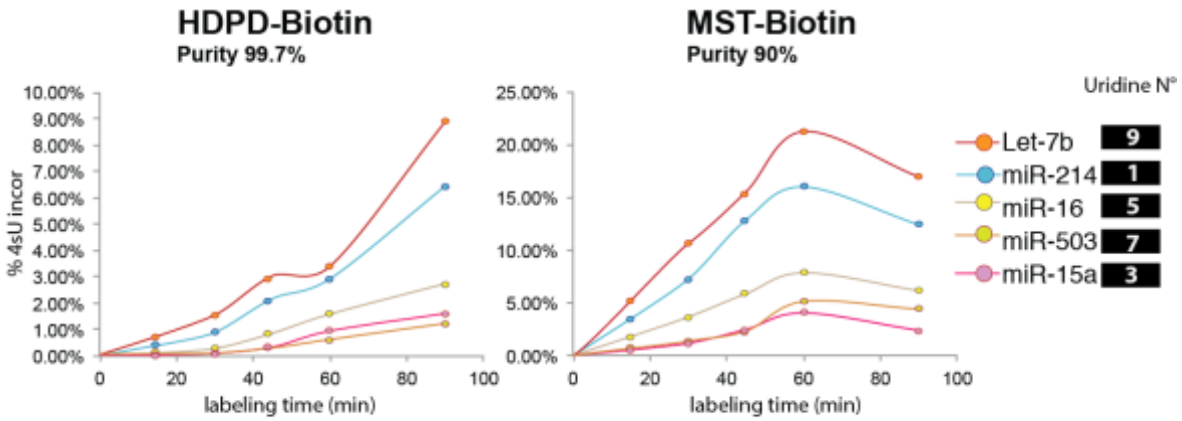

Figure 22. Comparison of HDPD-Biotin and MST-Biotin XX based method. Shown are percentages of 4sU incorporation starting from 40 ug of total RNA. miRNAs have been chosen depending on the uridine content number displayed close to the graph. 4sU incorporation were normalized on 4sU yield and amount of material loaded in qPCR runs.

4.1.5 Conclusions

In summary, we exploited 4sU as molecule for miRNAs labeling. In 3T9 murine fibroblasts, treatment of exponentially growing cells with 4sU at 300 uM for 3 hours was set as optimal for

miRNA labeling, as it does not perturb cellular metabolism and cell viability, is compatible with the entire biogenetic steps of miRNA generation, and allow the purification of labeled miRNAs with acceptable yield and good reproducibility and specificity. Overall, we observed that 4sU incorporation of mature miRNAs could vary, although is generally low, suggesting that these molecules are quite stable, in particular if compared to mRNAs, as previously said.

4.2. Measurement of microRNAs half-life through 4sU application

4.2.1 Pulse and Chase setting and preliminary data

Usually, pulse labeling of mRNA allows the indirect estimation of the half-life ($T_{1/2}$) by calculating newly transcribed-over-total RNA ratio (Dolken et al. 2008). As previously-mentioned, the complex biogenesis of mature miRNAs depends on multiple steps besides transcription, often regulated (for review see (Krol et al. 2010b)). If the contribution of miRNA maturation is not minimized, the calculation of half-lives is highly biased. To circumvent this issue, we developed a "pulse-chase" protocol (**Figure 23-LEFT PANEL**), in which miRNAs are labeled with 4sU (pulse) and then followed over time (chase) to measure the decrease of labeled molecules according to their intrinsic decay rates. Technically speaking, sub-confluent cells were treated with 300 uM 4sU for 3 hours to label miRNAs, the labeling was interrupted by replacing the medium with fresh one supplemented with 'cold' uridine (1000 uM final concentration) in order to wash out 4sU residues. At different time points (2h-4h-6h-8h-10h-12h-16h-24h-32h chasing time), RNA was purified to measure the decay of labeled molecules. **Figure 23- RIGHT PANEL** shows results on one representative experiment, with 4sU-RNA decreasing linearly and faster than cell division up to 12-16 hours of chasing, thus reflecting the degradation of total RNA. After 16h, 4sU-RNA recovery is too close to the negative control and with a slope similar to the simple dilution due to cell division.

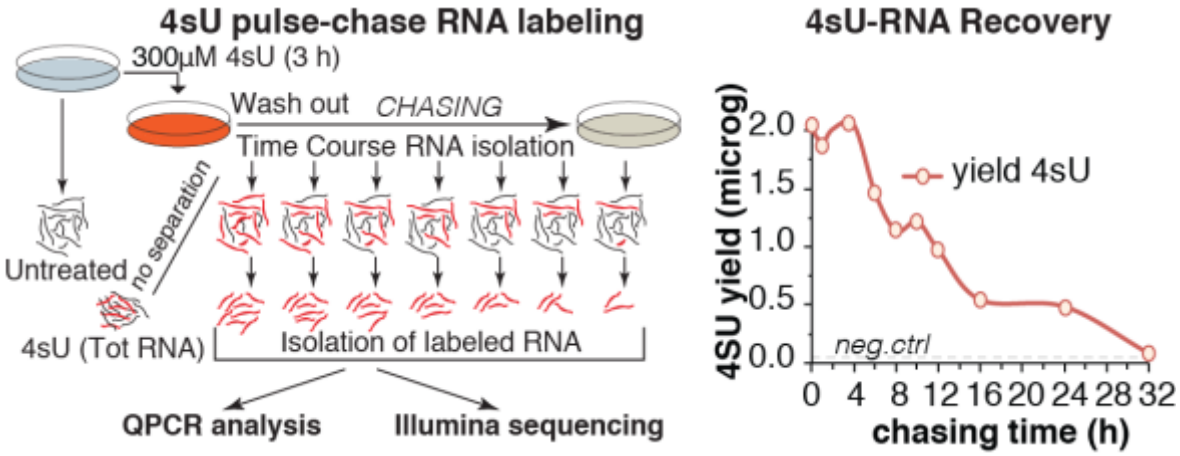

Figure 23. The pulse- chase approach to measure miRNA half-lives ($T_{1/2}$). **LEFT PANEL**- A scheme illustrates the experimental strategy of the 4sU pulse-chase approach used to follow miRNA decay dynamics. **RIGHT PANEL**- The yield of 4sU-RNA along the time course is reported. 40 µg of labeled total RNA were used at each time point. A dashed line marks the background level (yield of the negative control).

Thus, we used for the measurement of the half-lives ($T_{1/2}$) a fixed experimental window, comprising samples collected between 0 and 12 hours chasing-time. As validation, we measured the levels of different RNA species by RT-QPCR, fitted expression data derived from duplicate experiment linearly and calculated half-lives ($T_{1/2}$). R^2 of fitting and confidence interval were used to determine how well each tested RNA followed a linear decay. An example is shown below, (Figure 24), where the decay of c-Myc (using ActinB as reference) was calculated. The data fitted well (R^2>0.9) and the half-life was estimated less than 2 hours, in line with experimental observations made by others with independent approaches (Yang et al. 2003).

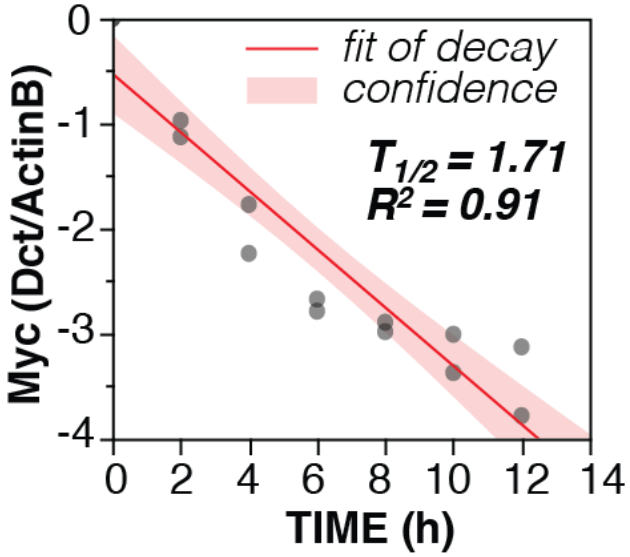

Figure 24. Example of fitting for half-life measurement. The half-life of Myc has been measured by RT-qPCR using the pulse-chase protocol according to a one-phase exponential fitting (N=2). Data were normalized on Actb levels, a highly stable gene (Yang et al. 2003)

For mRNAs and pri-miRNAs, we obtained half-lives of few hours, compatible with previous observations (Yang et al. 2003). As proof of concept, stable mRNAs (gapdh, ccne2) showed longer half-lives compared to less stable mRNAs (myc and pri-miRNAs) (**Figure 25-LEFT PANEL**). With this approach we could calculate half-lives of various miRNAs. Decay rates of mature miRNAs were heterogeneous, ranging from 3 to 24 hours. Of note, we exactly confirmed the short half-life of miR-503 ($T_{1/2}$=3.2hrs), which has been previously measured in growing fibroblasts by David Bartel's lab [$T_{1/2}$=3.6hrs, (Rissland et al. 2011)] (**Figure 25-RIGHT PANEL**).

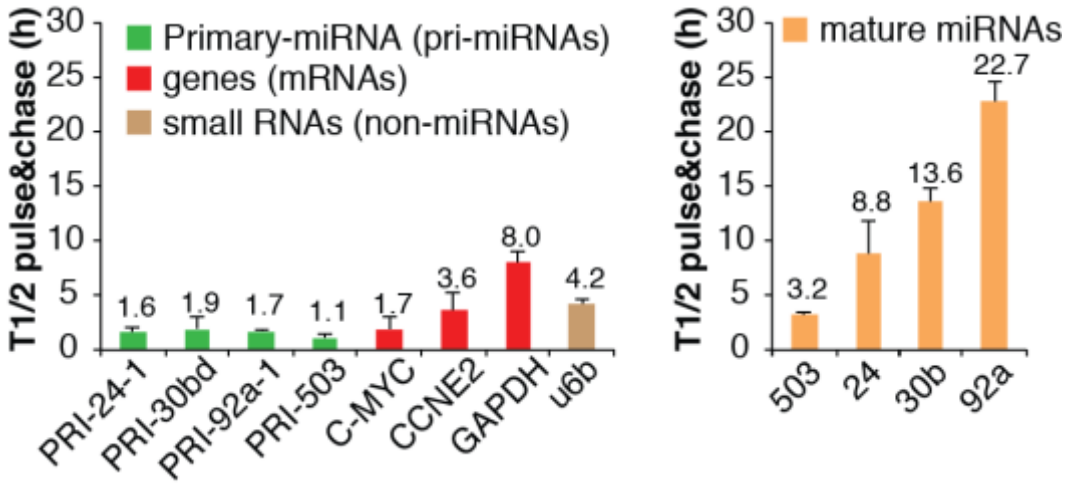

Figure 25. Half-life calculation for different RNA species. Half-lives of mRNAs, pri-miRNAs (**LEFT PANEL**) and small RNAs (**RIGHT PANEL**) were estimated as in *Figure 24*. Shown is the average and the s.e.m. of two independent experiments. Data of miRNAs were normalized on Snord72 levels, a highly stable short RNA.

We also compared half-life values measured through "pulse-chase" and "only-pulse" approaches, by calculating newly transcribed-over-total RNA ratios (Dolken et al. 2008). As expected, mRNAs and pri-miRNAs (red and green dots) showed very similar half-lives in the two methods (R^2=0.98, **Figure 26**). Conversely, the half-lives of miRNAs were profoundly different if calculated with the "only-pulse" and "pulse-chase" methods (correlation, R^2=0.10). According to the 'pulse', miR-503 would be an extremely stable miRNA ($T_{1/2}$ >24hrs), an assumption that does not hold true.

Hence, we concluded that "pulse-chase" approach is the only way to precisely determine miRNA decay rates.

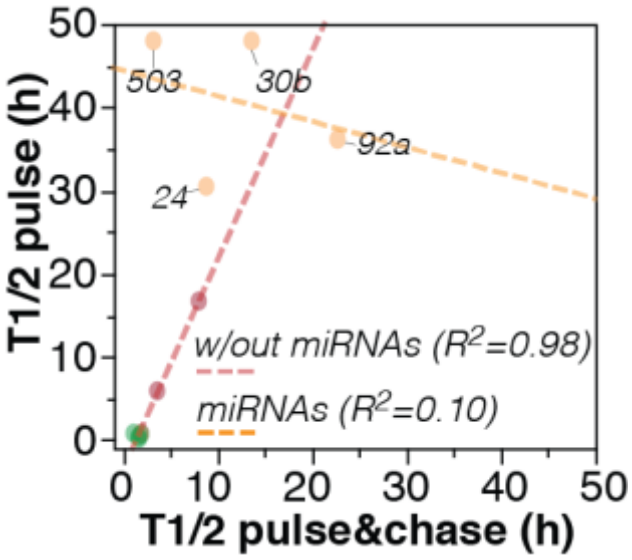

Figure 26. Comparison between "only ulse" and "pulse-chase" methods. Half-lives calculated using the pulse-chase were compared with those indirectly determined by 4sU labeling, as in (Dolken et al. 2008). A linear correlation has been calculated for mRNAs/pri-miRNAs (red dashed line) or miRNAs (yellow dashed line).

4.2.2. Genome-wide analysis of miRNA degradation rates in growing fibroblasts through Illumina sequencing

4.2.2.1 Small RNA sequencing, normalization and technical notes

To obtain a global picture of miRNA decays, we performed high-throughput sequencing (Illumina) using samples from three independent "pulse-chase" experiments. We produced a total of 21 libraries, using 4sU RNA isolated from 7 time points and 3 biological replicas, plus control libraries, including a negative control (background of 4sU purification) and libraries from total RNAs (untreated and 4sU treated). The last two controls confirmed that 4sU treatment does not affect the global level of miRNAs in the cell, as showed by the very high correlation observed by comparing miRNA expression (total reads) in untreated vs. 4sU treated RNA (R2=0.99, **Figure 27-LEFT PANEL**). From the pulse-chase experiments we obtained a total of 125 million reads that constitute the "decay dataset". The dataset was analyzed with the *IsomiRage* tool, a bioinformatics pipeline developed in our lab for the characterization and analysis of miRNAs and their variants in next-generation sequencing datasets (Muller et al. 2014) **Figure 27-RIGHT PANEL**). By analyzing raw expression data, we observed a gradual decrease of total reads along the time course. Since we prepared small RNA library starting from the same amount of materials (300 ng for each time point), this result suggests that the fraction of labelled miRNAs over the total pool of labelled species decreases during the time course. In other terms, miRNAs are less stable compared to other RNA species, most likely ribosomal RNA. Hence, it was not possible to normalize raw data by the size of the libraries, because this approach would have introduced a distortion in the analysis of miRNA decay. In fact, according to a library-size normalization many miRNAs would paradoxically increase their concentration over time.

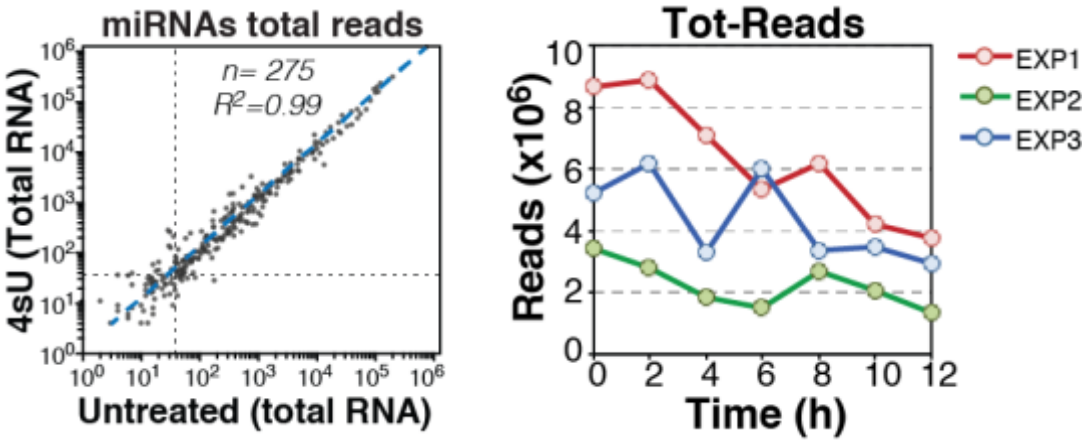

Figure 27. Analysis of miRNA reads from small-RNA libraries. **LEFT PANEL**- Effects of 4sU treatment on miRNA expression have been evaluated by small RNA sequencing (Illumina). Scatter plot shows expression of miRNAs (as reads in log10 scale) from control (untreated) and 4sU treated (4sU) samples. A total of 275 miRNAs were expressed above the threshold (>10reads, marked by gray dashed lines) and considered in the analysis. A blue dashed line highlights the linear correlation. The two samples are highly correlated (R^2= 0.99). **RIGHT PANEL**- The plots show the fluctuation of raw total reads (right) at each time-point in the three independent biological experiments that compose the decay dataset.

Thus, we decided to normalize decay libraries by an internal highly stable miRNA (T1/2 > 24 hours), abundant and ubiquitously expressed (**Figure 28 and Figure 25-RIGHT PANEL**). Such an internal reference has the advantage to normalize for biases deriving from 4sU dilution by cell division (specifically for fast-decaying miRNAs), different proliferation status of the cells (cells are in diverse metabolic states and, thus, 4sU incorporation might be difference) and possible biases in point-by-point 4sU extraction. Among the candidate miRNAs, we used miR-92a-3p as internal reference as it has been observed as long lasting miRNAs in the preliminary RT-QPCR analysis and for which we had confirmation of the very high stability in mammalian cells from knock-out model (Ventura's lab, personal communication).

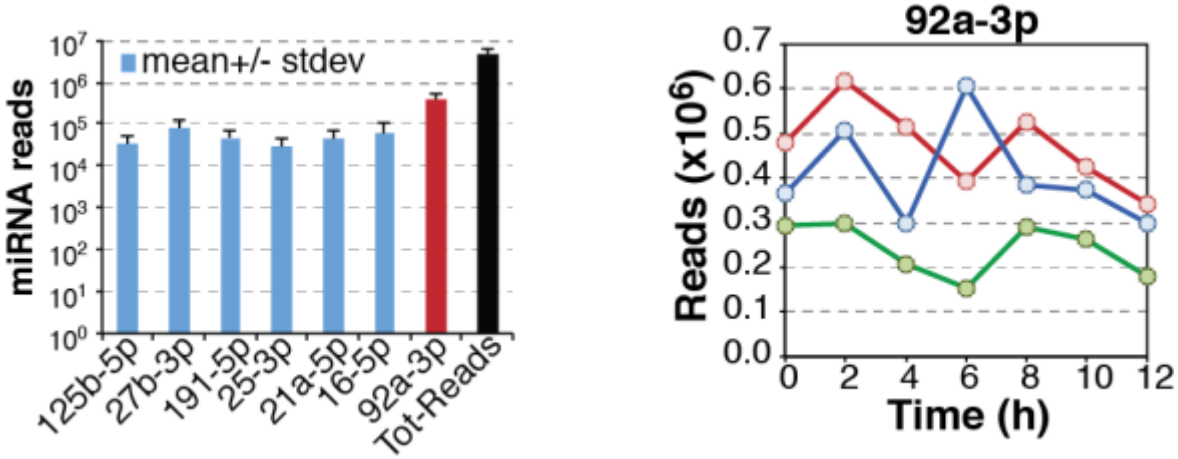

Figure 28. miR-92a-3p expression in small-RNA libraries. **LEFT PANEL** -Average read counts (N=3) for the most stable miRNAs in the decay dataset. MiR-92a-3p is marked in red while reads for all miRNAs (library size) are marked

in black. **RIGHT PANEL** - The plots show the fluctuation of miR-92a-3p total reads (right) at each time-point in the three independent biological experiments that compose the decay dataset.

Nevertheless, to demonstrate normalization consistency, we further selected 5 miRNAs that showed similar characteristics compared to miR-92a, in terms of stability and expression (mir-27b-3p, miR-191-5p, miR-25-3p, miR-21a-5p, miR-16-5p, **Figure 28-LEFT PANEL**). We normalized the libraries either on each single miRNA or the sum of all and we observed no significance differences on final data compared to the alternative normalization protocols (**Figure 29**).

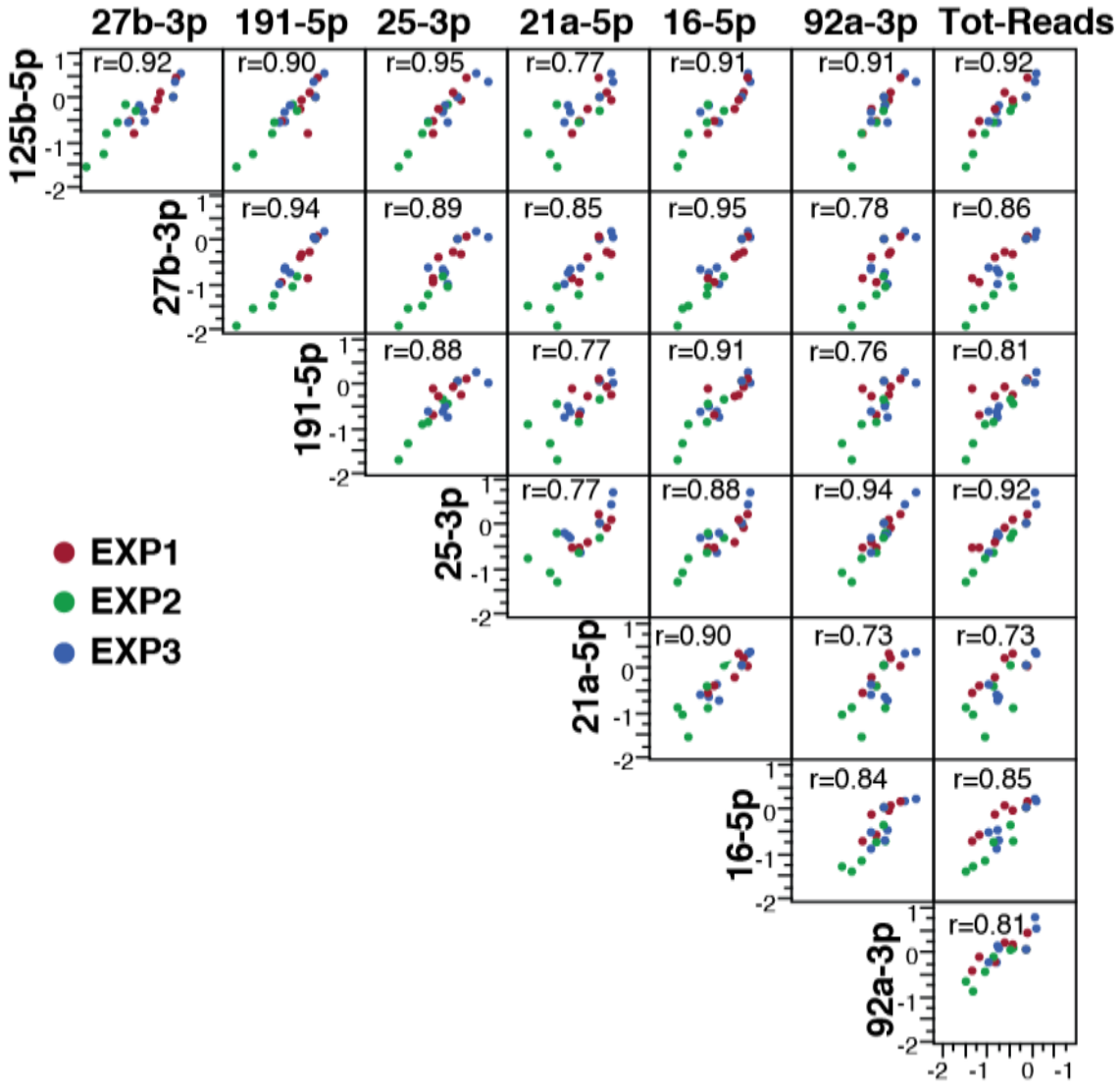

Figure 29. Correlation analysis between different normalization strategies. Each dot represents the log2 ratio of the time-points over the 0 hrs in each experimental set, while different experiments are marked with different colors.

As further control, we looked for major biases as a consequence of the purification protocol, due to miRNA length or base composition (with particular respect to Uridine number). We plotted the

miRNA incorporation ratio (miRNAs reads in 4sU-fraction/miRNA reads in total expression) against miRNAs length and nucleotides composition (**Figure 30**). Globally, neither of the two could affect significantly 4sU incorporation and small RNA sequencing results, confirming the consistency and reliability of the purification method.

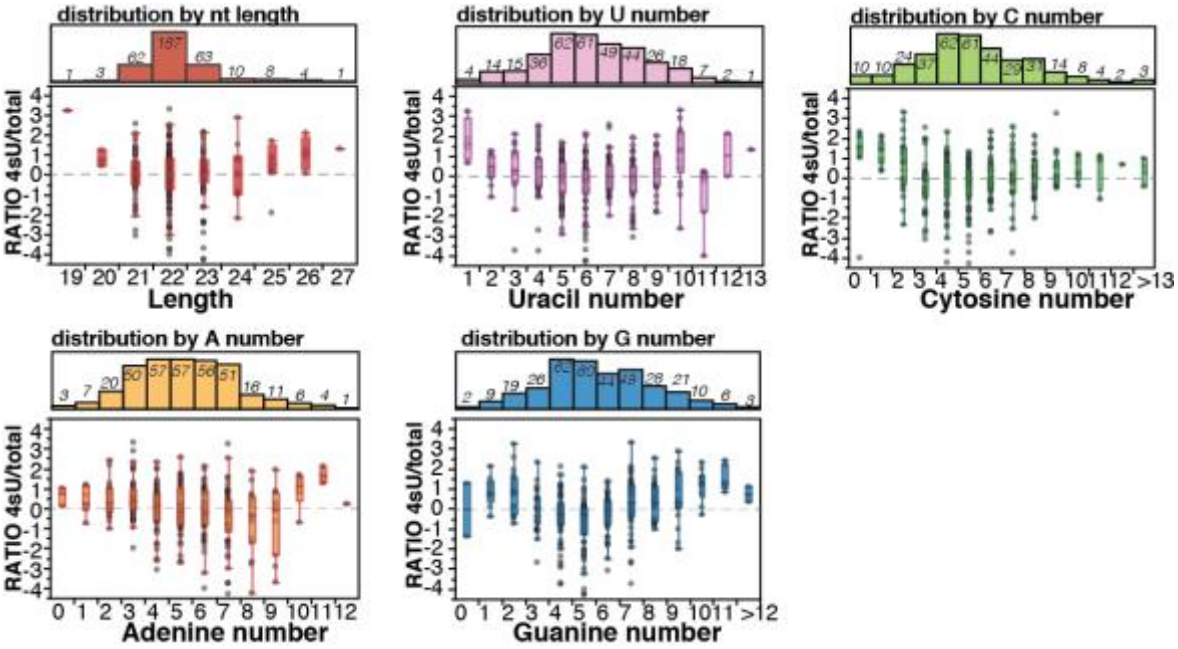

Figure 30. The nucleotide composition and the length of miRNAs sequencing. Analysis of nucleotide composition and length of miRNAs respect to 4sU incorporation levels. Each box plot shows the 4sU incorporation rate [i.e. ratio of raw reads obtained by 4sU RNA libraries (0h, N=3) as compared to total RNA (UNT + 4sU treated, N=2)] according to miRNA length or the number of Uridine, Cytosine, Adenine, Guanosine. No biases in miRNA length or base composition (with particular respect to Uridine number) were observed as consequence of the labeling and purification procedure.

4.2.2.2. Degradation rates of miRNAs in growing cells

After normalization, we moved to calculate miRNA degradation rates. We set a threshold of expression along the entire time-course (>10 reads) to select only those miRNAs reasonably expressed in the system and for which it is possible to mathematically infer half-lives. We retrieved data for 564 species (canonical miRNAs and variants). We focused on canonical miRNAs (186 species, see Table 1) and calculated half-lives of miRNAs assuming a one-phase exponential decay, fitting on the average of three independent biological replicas ($T1/2_{ave}$) with 95% confidence intervals ($T1/2_{min}$ and $T1/2_{max}$) for the best-fit. **Figure 31** shows two representative examples of fitting, with points indicating individual data of time points in each replicate experiment. According to the fitting, miR-182-5p has a fast turnover, as previously shown in neuronal cells (Krol et al. 2010a), with an half-life ($T1/2_{ave}$) of 7 hours, while miR-25-5p displays a more stable

behavior, with an half-life ($T1/2_{ave}$) of 20 hours. In all cases, we found that a simple one-phase exponential decay model fitted the data better than more complex models, such as a two-phase-decay, arguing against the existence of multiple pools of the same miRNA with different stability within the cell.

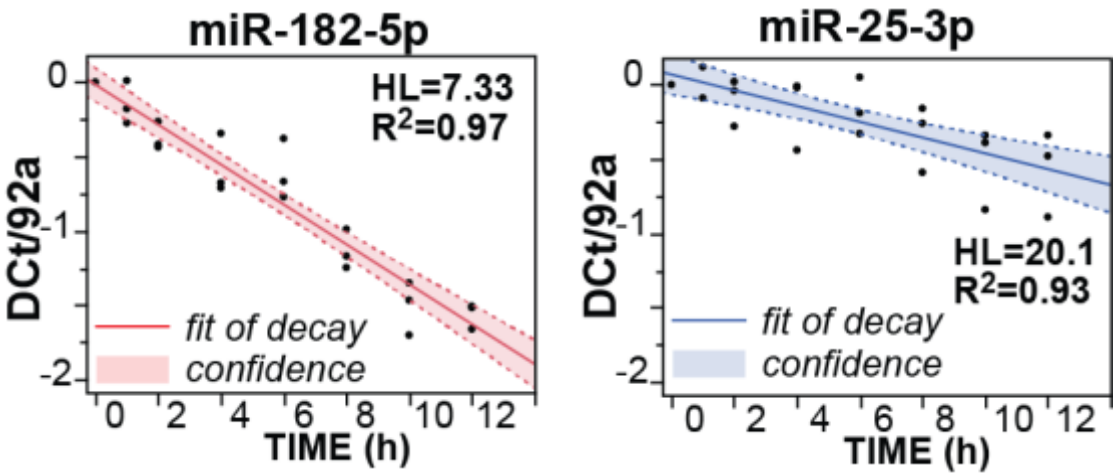

Figure 31. Examples of fitting for measurement of miRNA half-life. Shown are examples of fitting from three replicas for miR-182-5p and miR-25-3p which have fast and slow decay properties, respectively. Red and blue line show the linear fitting and R^2 have been calculated for information about the quality of the fitting. The highlighted area displays the confidence interval.

Looking at the distribution of half-life values (shown in **Figure 32**), we found they are quite heterogeneous. Such distribution has a bimodal shape, with many canonical miRNAs (57/186, 30.6%) showing half-lives >1day and behaving as very stable molecules, consistent with previous reports (Ruegger and Grosshans 2012). Nonetheless, a peak in the distribution is centered on 12h, with 61 miRNAs (32.8%) with a relatively short decay (T1/2<12h) and some of them quickly disappearing (T1/2<8h; N=28) (**Figure 32-LEFT PANEL**). It is important mentioning that the time-points used for half-life determination are between 0 and 12 hours. Accordingly, half-lives calculation is more precise for those species that are quickly disappearing (HL <12hr) than of those with a slow turnover. As a result, the accuracy of half-life measurement is directly related to the decay behavior of the molecule. This is clearly showed by plotting the average of the confidence intervals for each half-life values as in **Figure 32- RIGHT PANEL**, where the margin of error of miRNAs with high half-life (blue dots) is larger compared to those that decay within 12 hour. For some miRNAs, the turnover is so slow that the half-life could not be precisely fitted (the labeled molecules remained almost the same in the time course) and, hence, it was arbitrary set as ≥ 48h.

Based on this distribution of half-lives (**Figure 32**), we could formally categorize miRNAs into two three classes:

- **A "fast" decay group (N=42**, marked in red**)**, which contain miRNAs with $T1/2_{ave}$<14hrs and $T1/2_{max}$<20 hrs;
- **A "slow" decay group (N=40,** marked in blue**)**, which contains miRNAs with $T1/2_{ave}$>24hrs and $T1/2_{min}$>15hrs.
- The remainder of miRNAs, defined as **"other" group (N=107).**

The classes were defined in a way that the "fast" and the "slow" group do not overlap. Many of the analyses showed in this thesis will refer to these decay groups.

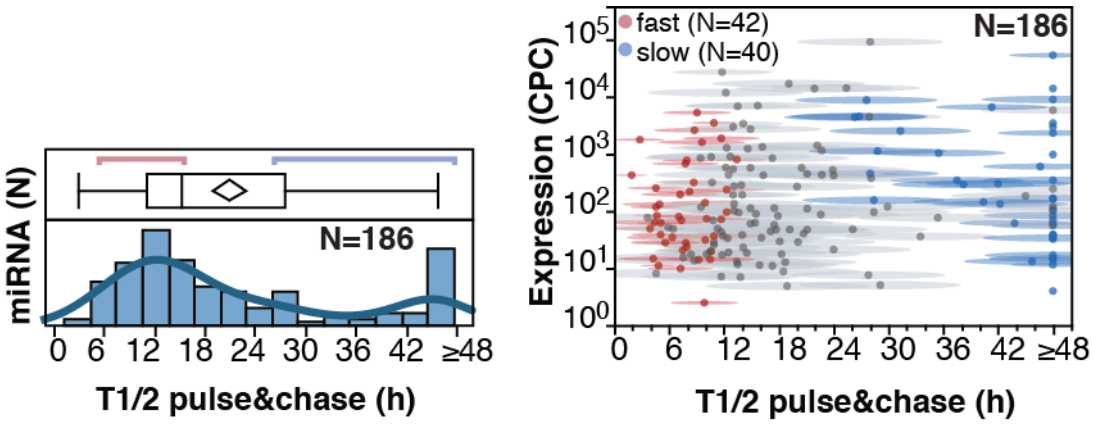

Figure 32. Distribution of measured miRNA half-lives. **LEFT PANEL-**Red and blue lines mark boundaries of fast- and slow-decaying species. **RIGHT PANEL** -Half-lives (mean with confidence interval) are plotted against miRNAs expression (copies per cell, CPC).

4.2.2.3. Decay of guide and passenger miRNAs

Each miRNA hairpin could generate two mature miRNAs. Typically just one of the two molecules is preferentially retained onto the RISC complex, termed as "guide" miRNA, while the other (called the "passenger" miRNA) is released in the cytosol and quickly degraded (Krol et al. 2010b). As consequence, just the guide miRNA accumulates in the cell, while the passenger miRNA is poorly expressed. We speculated that "passenger" miRNAs should have a 'fast' decay and, more generally, should decay faster than their cognate guide miRNA. We retrieved guide and passenger miRNAs in the decay dataset (**Figure 33-LEFT PANEL**), as defined by the miRNA database (miRbase 21) and with very different expression expression (the guide is much more expressed then the passenger). In a few cases (n=7) expression of the two species were roughly the same (ambiguous forms in **Figure 33-LEFT PANEL**), meaning that there is no a preferential strand

selection for that particular hairpin. In total we could identify 44 guide/passenger pairs. When we looked at the distribution of half-lives, we found that passenger miRNAs were actually decaying fast (average 12h), in particular when compared to their paired "guide" miRNAs (p-value <0.0004, **Figure 33-RIGHT PANEL**).

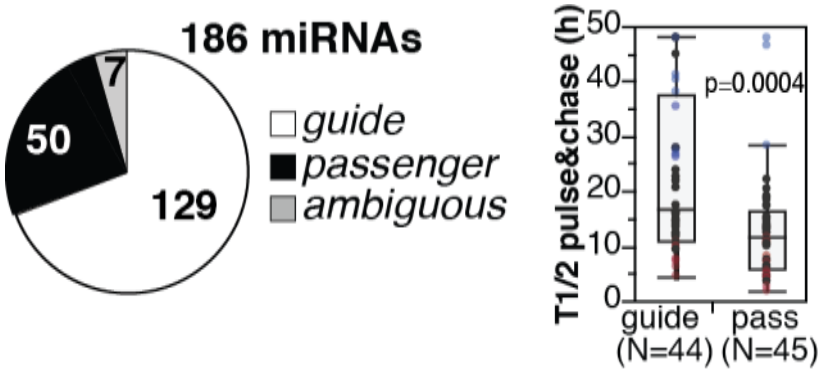

Figure 33. Guide and passenger miRNA in the decay dataset. **LEFT PANEL-** Canonical miRNA species analyzed in the "decay datasets", distinguished into guide and passenger miRNAs, according to miRbase and Targetscan databases. **RIGHT PANEL-** Box plot shows the distribution of half-lives for matched guide and passenger species. P-value (Wilcoxon-test) is shown.

We argued that the heterogonous behavior of miRNA decay, with two opposing classes (fast and slow), could be just dependent on the presence of guide and passenger miRNAs in the dataset. Indeed, for passenger miRNAs the 'fast' turnover behavior depends on their biogenesis rather than a decay mechanism (they are simply poorly loaded on Ago). Focusing on the "guide" miRNAs (N=129), we could still distinguish the two opposing behavior. The heatmap in **Figure 34** shows two groups, i) one composed of miRNAs with "fast" (N=25) decay with half-lives ranging from 4 to 14 and that, in a reproducible manner, quickly disappear in the pulse-chase time course, opposed to ii) a "slow" decaying group of miRNAs (N=32), with half-lives ranging from 24 to ≥48

hours, which are stable in the time-course, almost unaffected (**Figure** 34**).**

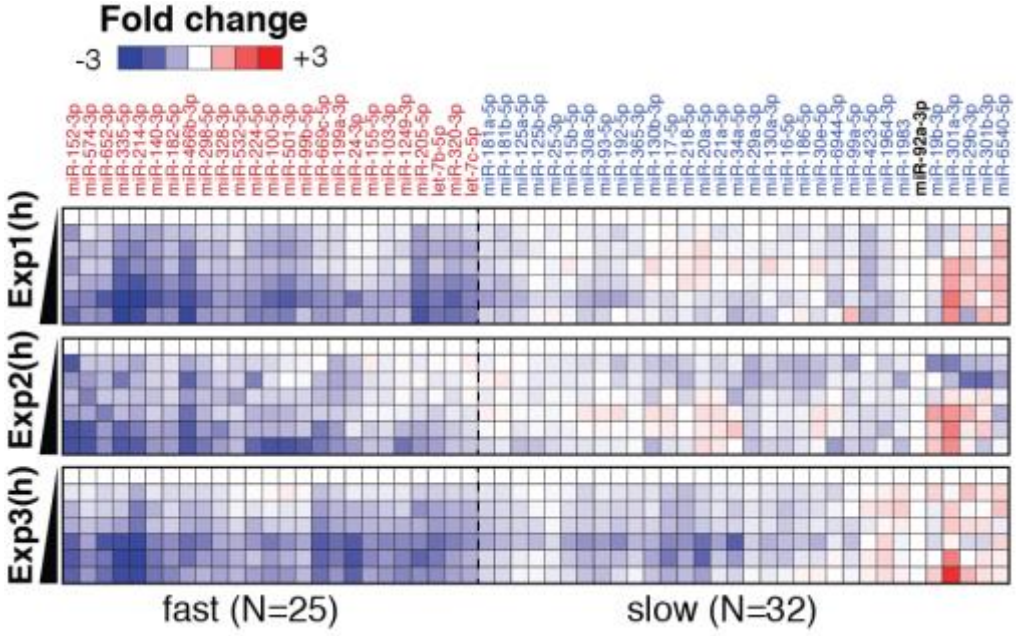

Figure 34. Degradation dynamics of miRNAs. Fast (N=25, T1/2<14h) and slow (N=32, T1/2>24h) guide miRNAs are shown along the time-courses. Data were normalized on miR-92a-3p and reported as log_2 fold change (over the 0 hrs time-point).

Importantly, when we looked at the loading on Ago2, the 'fast' and the 'slow' groups displayed a very similar loading, suggesting that the different decay is an intrinsic property of the miRNA, not related to their loading efficiency (**Figure 69**Based on these results, we could conclude that miRNA decay are heterogeneous, and fast turnover is not just an exception of few species (i.e. miR-182-5p or miR-503), but an intrinsic properties of a consistent group of miRNAs.

4.2.2.4. Analysis of decay dynamics with miRNA genomic and functional proprieties

We investigated the relationship between miRNA decay and their genomic or functional organization. MiRNA genes could be distinguished based on their genomic organization as 'intronic', which are located within introns of the 'host' protein coding genes and share the transcriptional regulation; and 'intergenic' miRNAs, which constitute an independent transitional unit. We found that half-lives were not different for miRNAs in intergenic regions as compared to those within introns of coding genes (**Figure 35-LEFT PANEL**); moreover, they were not influenced by any specific chromosomal location (**Figure 35-RIGHT PANEL**).

Next, we asked whether other functional properties of miRNAs (transcriptional and functional organization) are associated with miRNA turnover. About half of the miRNAs in mammals are organized in polycistronic transcriptional unit (miRNA clusters) and share common transcriptional

regulation. In most instances, miRNAs belonging to the same transcriptional cluster show a similar decay (25/33 coherent clusters; **Figure 36-LEFT PANEL**), suggesting that transcription and decay might be coupled. We, then, looked at those miRNAs belonging to the same miRNA family, which share sequence and functional similarities. Also in this case, related miRNAs showed a coherent behavior in decay rates (10/17 coherent families, **Figure 36-RIGHT PANEL**). We have to point out that clusters and families are often overlapped each other and, indeed, clusters with similar half-life contains families with coherent half-lives too.

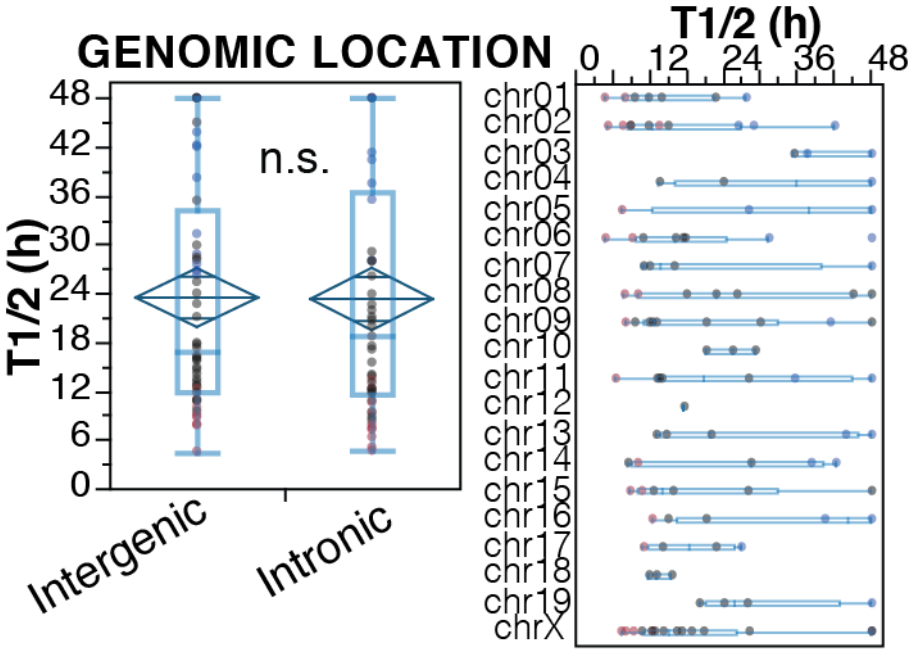

Figure 35. miRNA genomic features and half-lives. **LEFT PANEL**- the distribution of half-lives for intergenic vs. intronic guide miRNAs (N=129) is shown (p=0.7488, Wilcoxon-test). **RIGHT PANEL**- miRNA half-lives are reported according to chromosome location of miRNA loci.

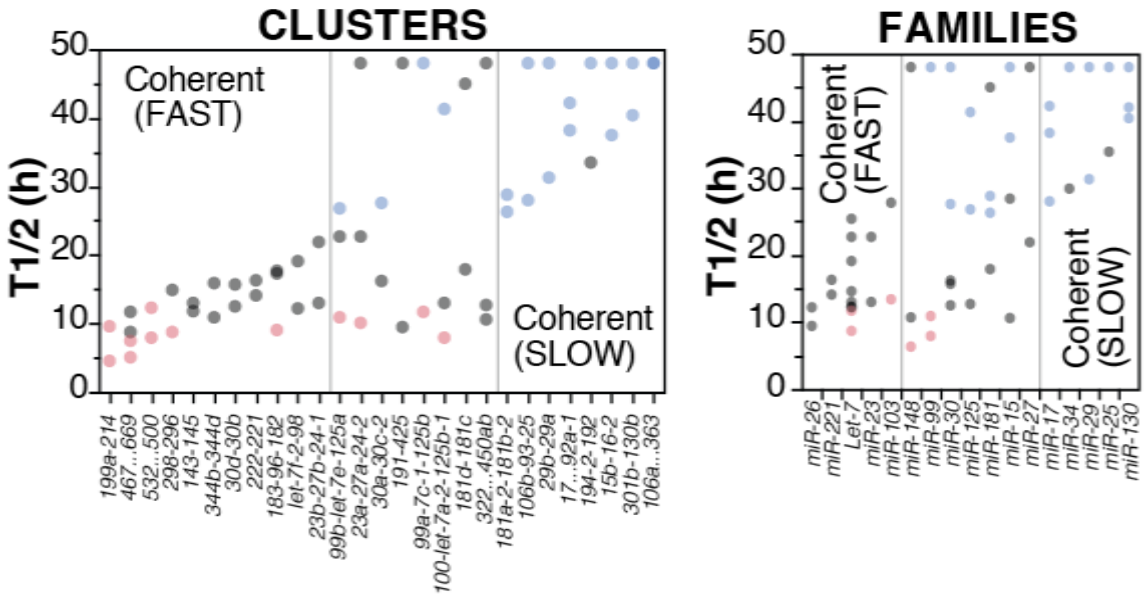

Figure 36. Clusters, families and decay. MiRNAs belonging to the same transcriptional unit (cluster) or sequence similarity group (family), according to miRBase 21, were analyzed. Clusters (**LEFT PANEL**) and families (**RIGHT PANEL**) with coherent behavior (differences in $T_{1/2}$ <12hrs) are highlighted. A color code indicates miRNA decay class (red, 'fast'; blue, 'slow')

4.2.2.5. 4sU labeling is a read out of miRNA stability in human BJ fibroblast and HeLa cells

Although 4sU incorporation could not be used to determine miRNA degradation dynamics (see **Figure 26**), we speculated that difference in 4sU incorporation might somehow reflect difference in decay behavior. In particular, as the percentage molecules labeled with 4sU depends on both the number of newly synthetized molecules and how quickly the old molecules are cleared, we reasoned that 'fast' turnover could be associated to increased 4sU labeling. Globally, we found that fast-decaying miRNAs significantly incorporate more 4sU compared to slow-decaying miRNAs ($p<0.0001$, **Figure 37-LEFT PANEL**) By distinguishing miRNAs into quartiles according the 4sU incorporation rate, we found a remarkable reciprocal relationship (**Figure 37-RIGHT PANEL**, $p<0.0001$ contingency test), whereby miRNAs displaying a very high incorporation rate (1^{st} quartile of the distribution in **Figure 37-LEFT PANEL**) were strongly enriched in 'fast' species, while those with a very low incorporation rate (last quartile of the distribution; <3% 4sU) were enriched for 'slow' miRNAs. A bivariate analysis directly comparing 4sU incorporation rate (Y) with miRNA half-lives (x), confirmed an inverse relation, which could be formally expressed as $Y = f(\frac{1}{x})$ (**Figure 38**).

Overall, these results suggested that miRNA incorporation rates, even if could not allow the determination of miRNA half-lives, could serve as a proxy to qualitatively infer turnover rates of miRNAs in a given biological system.

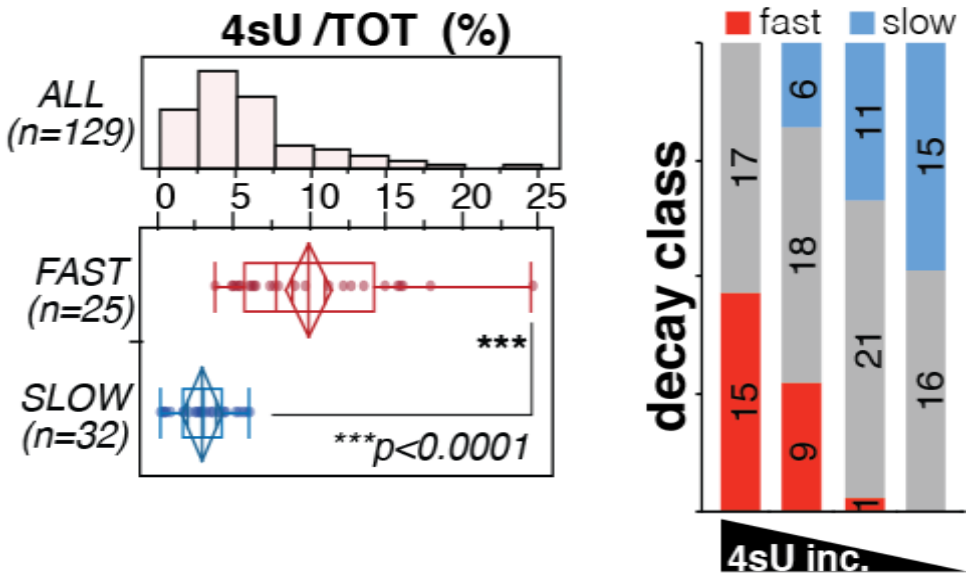

Figure 37. 4sU incorporation of miRNAs has been correlated to decay. **LEFT PANEL**-The histogram shows the distribution of incorporation rates of guide miRNAs, while a box-plot compares fast vs. slow decaying miRNAs ($p<0.0001$, Wilcoxon-test). **RIGHT PANEL**- Guide miRNAs were distinguished into four classes (quartiles of 4sU incorporation rates). Shown is the distribution of 'fast' and 'slow' miRNAs along the incorporation classes by contingency ($Chi^2=44.8$, $p<0.0001$).

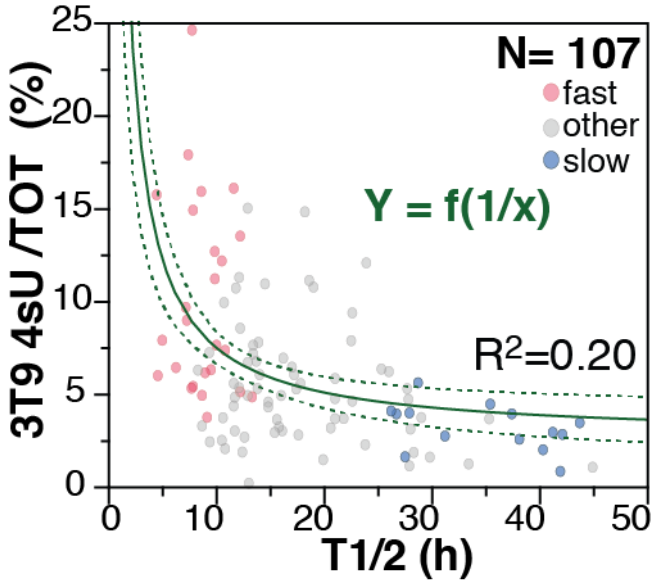

Figure 38. Half-lives are plotted against incorporation rates. A curved line highlights the reciprocal relationship. Dashed curves mark confidence intervals. Red and blue dots represent fast and slow miRNAs, respectively.

Based on this finding, we investigated decay dynamics into different cell models by 4sU incorporation. We focused on human BJ fibroblasts (the human counterpart of murine 3T9 fibroblast) and HeLa cells. As mentioned above, the choice of the right concentration for 4sU administration is pivotal for the success of the experiment; thus, we performed preliminary studies aimed at finding a non-toxic concentration for 4sU labeling. We chose final concentration of 100

μM for both cell lines, which was used to label cells for 3 hours. We performed small RNA sequencing on total and 4sU labeled RNAs and determined incorporation rates, whose distribution is shown in **Figure 39**. We focused on the common miRNAs that are perfectly conserved in human and mouse (N=72) and observed a very good correlation in 4sU incorporation rates (**Figure 39-RIGHT PANEL**), suggesting that decay rates were similar in the two models. To verify this contention, we performed 4sU pulse-chase on BJ fibroblasts and calculated turnover rates of a bunch of miRNAs by means of RT-QPCR. BJ half-life data were much similar to those previously measured in 3T9 cells in most cases (7/8, **Figure 41**), confirming our hypothesis. We also compared incorporation rates of human fibroblasts (BJ) and epithelial cells (HeLa) and observed a strong correlation (R^2=0.67, **Figure 40**), which supports the hypothesis that turnover rates are an intrinsic feature of miRNAs, which could be maintained across different cell lines and organisms.

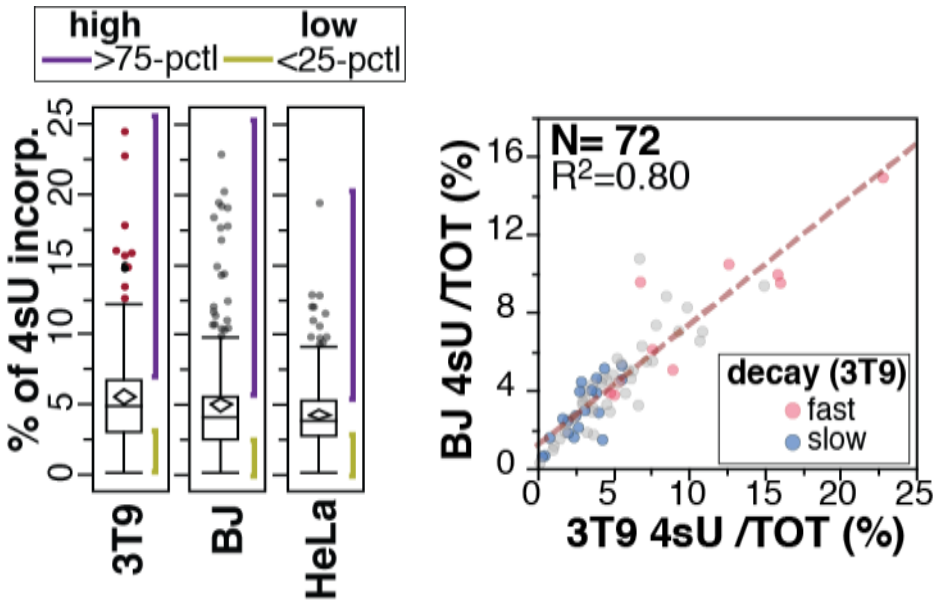

Figure 39. Incorporation rate of 3T9, BJ and HeLa cells. **LEFT PANEL** The box plots show the distribution of 4sU incorporation rates into different cell lines. Purple and yellow lines mark the area of high (>75pctle) and low (<25pctle) incorporating species, respectively. **RIGHT PANEL**-4sU incorporation rates of human (BJ) and mouse (3T9) fibroblasts are compared by scatter plot. Only miRNAs perfectly conserved between human and mouse were considered (N=72)

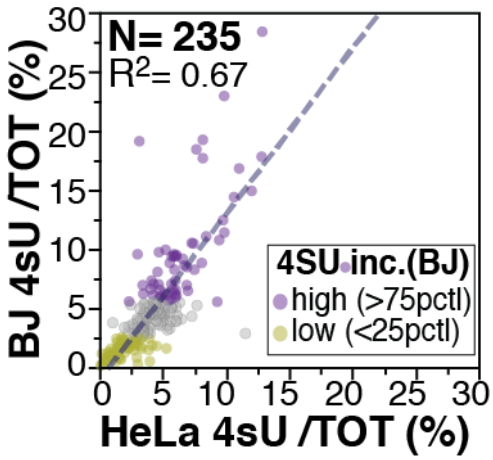

Figure 40. Correlation of 4sU incorporation data of Hela vs BJ cells. 4sU incorporation rates of HeLa and BJ human cells are compared by scatter plot. A dashed line highlights the linear correlation. Yellow and purple dots refer to percentile distribution as in *Figure 39*.

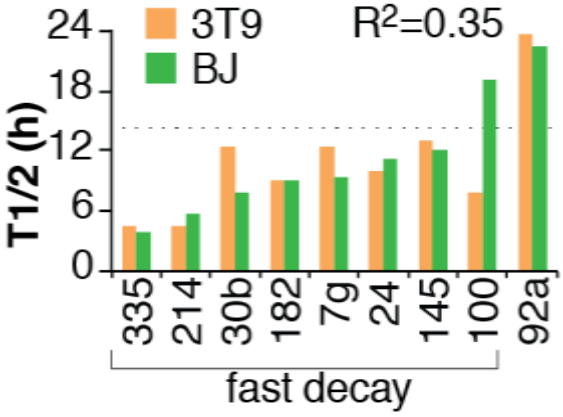

Figure 41. Half-life of miRNAs in BJ and 3T9 cells . Half-lives of 9 miRNAs were measured in human BJ cells by pulse and chase and compared with those from mouse 3T9 cells. Those miRNAs previously classified as fast decaying (<14h, dashed line) are boxed.

4.3. Transcription and decay contribute to the regulation of the miRNA pool

4.3.1 miRNA degradation rates are slightly associated to miRNA abundance

We defined the decay behavior of 186 canonical miRNAs and we described some features of the fast and slow classes. Next, we questioned about the processes that govern miRNAs regulation and their abundance. At first, we hypothesized that degradation rate might be a determinant of miRNA expression level. To test this hypothesis, we decided to measure absolute miRNA expression levels by means of digital PCR (ddPCR, see Material and Method), and determined how many copies for each miRNA are present in cells in growing conditions (copies per cell, CPC). The distribution of miRNA expression levels (CPC) is shown in **Figure 42-LEFT PANEL**. According to this, we subdivided miRNAs into four classes of expression (quartiles), useful for correlation analysis with miRNA decay. We observed just a trend of correlation between miRNA expression and decay rates (**Figure 42 – RIGHT PANEL**), which was close to significance (P=0.0599) when fast and slow classes were directly compared (**Figure 42 – MIDDLE PANEL**), implying that the decay contributes partially to miRNAs abundance.

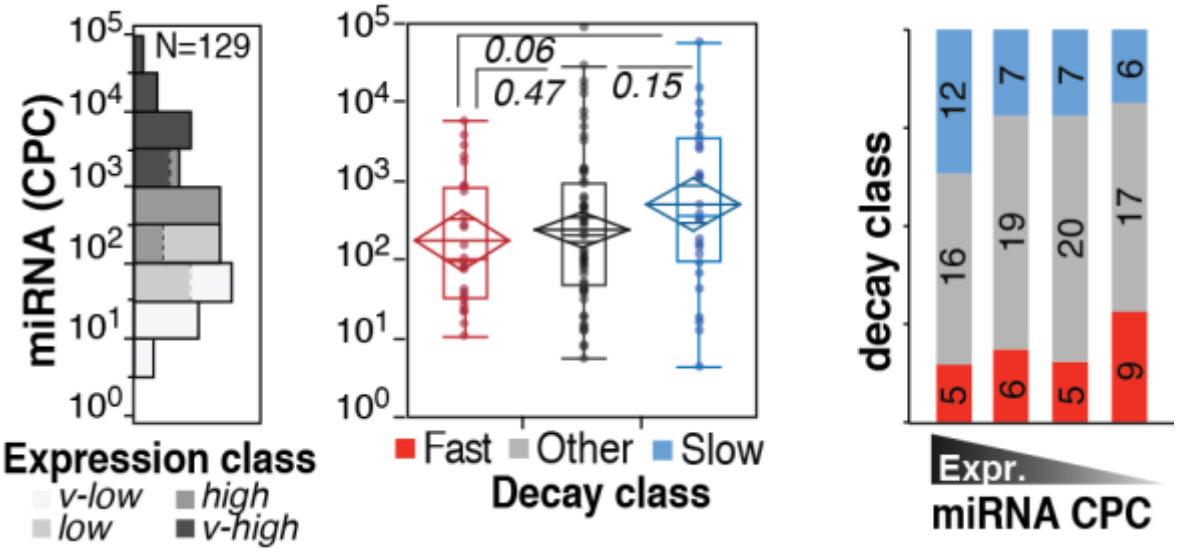

Figure 42. Absolute expression of miRNAs in cells correlated with miRNA decay. **LEFT PANEL**- According to the distribution of miRNA expression in 3T9 cells, four classes (quartiles, highlighted by a colored code) could be defined. **MIDDLE PANEL**-The box-plot (right) shows the abundance of miRNAs by decay class. P-values were calculated by Wilcoxon-test. **RIGHT PANEL** -The distribution of miRNA decay rates along the expression classes was analyzed by contingency (Chi^2=4.7, p=0.585).

4.3.2 Modeling of miRNA abundance regulation by transcription, maturation and decay

In principle, all the different processes that are involved in the determination of miRNA levels could be schematized into three kinetic processes. Thus, with the help of Dr. Cerruti, a biophysicist in the lab, we performed a kinetical analysis as outlined in **Figure 43.**:

- TRANSCRIPTION, in which miRNAs loci are transcribed by RNA-Pol2 and precursor molecules (PRI-miRNAs – PRI) are generated at rate called as transcription rate, *k1 (# of molecule time^{-1});*
- MATURATION, which summarizes all the events necessary to convert the precursor into the mature form (PRI to PRE-miRNAs, export in the cytosol and PRE-miRNAs to mature miRNA – μ). These steps could be simplified in a single kinetic process (maturation), described by constant, *k2 (time^{-1})*;
- DECAY, in which mature miRNAs (μ) are cleared. As previously said, this process depends on decay rate, *k3 (time^{-1})*. Decay rate (k3) is related to half-life, but also depends on dilution by cell division (*α*, which is $1/T_D$ – cell doubling time) according to the following formula: $k3 = \ln(2)/T_{1/2} - \alpha$;

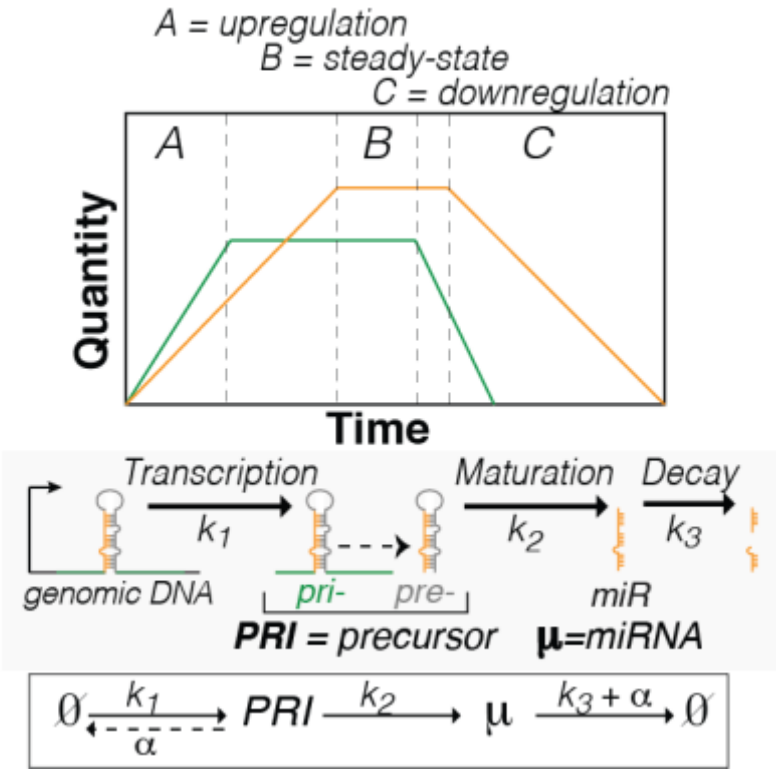

Figure 43. Scheme of miRNA lifespan. The scheme describes the variations of miRNA (yellow) expression in time according to changes in transcription of primary miRNA (pri-miRNA, green). The regulation of miRNA expression (μ) is

dependent on transcription, maturation and decay rates (k_1, k_2 and k_3, respectively) and on dilution by cell division (α). Half-life (T1/2) and k_3 are related [$T_{1/2}=\ln(2)/(k_3+\alpha)$].

The transformation of Primary miRNA transcript ($\dot{PRI}$) into mature miRNA (μ) can be written through two coupled differential equations:

$$\dot{PRI} = \frac{dPRI}{dt} = k_1\text{-}(k_2 + \alpha)PRI \qquad (1)$$

$$\dot{\mu} = \frac{d\mu}{dt} = k_2 PRI\text{-}(k_3 + \alpha)\mu \qquad (2)$$

Three possible situations could be depicted for miRNA expression regulation (**Figure 43**):

- UPREGULATION (A), when transcription is on, PRI-miRNA (green line) increases up to a plateau, and mature form (yellow line) starts accumulating, the gap between PRI-and mature miRNAs depends on maturation. This is a complex situation since all the processes contributes to the miRNA pool and none of them is at equilibrium.
- STEADY-STATE (B), when all the processes are at equilibrium and the generation of new molecules matches the degradation of old one.
- DOWNREGULATION (C), when transcription is off, mature miRNAs are disappearing according to their turnover rates. This is a simple situation (no contribute of transcription and maturation) and just decay play a role. It also reflects what happens during the chase experiment, which has been used to calculate miRNA decay rates.

Of note, at steady-state (e.g. exponentially growing cells) the generation and degradation of miRNAs are at equilibrium and, hence both equations (1) and (2) are equal to zero.

Thus, we can obtain the values of the plateau $\overline{PRI}$ and $\bar{\mu}$:

$$\overline{PRI} = \frac{k_1}{k_2 + \alpha} \qquad (3)$$

$$\bar{\mu} = \frac{\overline{PRI}\, k_2}{k_3 + \alpha} = \frac{k_1\, k_2}{(k_2 + \alpha)(k_3 + \alpha)} \qquad (4)$$

A further simplification could be made, assuming that maturation is much faster than cell division ($k_2 >> \alpha$), an assumption that hold true since miRNA maturation is thought as a quite efficient process that lasts few hours (unless in case of more complex regulations, such as polycistronic miRNAs or miRNAs with regulated processing).

$$\bar{\mu} = \sim \frac{k_1}{k_3 + \alpha} \qquad (5)$$

Hence, at steady state miRNA amount (μ) could be calculated by just three parameters: the transcription rate (k_1), the degradation rate (k_3) and the dilution by cell division (α), of which two are known (k3 and alpha).

4.3.3 miRNA genomic loci definition and transcription rate (k1) absolute quantification

We next sought to determine transcription rates (k_1) of miRNA primary transcripts (PRI-miRNAs) in exponentially growing fibroblasts. We decided to exploit short pulse of 4sU, as an approach to measure transcription. Providentially, Bruno Amati's lab already performed RNA-sequencing of 4sU short pulsed (10') 3T9 fibroblasts in growing conditions (triplicate experiment) and granted us the access to raw data. To calculate transcription rates of PRI-miRNAs, we had to know exactly the transcriptional unit, an issue which is not trivial, since transcription start sites of miRNA genes (TSS) could be many kilobases distant from miRNA genes and, until very recent studies, (Chang et al. 2015) were poorly annotated.

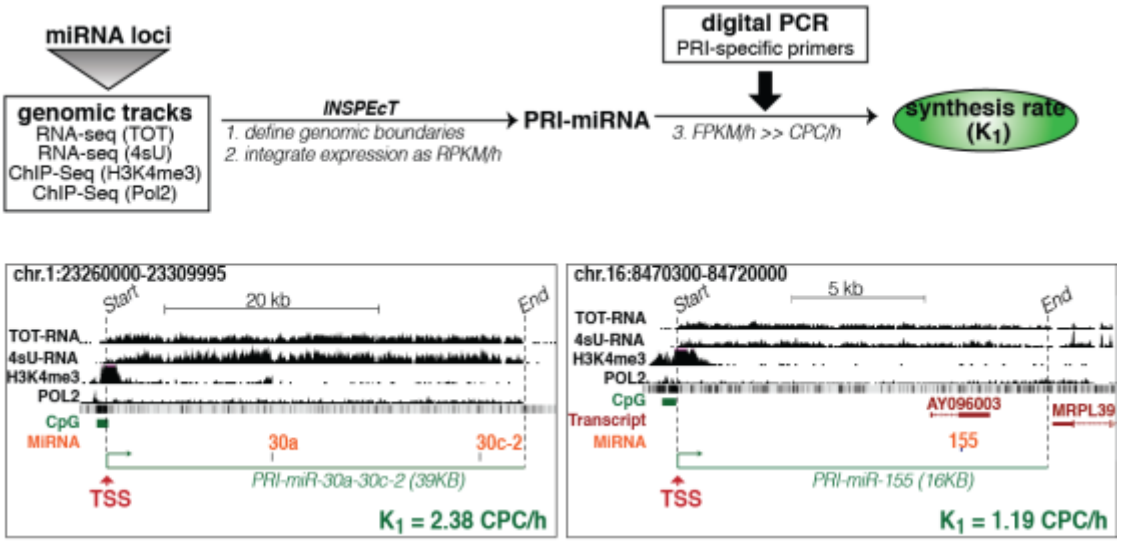

Figure 44. Definition of miRNA loci and INSPEcT tool. **UPPER PANEL**-The scheme illustrates the strategy used to define genomic boundaries for miRNA primary transcripts (pri-miRs) and to calculate the synthesis rate (k_1). Examples

are shown in **LOWER PANEL**. RNA-seq (TOT and 4sU) are the results of triplicate experiments (biological replicas). In order to infer synthesis rates, RPKMs of 4sU- and TOT-RNA-seq were provided to the R/Bioconductor software INSPEcT (de Pretis et al. 2015), which integrates expression as synthesis rate (RPKM/h)

We manually defined genomic boundaries of PRI-miRNAs in growing 3T9 fibroblasts according to a combination of 4sU-RNA-seq and ChIP-seq (Pol2 and H3K4me3, also provided by Amati's lab) tracks, which mark the transcriptional unit and the promoter region, respectively. In figure are reported two representative examples (miR-30a/c-2 and miR-155 loci, **Figure 44-LOWER PANEL** and **Table 2**). In particular, in case of intergenic species, primary transcripts were defined as regions with i) a continuous 4sU transcriptional track, ii) not overlapping with intervening transcripts and iii) associated with a clear Pol2 signal in the close proximity of a H3K4Me3 peak at the putative promoter. In the case of intragenic species, the analysis was restricted just to the intron containing pre-miRNA species.

We also took advantage of another bioinformatics tool, named as INSPEcT (de Pretis et al. 2015) (**Figure 44-UPPER PANEL**), developed by our colleagues to specifically calculate transcription rate from 4sU RNA sequencing data. Such synthesis rate (k_1) are expressed as Reads per kilobase per million mapped produced per hour (RPKM/h). As we aimed at a quantitative analysis of miRNA expression, we sought to convert such value into an absolute value (CPC/h). Again, we took advantage from digital PCR, and measured different PRI-miRNAs (N=6, **Figure 45**). We chose PRI-miRNA transcripts with known different expression levels, and by using the absolute values obtained by digital qPCR, we calculated a linear scaling factor to convert RPKM/h into CPC/h.

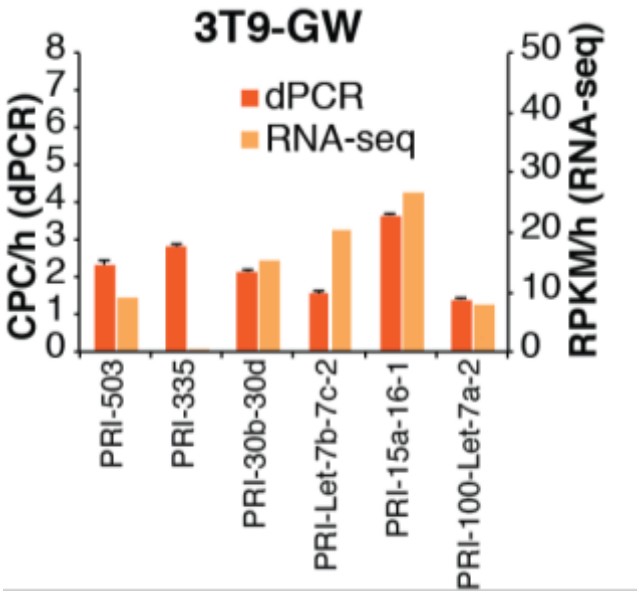

Figure 45. Comparison of ddPCR and RNAseq data and transcription rate (k1) distribution.Six different pri-miRNAs were quantified from 4sU and total RNA extracted from growing (3T9-GW) or quiescent (3T9-SD) cells. As shown in the bar graph, ddPCR and RNA-seq data are highly correlated, thus it was possible to calculate a scaling factor (SF=7.36) used to convert RPKM/h into CPC/h.

4.3.4 miRNA transcription rate is a major determinant of miRNA abundance

Overall, we could calculate the transcription rate for about one hundreds of different miRNA loci (including 82 out of the 129 guide miRNAs included in this study), with values ranging from 0.1 to 30 CPC/h (**Figure 46-LEFT PANEL** and **Table 2**). We distinguished four groups (quartile) of transcription, useful for correlation analysis. At first, we compared the classes of miRNA transcription (k1) with miRNA expression levels in cells. The correlation with miRNA amount (expressed as copies per cell) is notable, suggesting that transcription rate is a major determinant of miRNA expression level. Low transcribed loci showed significantly less abundant miRNA levels compared to those genes highly processed ($p<0.0001$), either by box plot analysis ($p<0.0001$, **Figure 46-MIDDLE PANEL**) or by contingency classes (11/12) (**Figure 46-RIGHT PANEL**).

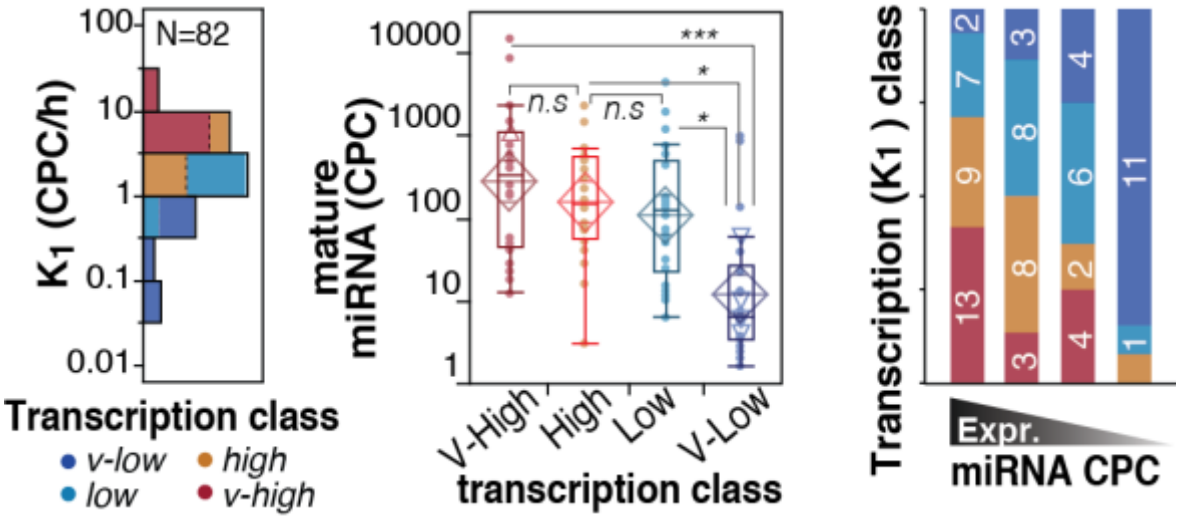

Figure 46. Correlation analysis of miRNA transcription and miRNA abundance. **LEFT PANEL**- Distribution of transcription rate of 82 miRNA loci. A color code highlights four classes (quartiles) of the distribution **MIDDLE PANEL**-The abundance of miRNAs has been correlated with transcription classes as in B. Asterisks mark significant values (*=p<0.05, ***= p<0.001; Wilcoxon test). **RIGHT PANEL**-The distribution of miRNA transcription rates along the expression classes was analyzed by contingency (Chi^2=38.07, p<0.0001).

Then, we explored the relationship between transcription and decay rate. We found that those miRNAs with low synthesis rate (low k_1) were enriched for 'fast' decaying species (and, vice versa, those species actively transcribed (high k_1) were enriched for 'slow' miRNAs (**Figure 47-LEFT PANEL**). Furthermore, "fast" species displayed a lower transcriptional rate than other classes (**Figure 47-RIGHT PANEL**), meaning that transcription and decay might be coupled.

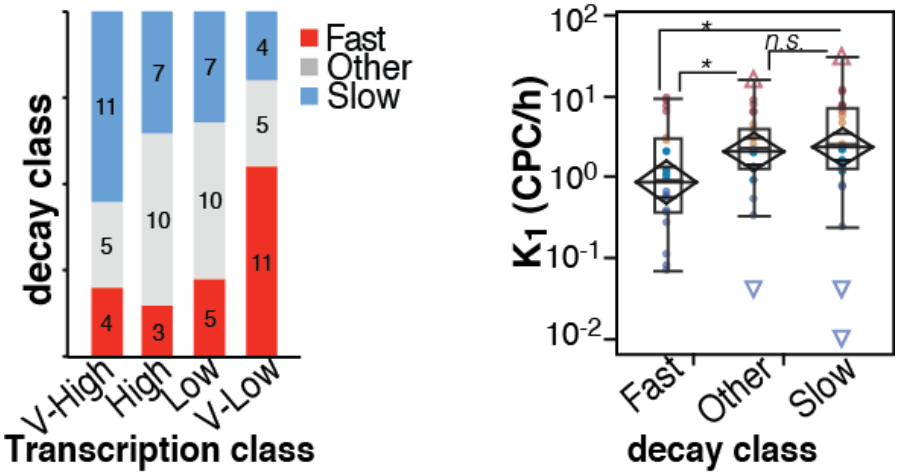

Figure 47. Correlation analysis of miRNA transcription and decay. **LEFT PANEL**-The transcription of miRNAs has been correlated with decay of mature miRNAs by contingency test (Chi^2=13.06 p=0.0421) and by one-way analysis (**RIGHT PANEL**). Asterisks mark significant values (p<0.05).

4.3.5 miRNA abundance inferred by transcription and decay rates

As mentioned before, at steady-state miRNA expression (μ) is just dependent on transcription (k1), decay (k3) rates and on dilution by cell division (α) (**Figure 43**). Since we know all these parameters, we could then infer miRNA abundance. We calculated such "theoretical" miRNA abundance and correlated the values with those experimentally measured. We found a remarkable linear correlation, with fitting (R^2=0.47), but only for miRNA loci that are organized as single (non-clustered) transcriptional units (N=25, **Figure 48-LEFT PANEL**). On the contrary, miRNAs that belong to clusters (N=57) could not be modeled properly (**Figure 48-RIGHT PANEL**, R=0.12), suggesting that the assumption made about the maturation step (k_2>>α) is not verified, and processing has to be taken into account. Overall, we can also conclude that the mathematical

model that we generated to interpret miRNA regulation by biosynthetic and decay processes is verified.

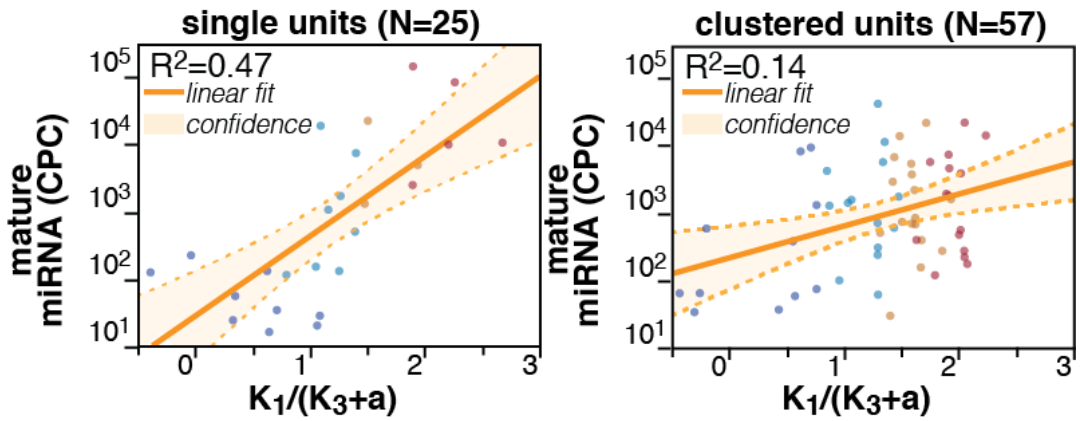

Figure 48. Correlation analysis between theoretical and experimental abundance. The expression of miRNAs at steady state was inferred using the kinetic parameters (k1 and k3), which were measured by pulse and pulse-chase experiments, respectively. Scatter plots show the fitting of experimental (CPC, log scale) and theoretical (k1/(k3+α), log scale) copies, for miRNAs transcribed as single units (**LEFT PANEL**) or clustered units (**RIGHT PANEL**). Straight and dashed lines mark linear correlation and confidence intervals, respectively.

4.3.6 The impact of transcription and decay on miRNA dynamic regulation

Next, we sought to exploit the mathematical model to understand the impact of transcription, maturation and decay on the dynamic regulation of miRNAs (Table 3). To answer this question, we generated time-evolution curves of miRNA expression levels, using kinetic parameters (k_1, k_2, k_3, α) in the range of those measured experimentally in 3T9 cells. In particular, we sought to highlight the difference between a 'fast' decay behavior ($T_{1/2}$=4h) over a 'slow' decay ($T_{1/2}$=24h). We performed the analysis also considering the impact of cell proliferation (by alpha), considering cells that are not dividing (α=0, quiescent or differentiated cells), cell slowly dividing (α=1/48) and cells rapidly dividing (α=1/24). The time-evolution models also consider a switch in transcription (on/off, thin black line) after a fixed time to model both the upregulation and downregulation of miRNAs. As shown in the figure, the shape of the curve that describes miRNA expression during time is profoundly different between different decay classes. In particular, fast miRNAs ($T_{1/2}$=4, thick red line) reach quickly the plateau upon upregulation (**Figure 50- RIGHT PANEL**) and are also quickly downregulated when transcription is off, independently on the other kinetic parameters (k1, k2 or alpha -**Figure 49**).

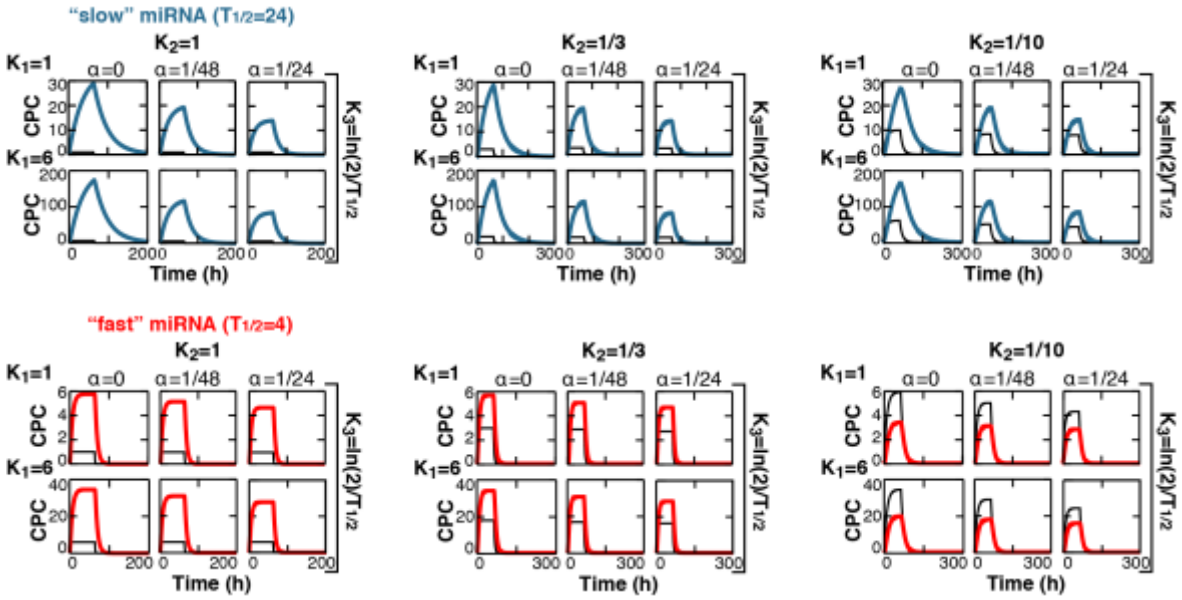

Figure 49 Time evolution model of the impact of transcription and decay on miRNA regulation. Mathematical modeling of accumulation and degradation dynamics of miRNAs (thick colored line) and pri-miRNAs (thin black line) by defined kinetic parameters and according to different proliferation states ($\alpha=1/T_D$, duplication time). A dashed vertical line marks when synthesis has been shut off. The blue and the red lines highlight the behavior of slow and fast decaying miRNAs, respectively. Analysis were performed at two different proliferation rates [low proliferation rate (K1=1) and high proliferation rate (K1=6)] and three different maturation rates [fast (k2=1), slow (k2=1/3) and very slow maturation (k2=1/1, meaning 10 hours to maturate 50% of transcribed molecules)]

Decay rates also influence miRNA expression (copies at plateau) and times to reach 90% expression of plateau although the rate of transcription (k1) appears as the primary determinant (**Figure 50-LEFT PANEL**). Of note, different maturation rate did not influence much the dynamic of miRNA regulation, but just the equilibrium between precursor and mature miRNAs.

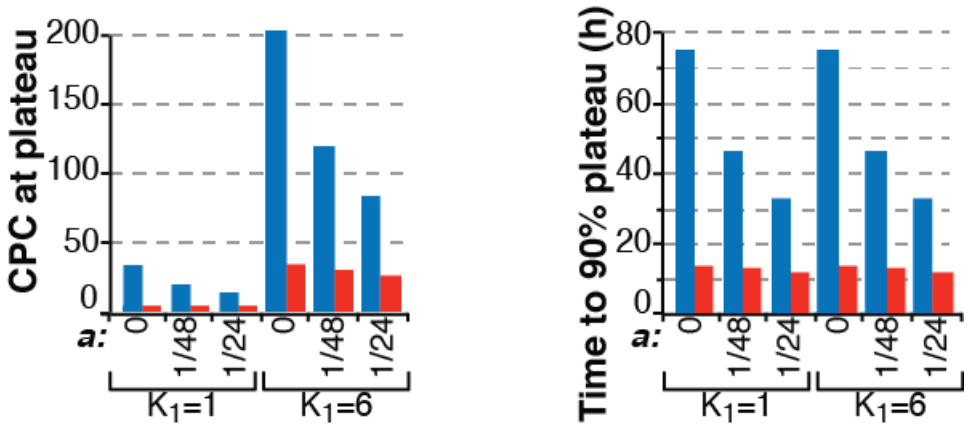

Figure 50. Decay rate and miRNA expression. Bar graphs show the theoretical values of miRNA abundance at plateau (CPC - **LEFT PANEL**) or the time required to reach the 90% of the plateau (hours – **RIGHT PANEL**) inferred by modeling. Values are reported according to indicated k1 and T1/2 in cells, further distinguished by cell proliferation rates (α)

Hence, we can conclude that the decay rate is controlling the dynamics of miRNA regulation. In regard to miRNA decay behavior, we can say that only miRNAs with fast decaying behavior could

give rise to sharp and quick changes in miRNA levels (i.e. the time to shift from two different steady levels upon a change in k_1), which is minimally influenced by cell proliferation. Conversely for slow miRNAs, both the accumulation and degradation are very slow and mainly dependent on dilution by cell division (**Figure 50**).

4.4. Mechanisms behind miRNA decay

4.4.1. A target per miRNA ratio (TPM) associates with miRNA degradation dynamics

MiRNAs function through RISC complex by silencing the expression of target genes (TG) (Carthew and Sontheimer 2009; Jonas and Izaurralde 2015). It has also been shown that high affinity targets (TG) could influence miRNA stability by promoting the unloading from Ago2 (De et al. 2013) and miRNA degradation, a mechanism called target-induced (or -directed) miRNA decay (TIMD or TDMD). Hence, we sought to investigate the relationship between RNA targets and miRNA decays.

We exploited the in-house RNAseq dataset from 3T9 (provided by Amati's lab), scouting for targets (the strategy is schematized in types **Figure 51-LEFT PANEL**). We relied on TargetScan database, using rules that enriches for high confidence targets (context score <-0.2; targets with 8mer and 7mer-m8 "seed" match). Both conserved and non-conserved targets were considered (CS and NSC). Recently, it has been pointed out that other regions outside the 'seed' could also play a role, in particular the binding at the 3' end of the miRNA (3' complementary site – 3C) (Bartel 2009). Hence, we took into account different classes of high confidence targets: i) only the "seed" (TG_seed), ii) the seed plus a partial region at the 3'site (TG_3C.03 with 3'-end pairing <-0.03), iii) the seed plus an extensive region at the 3'site (TG_3C.05 with 3'-end pairing <-0.05). Examples are shown in **Figure 51-RIGHT PANEL**. For inferred target expression by sequencing and as previously said, we converted RPKM values into absolute expression values (copies per cells, CPC).

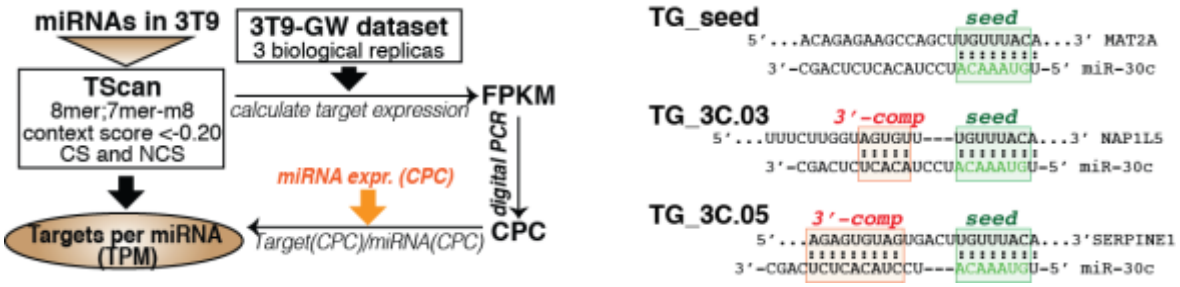

Figure 51.TPM calculation and target complementarity. **LEFT PANEL**-Scheme of strategy used for the target:miRNA ratio calculation. **RIGHT PANEL**-Targets of miRNAs were further distinguished according to the complementarity to the miRNA 3' end. TG_seed, seed interaction; TG_3C, seed plus 3' compensatory site with moderate (3C.03) or extensive (3C.05) interaction.

To study quantitative relations between miRNAs and RNA targets we estimated a ratio of the number of target molecules per miRNA (target per miRNA ratio – TPM). We followed the simplest hypothesis that no competition occurs for the same binding site between different miRNAs and calculated the ratio diving the target expression (target CPC) by miRNA expression (miRNA CPC), taking into account also the number of miRNA responding elements (MRE) present in each target (**Figure 51**). As we defined three sets of targets (seed, 3C.03 and 3C.05) we obtained three corresponding sets of TPM (TPM_seed, _3C.03 and _3C.05). Below is shown the distribution of TPM_seed in 3T9 fibroblasts, from which we distinguished classes of TPM (quintiles) that ranged from a 1:1 ratio (low TPM) to thousands of target copies (high TPM) for a single miRNA (**Figure 52-LEFT PANEL)**. The inclusion of extended 3' complementarity increases the specificity for miRNAs (few targets shares more than one miRNA) and greatly reduced the number of target molecules for each miRNA, with a maximum of hundreds or tens of binding sites, respectively for TPM_3C.03 and TPM_3C.05 (**Figure 52-RIGHT PANEL** and **Figure 53**).

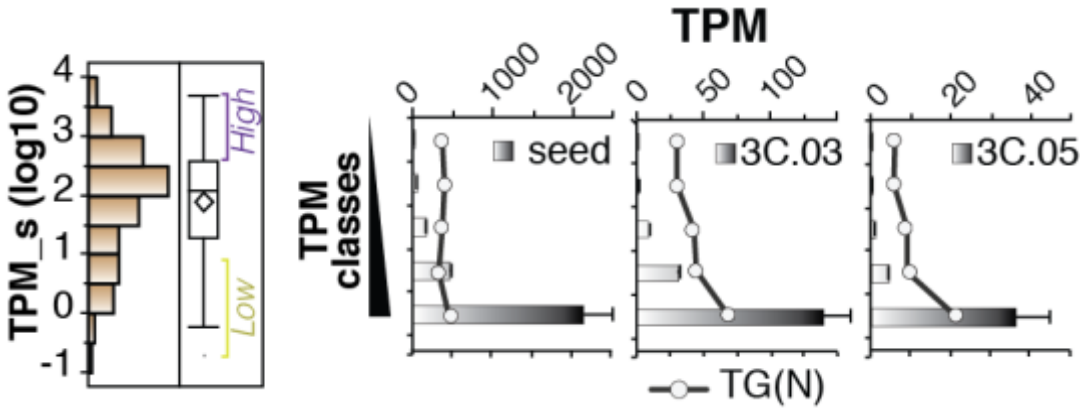

Figure 52. Distribution of target:miRNA ratios (Targets per miRNA – TPM). **LEFT PANEL**- Shown is the distribution of TPM for targets with seed interaction (TPM_s). Based on the distribution, the two most distant classes were selected: 'High' (N=22, TPM > 80th pctle); 'Low' (N=22, TPM < 20th pctle). **RIGHT PANEL**-A bar graph summarize the TPM and the number of targets [TG (N]. Asterisks mark significant values (*=p<0.05, **=p<0.01; Wilcoxon test).

	CLASS	TPM (mean ±s.e.m.)	# of TG (mean ±s.e.m.)	TG (CPC) (mean ±s.e.m.)
seed	FAST	587 ± 142	376 ± 47	5608 ± 775
	SLOW	287 ± 135	432 ± 40	5735 ± 641
3C.03	FAST	51 ± 16	55 ± 13	583 ± 135
	SLOW	18 ± 8	42 ± 5	358 ± 55
3C.05	FAST	14 ± 8	19 ± 7	155 ± 56
	SLOW	5 ± 3	8 ± 1	59 ± 13

Figure 53. Table of TPM values. A table summarizing the TPM, the number of targets [TG] and their level of expression in 'fast' vs. 'slow' miRNA classes. Values are displayed as mean with s.e.m.

Then, we analyzed the correlation between TPM and miRNA decays. We focused our analysis on the two main decay classes, revealing that 'fast' miRNAs displayed higher TPM values respect to 'slow' miRNAs (**Figure 54-UPPER PANEL** $p<0.01$). We performed also a reciprocal analysis using the two extreme TPM classes and observed that miRNAs with very high TPM (High, top 20% distribution) had a significant enrichment of 'fast' species and a shorter half-life compared to those with very low TPM (Low, bottom 20% distribution, **Figure 54-LOWER PANEL** and **Figure 55**).

These data strongly suggest that the total number of target molecules is a determinant of miRNA decay behavior, supporting TIMD as general mechanisms in control of miRNA stability. Accordingly, in most analysis the 3' complementarity (3C.03 and 3C.05) further increased the significance of the correlation, suggesting the importance of such complementary in the target-mediated degradation of miRNAs, something which has been only observed in vitro.

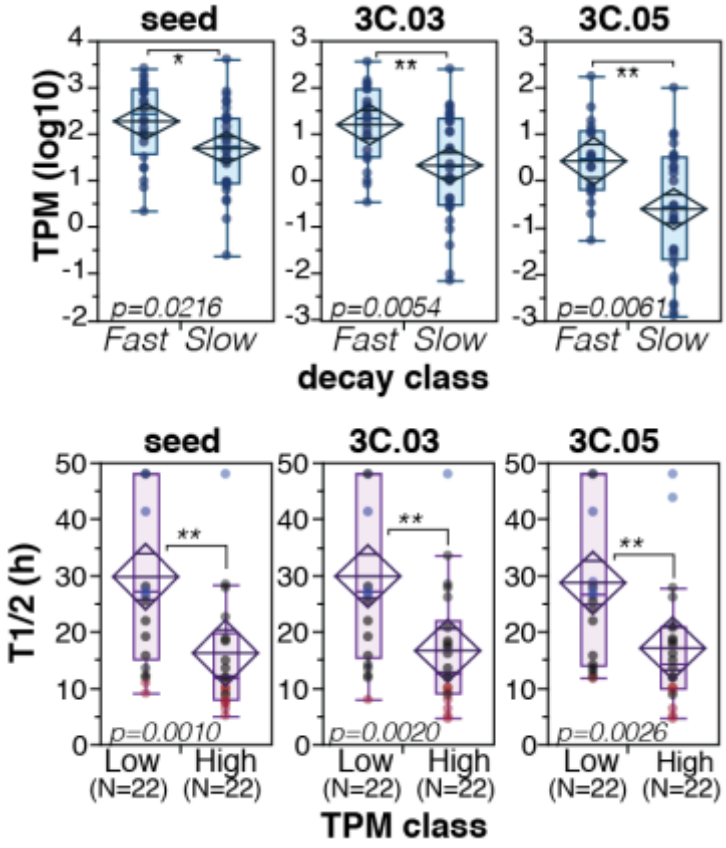

Figure 54. Correlation analysis between TPMs and decay rates. **UPPER PANEL**-Box-plots shows the distribution of the target:miRNA ratios (TPM) according to target complementarity, as shown in in fast' vs. 'slow' miRNAs. **LOWER PANEL**- MiRNA half-lives (T1/2) distribution within classes of miRNAs with low (<20th pctle) or high (>80th pctle) TPM. Blue and red dots represent slow and fast miRNAs, respectively.

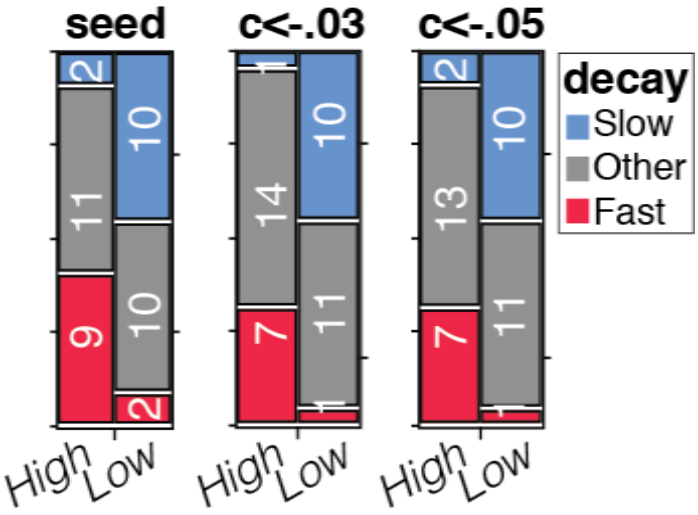

Figure 55 Contingency analysis between TPM classes and classes of miRNA decay. A contingency analysis is shown, correlating 'High' and 'Low' TPM classes with the classes of miRNA decay. TPM classes were further distinguished according to the type of complementarity between targets and miRNAs: seed, targets with seed interaction (Chi2=10.68 p=0.0048); 3C.03, targets with seed plus 3' compensatory site (Chi2=13.97 p=0.0022), targets with seed plus 3' compensatory site with extensive interaction (Chi2=11.05 p=0.0040)

Of note, the correlation with TPM and miRNA decay is far more significant that the association with either target (TG CPC) or miRNA abundance (miRNA CPC) (**Figure 56-LEFT** and **RIGHT PANEL**, respectively), suggesting that is the combination of the two that really matters.

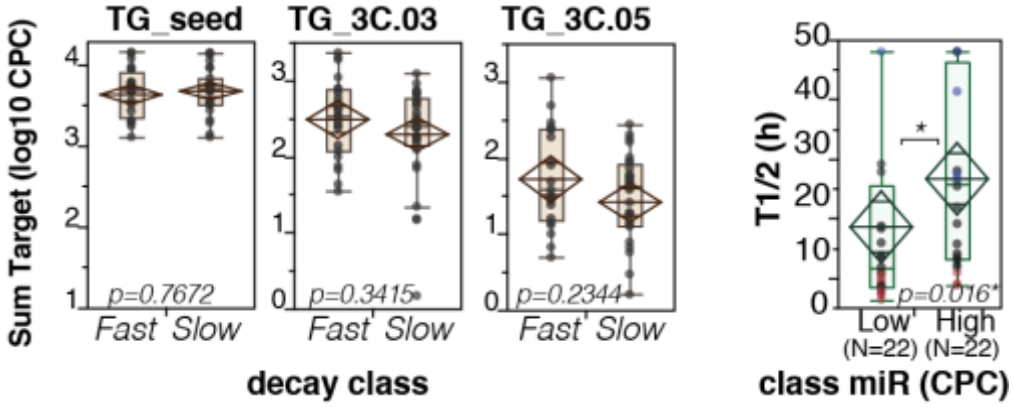

Figure 56.Correlation analysis of targets and miRNAs abundance to decay rate. **LEFT PANEL** Abundance of all targets (as copies per cell – CPC, log scale) is correlated with 'fast' and 'slow' miRNAs by box-plot. **RIGHT PANEL**-MiRNA half-lives (T1/2) were correlated with classes of miRNA expression with very low (<20th pctle) or high (>80th pctle) miRNA abundance.

A caveat in this model is that TPM values is calculated based on 'actual' copies of miRNAs. However, TPM also influences miRNA decay and, hence, miRNA expression. We wanted to verify our conclusion, by calculating TPM based on 'virtual' copies of miRNAs, defined as those copies that should be in the cell without differential decay behavior. We used the transcription rate to calculate miRNA 'virtual' copies with the above-mentioned mathematical model (having set a fixed k3 value). Those miRNAs with high "virtual TPM" still displayed shorter half-lives (**Figure 57-LEFT PANEL**), and the association was stronger with respect to that observed between

synthesis and half-life (**Figure 57-RIGHT PANEL**), suggesting that high TPM correlates with faster decay *per se*, and not as a result of reduced miRNA expression due to target-induced miRNA degradation.

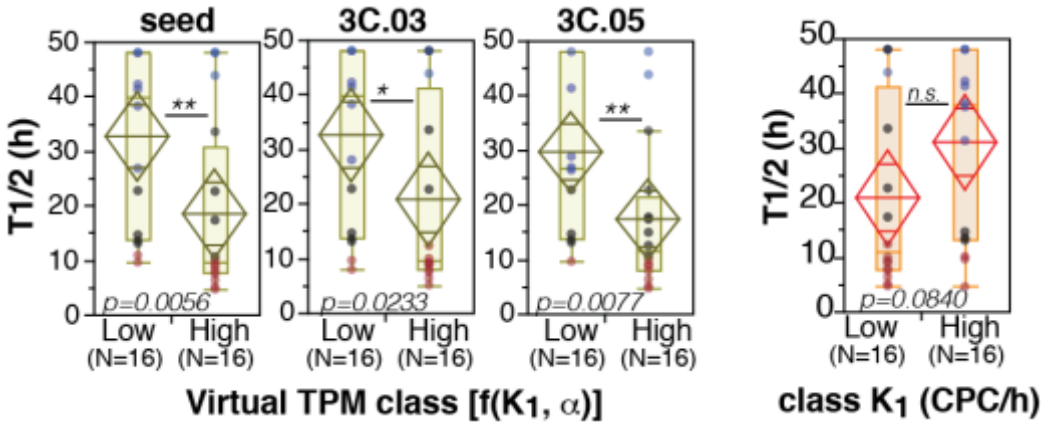

Figure 57. Correlation analysis between half-lives and virtual TPM classes. **LEFT PANEL**. Shown is miRNA half-lives (T1/2) distribution within classes of miRNAs with low (<20th pctle) or high (>80th pctle) virtual TPM classes calculated using data of transcription rate (k1) and cell duplication time (α). **RIGHT PANEL**. MiRNA half-lives (T1/2) were correlated with classes of miRNA synthesis rates with very low (<20th pctle) or high (>80th pctle) transcription rates (K1, CPC/h).

4.4.2. Target:miRNA dynamics could be recapitulated with the application of exogenous expression systems

Our analyses suggest that high target:miRNA ratios (TPM) might induce fast decay behavior of miRNAs, supporting an active role for targets in miRNA regulation. A corollary of this model is that at high TPM also the activity of a miRNA on its target should be affected, as previously suggested (Mullokandov et al. 2012; Bosson et al. 2014). We thought verify this contention by manipulating TPM ratio by tuning the expression of miRNAs and monitoring miRNA repression by a highly complementary reporter target (GFP). We selected a miRNA that is absent in 3T9 cells, avoiding background expression regulation of endogenous molecules, and generated an inducible expression vector (pSLIK-miR-9) used to infect 3T9 cells, to control the expression of miR-9 by tetracycline treatment. We selected for clones harboring just one viral integration. Concomitantly, we generated a constitutive expression vector to overexpress a synthetic highly complementary target (dGFP with 4x perfect complementary binding sites or a control sequence, **Figure 58**) together with a marker (ΔNGFR).

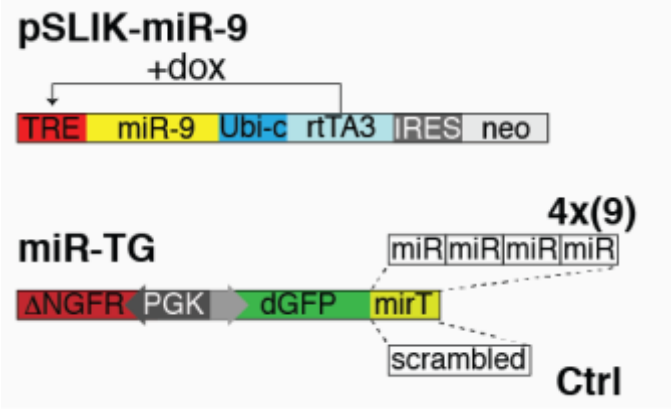

Figure 58 Schemes of pSLIK vectors. pSLIK vectors used for the inducible expression of miR-9 (pSLIK-miR-9, Tet-ON system) and the constitutive expression of a reporter target gene. This vector exploits a bidirectional PGK promoter that expresses both the dGFP reporter and a ΔNGFR gene, which could be used to normalize the expression levels of the target dGFP by Fluorescence Activated Cell Sorting (FACS).

Control (ctrl) or target (4x9) dGFP populations with similar ΔNGFR expression were selected by FACS. MiR-9 has been induced soon after sorting (50 ng/mL, 7 days – 'ON' condition) and exerted its inhibitor role on the GFP target. We, then, turned off transcription by removing doxycycline from the medium ('OFF') in order to gradually decrease miR-9 levels over time. Levels of miR-9 were quantified by digital (ddPCR) and shown as copies per cell (CPC). As expected, we found that, once miR-9 production was blocked upon doxycycline withdrawal from media, miR-9 decreased its abundance (**Figure 59-LEFT PANEL**) and target was "derepressed" (**Figure 59-RIGHT PANEL**).

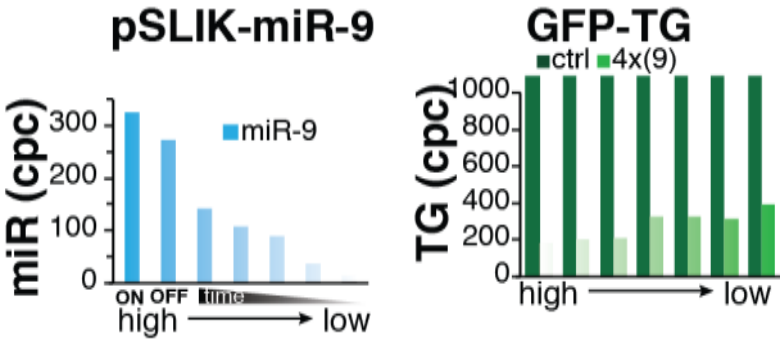

Figure 59. Expression levels of miR-9 and target. **LEFT PANEL**- Expression levels of miR-9, determined through ddPCR and expressed as copies per cell. Data were normalized on Snord72. **RIGHT PANEL**- Expression levels of control target (dark green) or 4x(9) target (light green) determined through ddPCR and expressed as copies per cell.

Thus, we determined TPM_3C.05 for miR-9, by dividing the number of target copies (endogenous target plus exogenous target) by miR-9 copies (measured by digital PCR) at each time points. Results are shown in figure below and revealed that strong target repression occurred with

TPM_3C.05 was <5, while repression was weakened at TPM_3C > 10 (**Figure 60**). If we compare these values with those determined experimentally in 3T9 cells (**Figure 53**), we could see that they are exactly in the same range of TPM values of 'fast' vs. 'slow' miRNAs, suggesting the ratio between high affinity targets and miRNA abundance plays a role in the definition of both miRNA activity and miRNA decay.

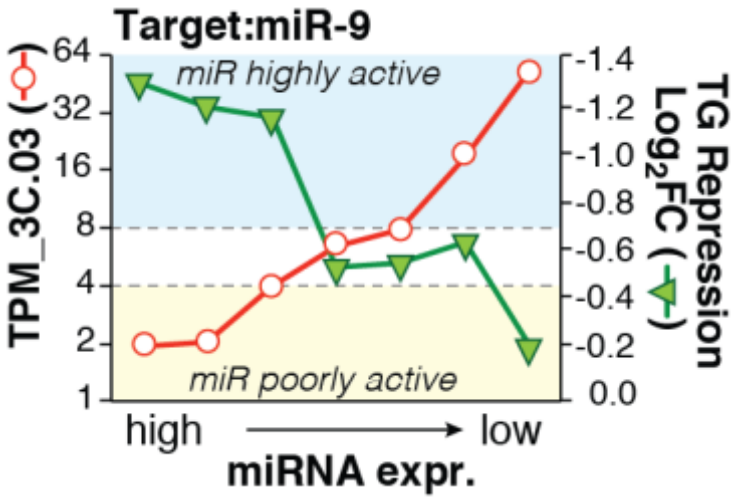

Figure 60. TPM estimation of Target:miR-9 system. The plot shows the fluctuations of target:miRNA ratios (TPM_3C, in red) together with the repression of target dGFP (TG, log2 fold, in green) upon miR-9 regulated expression. . Target:miRNA ratios were determined by computing both endogenous miR-9 targets (TG_3C) and target dGFP.

4.5. MiRNA decay and structural heterogeneity

4.5.1. IsomiRs are a sizable fraction in the decay dataset and enriched in fast decaying miRNAs

Thanks to the application of high-throughput sequencing to miRNA analysis we have recently discovered that sequences of miRNAs are quite heterogeneous and result into multiple isoforms (Neilsen et al. 2012), called "isomiRs" (see section "Determination and nomenclature of IsomiRs in Introduction). Certain isomiRs, such has shortened form (trimmed isomiRs) or urydilated forms, have been also linked to miRNA degradation and to target-mediated mechanisms (Ameres et al. 2010; Kim et al. 2010; Baccarini et al. 2011; de la Mata et al. 2015). We, thus, decided to investigate isomiRs in our decay dataset by exploiting an in-house bioinformatic tool, called IsomiRage tool (Muller et al. 2014), which has been developed in our lab to deconvolute miRNA sequence complexity from next-generation sequencing experiments. We categorized isomiRs into 4 classes: i) canonical miRs, which refer to canonical miRNA sequence plus those variants produced by imprecision processing events (defined as 'templated' variants, wince share the same precursor template), ii) 3' non-templated miRs (3'NT), which have nucleotide/s added ad the 3'-end as consequence of a tailing event (also known as 'tailing isoforms'), iii) 5' non-templated miRs (3'NT), which have nucleotide/s added ad the 5' end forms, and iv) trimmed isoforms (TRIM), produced by shortening.

We globally looked at the expression of miRNA isoforms in the decay dataset (Table 4). As expected, the canonical and templated forms represent the majority, with tailing (3'-NT) and trimming forms also significantly represented (>25%,**Figure 61-LEFT PANEL**). 5' variants (5'-NT) are instead very rare, as they generally associate with an alternative 'seed' and, hence, different target repertoire. As usual, adenylation and urydilation events were prevalent among 3'-NT isomiRs (**Figure 61-RIGHT PANEL**).

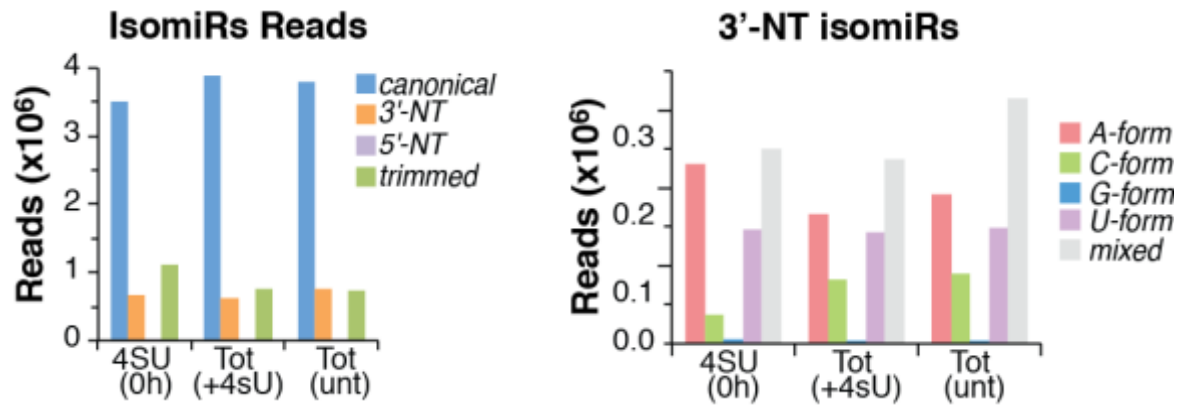

Figure 61. IsomiRs mapped reads in the decay dataset. **LEFT PANEL**- Shown are the number of mapped reads (average of three independent experiments) for canonical miRNAs or miRNA variants in the decay dataset. MiRNA isoforms were further distinguished into 5'-end non-templated (5'-NT), 3'-end non-templated (3'-NT) and trimmed forms. **RIGHT PANEL**-. 3'-end non-templated (3'-NT) forms were further distinguished according to the type of nucleotide added into A-, C-, G-, U- forms plus mixed variants (which contain more than one attached nucleotide type making impossible origin determination). Shown are the data of small-RNA sequencing from 4sU RNA (4sU - 0h), or total RNA isolated from cell with (Tot, +4sU) or without (Tot, unt) 4sU administration (300 μM, 3hrs)

We next looked at the relative distribution of isomiRs within decay classes. On average, tailing (3'-NT) and trimming contributed to 11.9% and 15.1% on the global composition, respectively (**Figure 62**, "All guide", N=129). If we just focus on 'fast' miRNAs, the distribution is significantly different, with enrichment in both tailing and trimming variants **(Figure 62,** "**FAST**"; p<0.001). Among 3'-NT isomiRs, both adenylation and urydilation was enriched in fast decaying species. No significant differences in the average composition were observed for slow decaying miRNAs, with a slight depletion in trimming variants. Of note, trimmed and tailed variants (adenylation and urydilation in particular) are exactly the forms that associated to miRNA degradation. Hence, such distribution is coherent with the hypothesis that fast miRNAs are more subjected to degradation than slow miRNAs. We termed such modification as 'decay-associated' isomiRs.

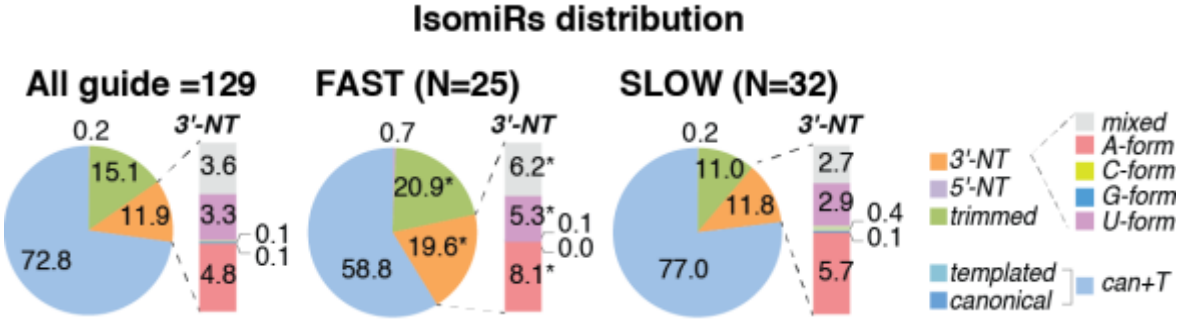

Figure 62. IsomiRs distribution in decay classes. The pie charts show the frequency of isomiRs for all the guide miRNAs included in the decay dataset, or just those of the 'fast' and 'slow' subsets. Data refers to the average of three independent sequencing experiments. Asterisks mark significant values (p<0.001, paired T-test).

We decided for a closer inspection of decay-associated isoforms. We found that most, but not all fast decaying miRNAs showed high levels of tailing (3-NT/TOT **Figure 63-LEFT PANEL**, p=0.0061), with 19/25 fast miRNAs falling in the top 50% tailing distribution (**Figure 63-RIGHT**

PANEL, p=0.0235). We did similar observations for trimming, with high levels of trimmed forms (p=0.0061,**Figure 64-LEFT PANEL**) and a high trimming frequency (**Figure 64-RIGHT PANEL,** p=0.0069) among 'fast' miRNAs.

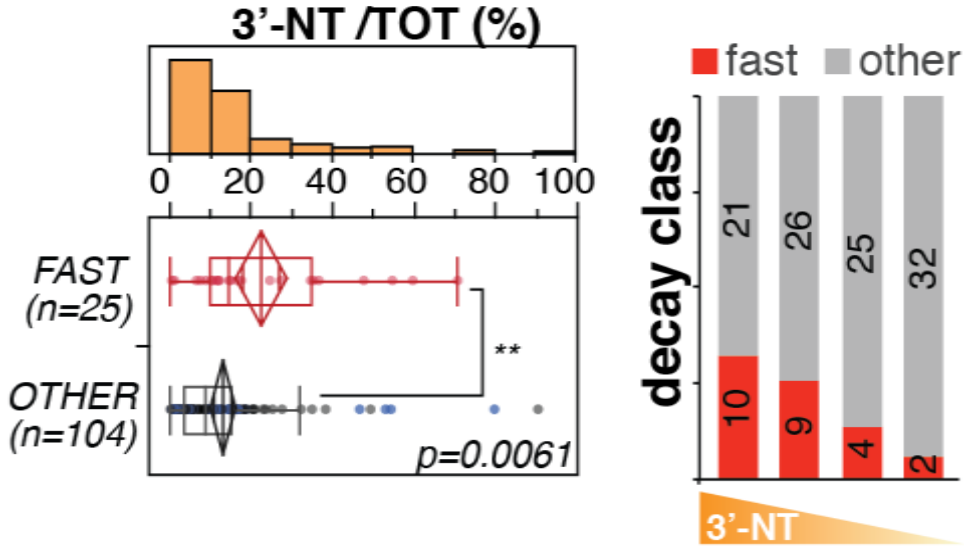

Figure 63 Correlation analysis between 3NT/TOT ratio and decay. **LEFT PANEL**-Distribution of 3'-NT isoforms in 'fast' miRNAs as compared to non-fast miRNAs. Asterisks mark significant values (**=p<0.01, Wilcoxon-test. Red and blue dots represent fast and slow miRNAs. **RIGHT PANEL**-Guide miRNAs were distinguished into classes (quartiles) according to the amount of 3'-NT modifications and correlated with 'fast' decay by contingency analysis (3'-NT Chi2=9.6, p=0.0235)

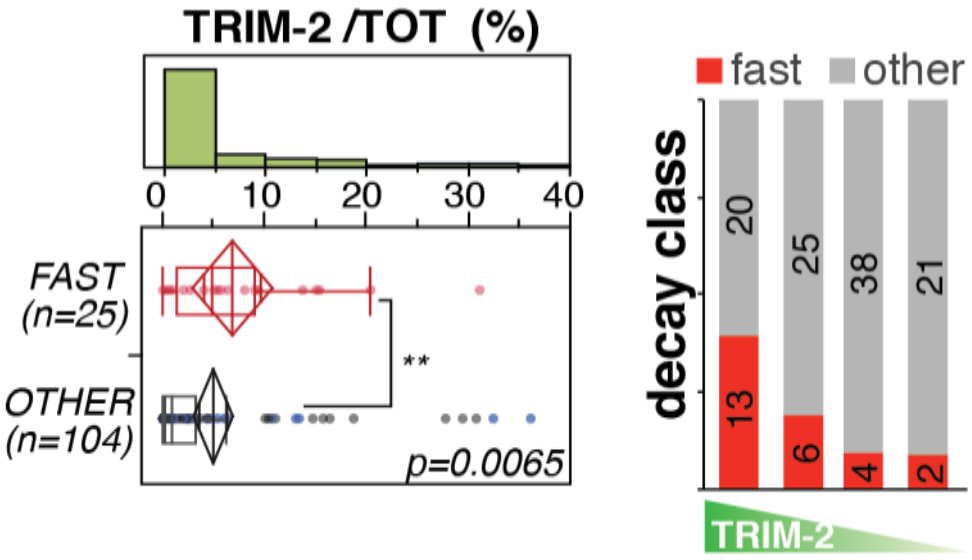

Figure 64. Correlation analysis between TRIM/TOT ratio and decay. **LEFT PANEL**-Distribution of trimmed isoforms ('Trim-2', which includes only species shortened by at least two bases), in 'fast' miRNAs as compared to non-fast miRNAs. Asterisks mark significant values (**=p<0.01, Wilcoxon-test) RIGHT-Guide miRNAs were distinguished into classes (quartiles) according to the amount of Trim-2 modifications and correlated with 'fast' decay by contingency analysis (Trim-2 Chi^2=12.1, p=0.0069).

It has been reported that tailing and trimming might be simultaneously present (Ameres et al. 2010). Indeed, we found that co-occurrence of these events was significantly high (**Figure 65-**

LEFT PANEL, p=0.0270), confirming that the two phenomena could be associated. To this respect, we found 15/25 (60%) 'fast' miRNAs, but only 8/32 (25%) 'slow' miRNAs, having a combination of high tailing and trimming (**Figure 65-RIGHT PANEL**, p=0.005).

These results indicate tailing and trimming as degradation intermediates in miRNA decay pathway.

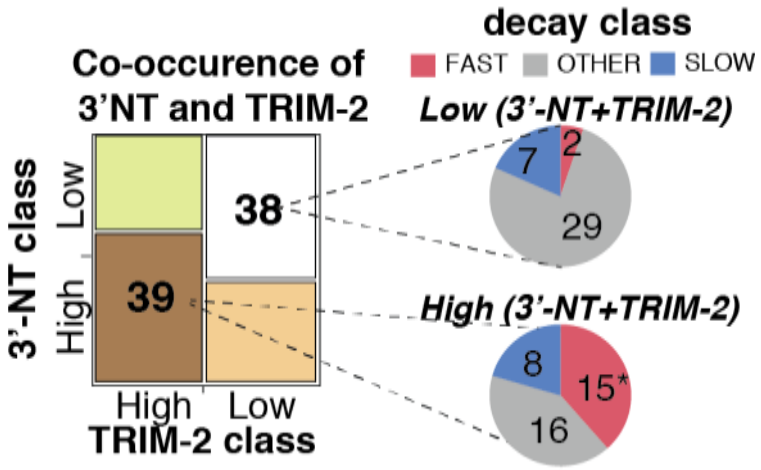

Figure 65. Co-occurrence of 3'-NT and Trim-2 modifications. **LEFT PANEL** Shown is the co-occurrence of tailing and trimming (Chi2=5.35, p=0.0207). **RIGHT PANEL** The two classes with concordant "high" or "low" tailing/trimming are highlighted and further distinguished by decay classes. Asterisks mark significant values (**=p<0.01, contingency test)

4.5.2. 3p- and 5p- arm isomiRs reveal specific features in tailing and trimming

Mature miRNAs could derive from any of the two arms of the pre-miRNA (hairpin structure), called 5p- and 3p- arm, for their proximity to 5'end and 3'end, respectively. This implies that the 3'-end is generated either in the nucleus by the Microprocessor (3p miRNAs) or in the cytosol by Dicer (5p miRNAs). We exploited this feature to assess whether the decay-associated modifications occur while miRNAs are in the nucleus or in the cytosol. Focused on the frequency of trimming between 5p and 3p miRNAs (**Figure 66-UPPER PANEL**) we did not observe any preferential differences, suggesting that this modification likely occurs in the cytosol on mature molecules, as previously shown (Krol et al. 2010b). On the contrary, 3'-NT modifications were more frequent for 3p miRNAs (**Figure 66-UPPER PANEL**, p=0.0012), implying that some tailing events might also occur in the nucleus at the level of the pre-miRNAs. This correlation was almost exclusively restricted to uridylation (**Figure 66-LOWER PANEL** "3'NT (U)", p=0.0144) and might be ascribed to the nuclear terminal uridylyl transferases (TUTase) (Krol et al. 2010b) (Lin and Gregory 2015). Conversely, adenylation, the most frequent tailing event in our cells, was

similar for 5p and 3p miRNAs, and likely occurs in the cytosol, as previously suggested (Lee et al. 2014).

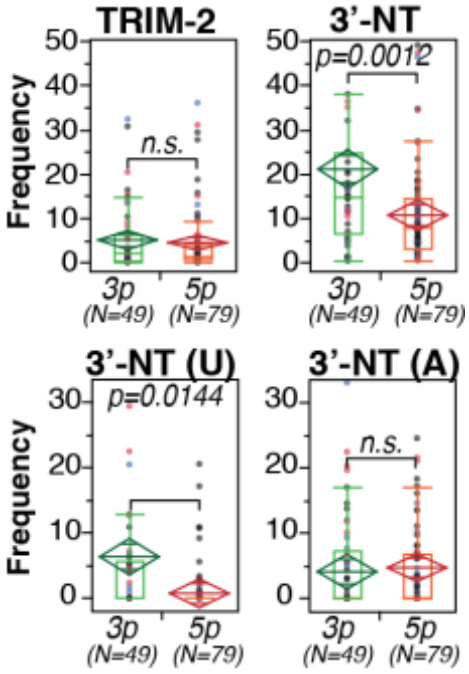

Figure 66. Frequency of 3'-NT or Trim-2 modifications. **UPPER PANEL** miRNAs were distinguished by arm type (3p or 5p) and frequency of Trim-2 and 3-NT was assessed. **LOWER PANEL** 3'-NT forms were further distinguished in uridylated (U) or adenylated (A) variants. Red and blue dots represent fast and slow miRNAs

4.5.3. Tailing and trimming occur directly on miRNAs loaded on Ago2

We, then, speculated that tailing and trimming might occurs while miRNAs are on the Ago and interact with the RNA targets, as previously suggested (De et al. 2013; de la Mata et al. 2015), further supporting the target-mediated decay mechanisms. We then performed small RNA sequencing on Ago2 bound RNA isolated by immunoprecipitation experiments (Ago2-RIP). As negative control, we used RNA bound to immunoglobulin (IgG), which could not precipitate Argonaute (**Figure 67**) and produced very few miRNA reads, as expected. As positive control we used total RNA ('input' of the IP). Of note, Ago2 bound miRNAs closely resembled the cellular total pool (**Figure 68,** R^2=0.91), confirming that miRNAs in cells are mostly loaded on Ago2.

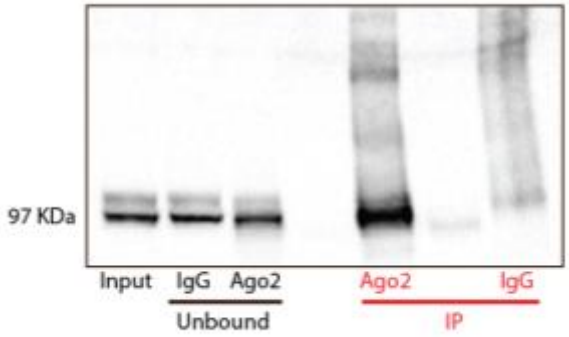

Figure 67. Western Blot of Ago2 IP. Shown is the western blot of Ago2-IP. In each lane has been loaded the same amount of protein content (5% of IP= 250K cells). Unbound fractions refer to wash through after antibody incubation.

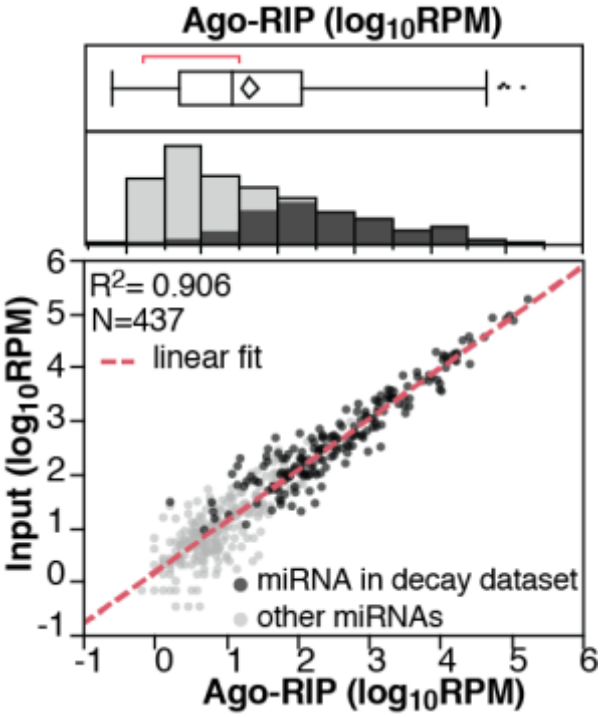

Figure 68- Ago-RIP reads scatter plot. The scatter plot shows the expression values of miRNAs from Ago2-RIP experiments as compared to total RNA ('input'). A total of 437 miRNAs were expressed above the threshold (>10reads) and considered in the analysis. Values are averages of three independent experiments. A red dashed line highlights the linear correlation (R2= 0.906). Dark gray dots mark miRNAs in common with the decay dataset.

Then, we investigated decay properties on Ago2-bound miRNAs. 'Fast' miRNAs neither displayed a different abundance on Ago2 (**Figure 69-UPPER PANEL**), nor were differently loaded (Ago2/Input ratio, **Figure 69-LOWER PANEL**) as compared to slow decay group, suggesting that the fast decay is not due to poor loading on the RISC complex.

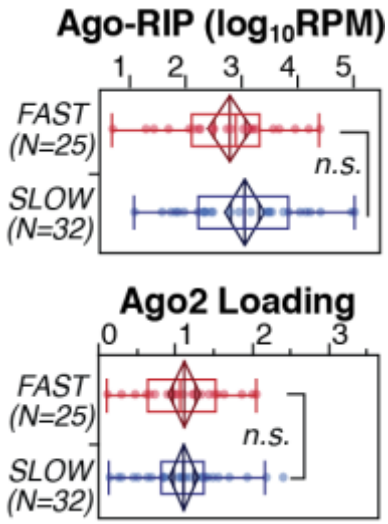

Figure 69. Ago2-IP loading analysis. Abundance (**UPPER PANEL**, RPM – reads per million, log scale) and loading efficiency (**LOWER PANEL**, Ago2/Input log2 ratio) of 'fast' and 'slow' miRNAs associated to Ago2, as measured by Ago2-RIP. Data are the average of three independent biological experiments. P-values were calculated by Wilcoxon-test.

Exploiting the IsomiRage pipeline, we looked at isomiRs distribution on Ago2. We found it was very similar to the one of total RNA (input) and confirmed the enrichment for decay-associated forms (trimmed and 3'-NT species) among "fast" miRNAs (**Figure 70**). Conversely, "slow" miRNAs were depleted of such isoforms.

Taken together, these results suggest that enzymatic activities able to modify miRNA 3' ends are in place and mediate miRNA degradation. Modifications likely occur in the cytosol while miRNAs are loaded on the Ago and could interact with their RNA targets.

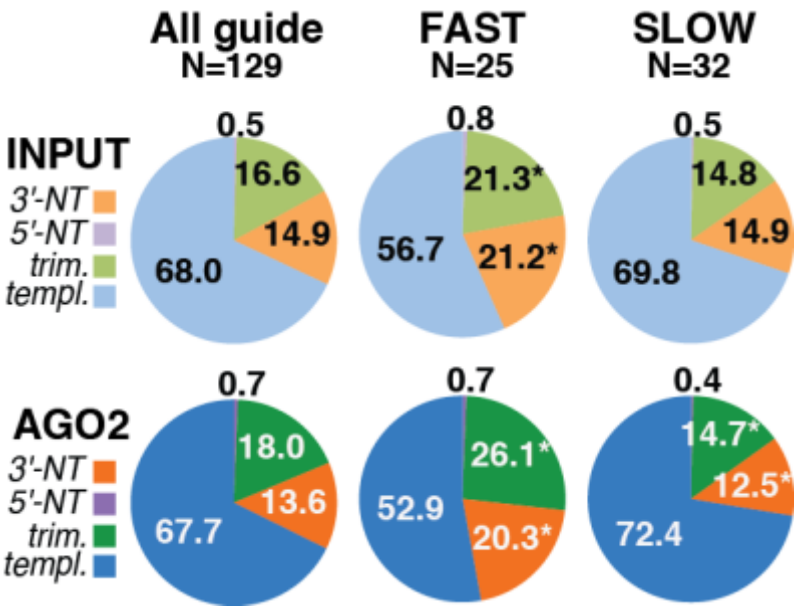

Figure 70. Ago2-loaded isomiRs distribution in decay classes. The pie charts show the frequency of isomiRs in the Ago2-RIP ("Ago2") experiments as compared to the total RNA ("Input"), used as input. Asterisks mark significant values ($p<0.001$, paired T-test).

4.6. miRNA decay and miRNA regulation in serum-induced cell cycle re-entry

4.6.1. miRNA downregulated in G1-S transition are fast decaying miRNAs

So far, we have investigated miRNA decay and its implication during a steady-state condition, on exponentially growing cells. We, then, decided to move to a dynamic situation, where miRNA expression could be regulated upon a stimulus. Such condition will be ideal to verify most of the conclusion made so far and to understand more directly the impact of miRNA decay into miRNA regulation. We decided to investigate the serum stimulation of quiescent fibroblasts (Figure 71). This is a physiological process, which involves fibroblasts (as 3T9 cells) and produce a consistent change in gene and miRNA expression (Rissland et al. 2011)in absence of cell division (α=0), thus miRNA dilution is negligible.

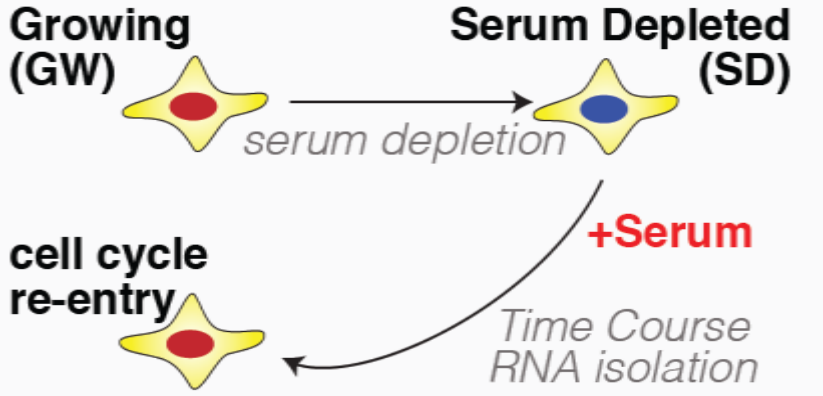

Figure 71- Schematic representation of the serum stimulation model in 3T9 mouse fibroblasts.

We grew 3T9 fibroblasts at low density (<70%), minimizing the effects of cell density on miRNA processing (Hwang et al. 2007; Mori et al. 2014). Next, we induced quiescence by serum depletion cells for 72h and stimulated cell cycle re-entry through serum, collecting samples every 2hr up to 12h, when cells enter into S-phase (as monitored by BrdU incorporation assay, **Figure 72-LEFT PANEL**). The entire time course has been repeated twice. We checked the serum stimulation also by looking at marker genes, such as early (FOSB and MYC) and late (CCNE1, UHRF1 and MCM6) serum-induced genes (**Figure 72-RIGHT PANEL**).

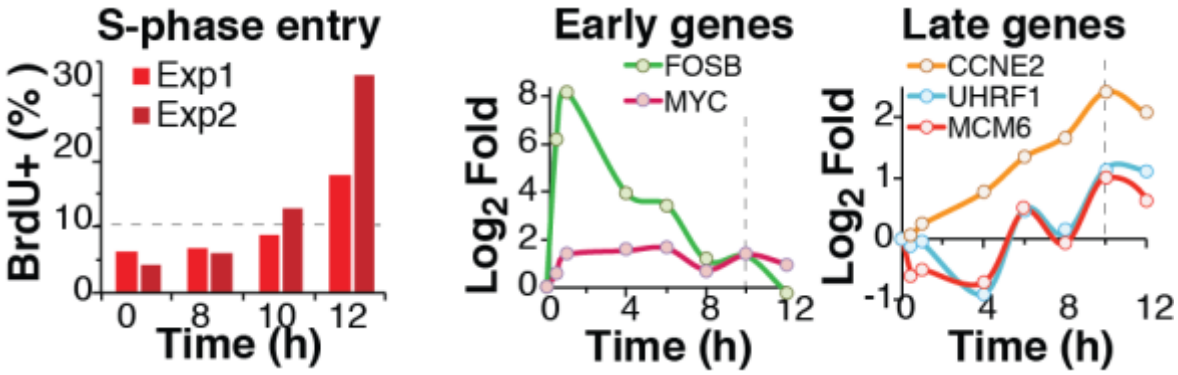

Figure 72. Analysis of G0-G1 transition. **LEFT PANEL**-The bar graph shows the quantification of cell-cycle re-entry induced upon serum stimulation by BrdU incorporation in two independent experiments. The expression of early (**MIDDLE PANEL)** and late (**RIGHT PANEL**) serum response genes has been measured along the time course of serum stimulation. The data are representative of one out of two independent experiments. A dashed line marks he G1/S transition boundary, as determined by BrdU assay.

We analyzed miRNA expression through small RNA sequencing, isolating a group of serum-regulated miRNAs (N=52, Table 5) consistent in the two experiments and in line with previous observations (Bueno et al. 2010). We normalized data both by library size and taking into account the RNA content per cell, which increase during serum stimulation and must be considered to avoid misinterpretation of gene regulation. We isolated a module of serum-induced miRNAs ("Up", N=39) and a module of serum-repressed miRNAs ("Down", N=13), whose down-regulation was observed even when data were normalized for RNA amplification induced by serum (**Figure 73**).

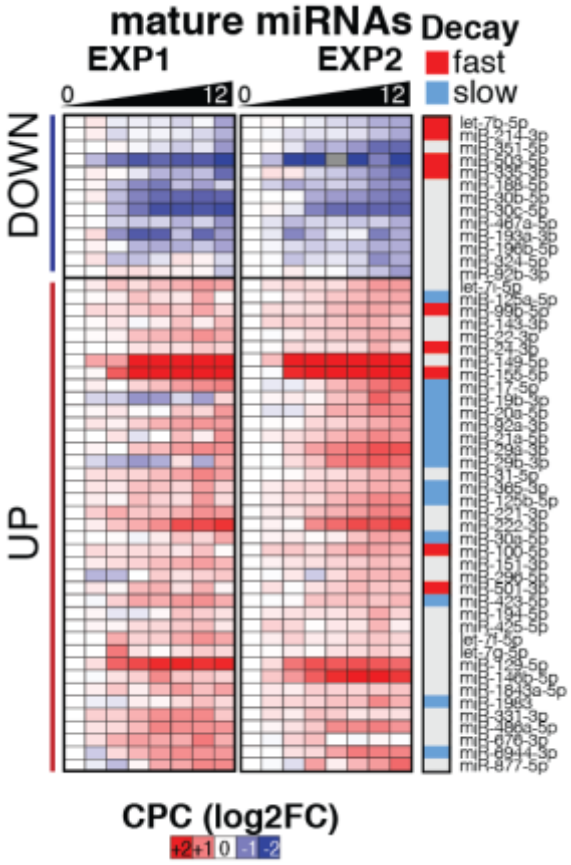

Figure 73. The serum signature. Heat-map shows fold-change (log2) of serum-regulated miRNAs (n=52) along the time course (0-12 hours) in two independent experiments. 'Fast' and 'Slow' decay miRNAs are highlighted by a color code.

We speculated that the downregulated miRNAs should have a 'fast' decay behavior in order to be downregulated in just few hours, without cell dilution effects. Indeed, the "down" group was completely depleted of "slow" miRNA and significantly enriched for 'fast' species (**Figure 74-LEFT PANEL**). When we analyzed the half-lives directly, we observed that the "down" group displayed substantially shorter half-lives (**Figure 74-RIGHT PANEL**, $p<0.01$), compatible with the kinetic of cell cycle re-entry (i.e. within 10-12 hours). This suggests that miRNA decays are, indeed, playing an important role in miRNA regulation.

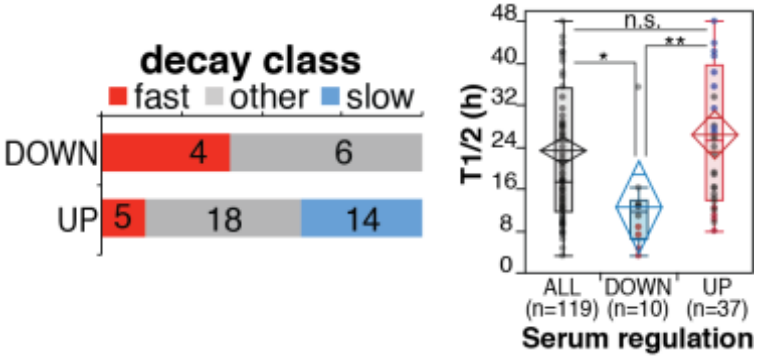

Figure 74. Correlation analysis of serum signature and decay classes. **LEFT PANEL**-Distribution of serum-regulated miRNAs within decay class has been analyzed by contingency (Chi=9.3, p=0.0096). **RIGHT PANEL**- Distribution of miRNAs half-lives (T1/2) within classes of serum-regulated miRNAs. The "ALL" class (N=119) contains all the common miRNAs of the serum-regulation and decay datasets

Next, we measured transcription rates of miRNA loci during serum stimulation (**Figure 75** and Table 5), using the same approach described previously (see **Figure 44**) by exploiting RNA sequencing on total and 4sU RNA (short pulse) and ad-hoc bioinformatics tools (de Pretis et al. 2015). Most of miRNAs changes could be ascribed to concomitant coherent variations in the synthesis rate of pri-miRNAs although in some cases (4/10, for instance miR-30a/c2 or miR-30b/d, **Figure 75** and **Figure 76**) we observed miRNA downregulation with no evidence of a significant reduction in the transcription rate, suggesting the presence of an active and dynamic mechanism of degradation.

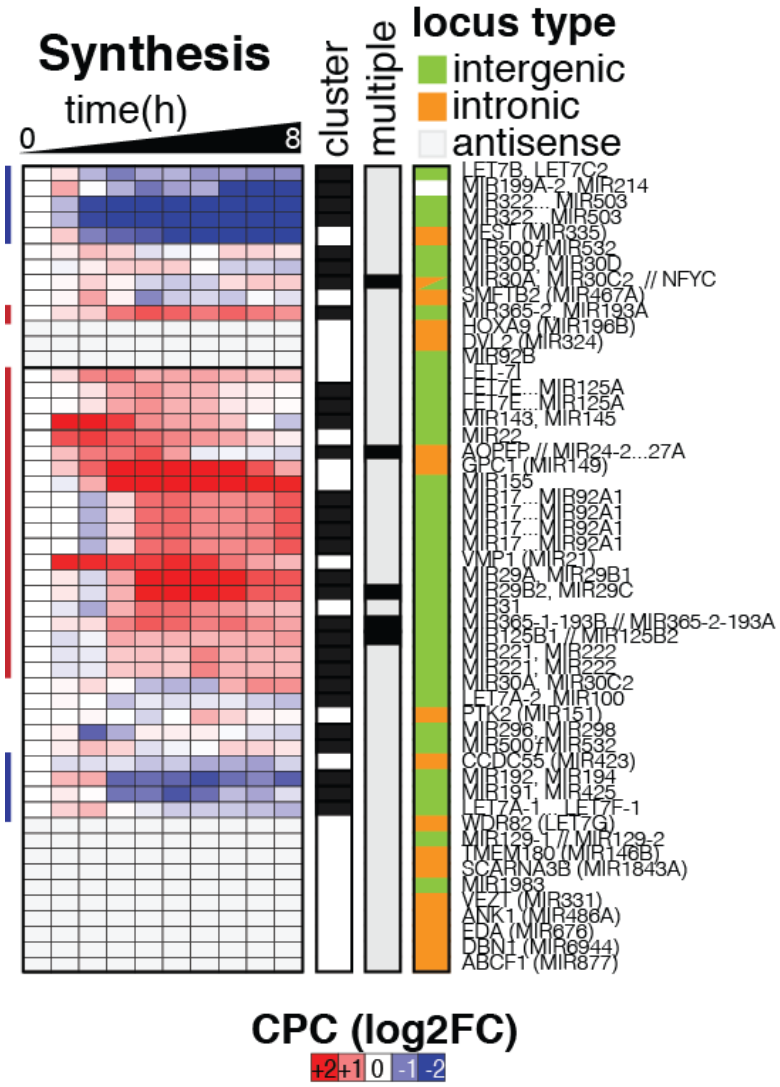

Figure 75. miRNA synthesis rates in serum stimulation. The heat-map shows the variation of miRNA primary transcripts (pri-miRs) along the time-course. Transcription of pri-miRs at each time point has been calculated as described previously (see *Figure 44*). Data are expressed as log2 fold change over the 0hrs time points. A color code highlights the decay of miRNAs plus the type of miRNA locus (intergenic, intronic and antisense)

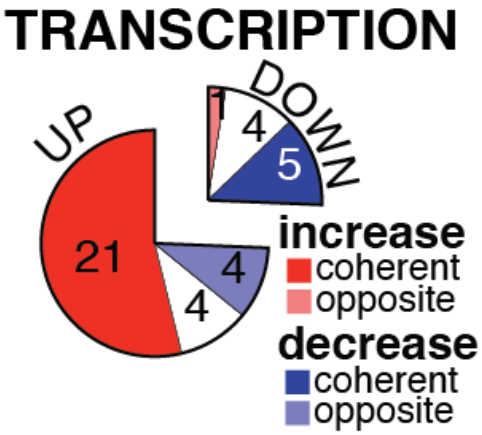

Figure 76. Coherent and opposite behaviors of miRNA transcription rate in G0-G1 transition. A pie chart summarizes the number of miRNAs with changes in transcription (Chi=12.8, p=0.0017; Contingency test) within classes of serum-regulated miRNAs

4.6.2. IsomiRs signature in serum stimulation mirrors miRNA dynamic regulation

We previously described an accumulation of decay-associated miRNA isoforms (3'-NT and trimmed) for 'fast' decaying miRNAs. Thus, we characterized isomiRs upon serum stimulation looking for dynamic regulation of tailing and trimming that could highlight the regulation of miRNAs along the time-course (**Figure 77**). We found a significant increase in the distribution of tailing and trimming forms for "down" miRNAs, which follow their dynamics of regulation. Similarly, a decrease in decay-associated isomiRs, more evident for trimming forms, emerged for "up" miRNAs **(Figure 78**).

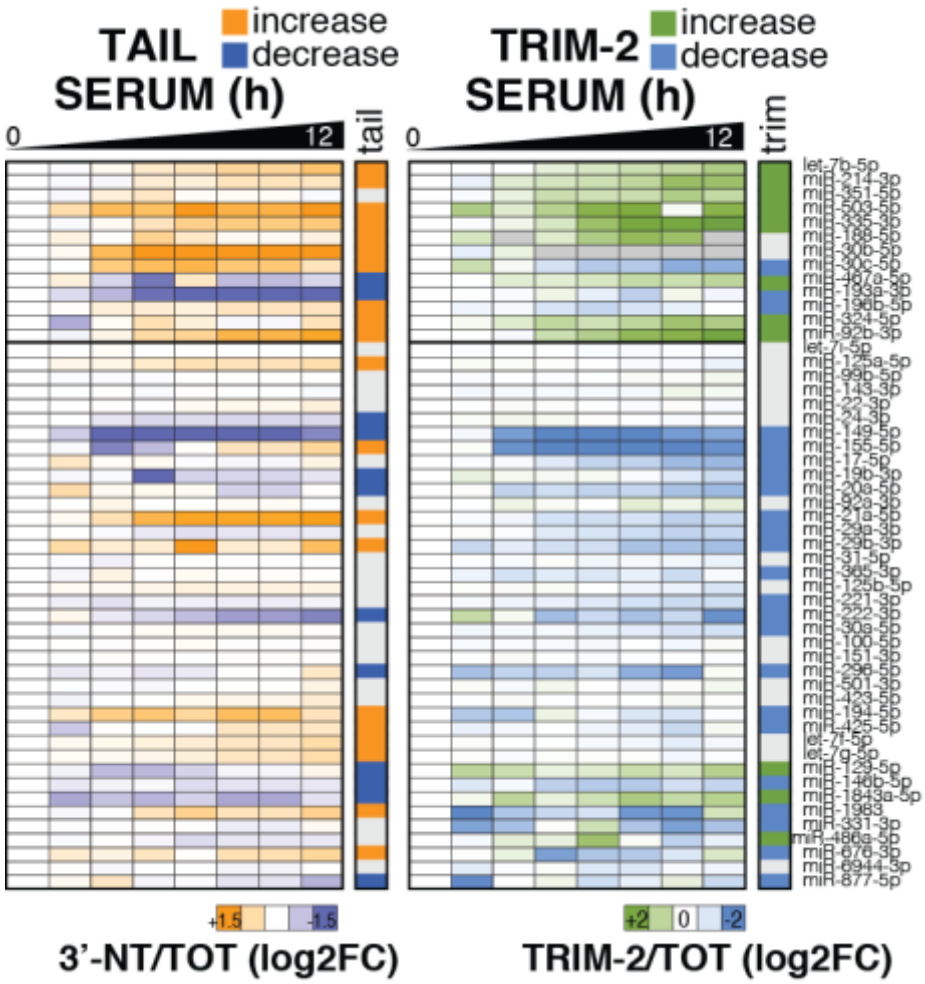

Figure 77. Tailing and trimming in serum stimulation. Heat-maps show the variation of tailing (3'-NT/TOT, LEFT) and trimming (TRIM-2/TOT,RIGHT) frequencies along the time-course.

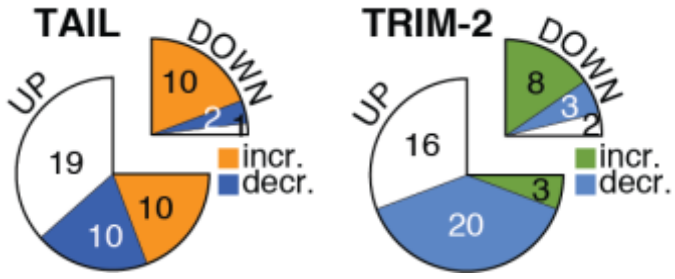

Figure 78. Tailing and Trimming enrichment in serum signature. The pie charts show number of miRNAs with changes in tailing (Chi=12.0, p=0.0025) and trimming (Chi=15.2, p=0.0005) within classes of serum-regulated miRNAs.

Some specific examples are shown below, putting together miRNA regulation (Total – T), trimming and tailing distribution (3NT/T and TRIM2/T) and transcription rate (CPC/h) along the time course (**Figure 79**). It clearly appears that fluctuations in tailed and trimmed forms were the mirror image of the regulation of miRNA. Down-regulated miRNAs (miR-30b-5p and let-7b-5p, **Figure 79-UPPER PANEL**) accumulated decay forms in the time course, while up-regulated species (miR-155-5p and miR-221-3p **Figure 79-LOWER PANEL**) are depleted for such forms.

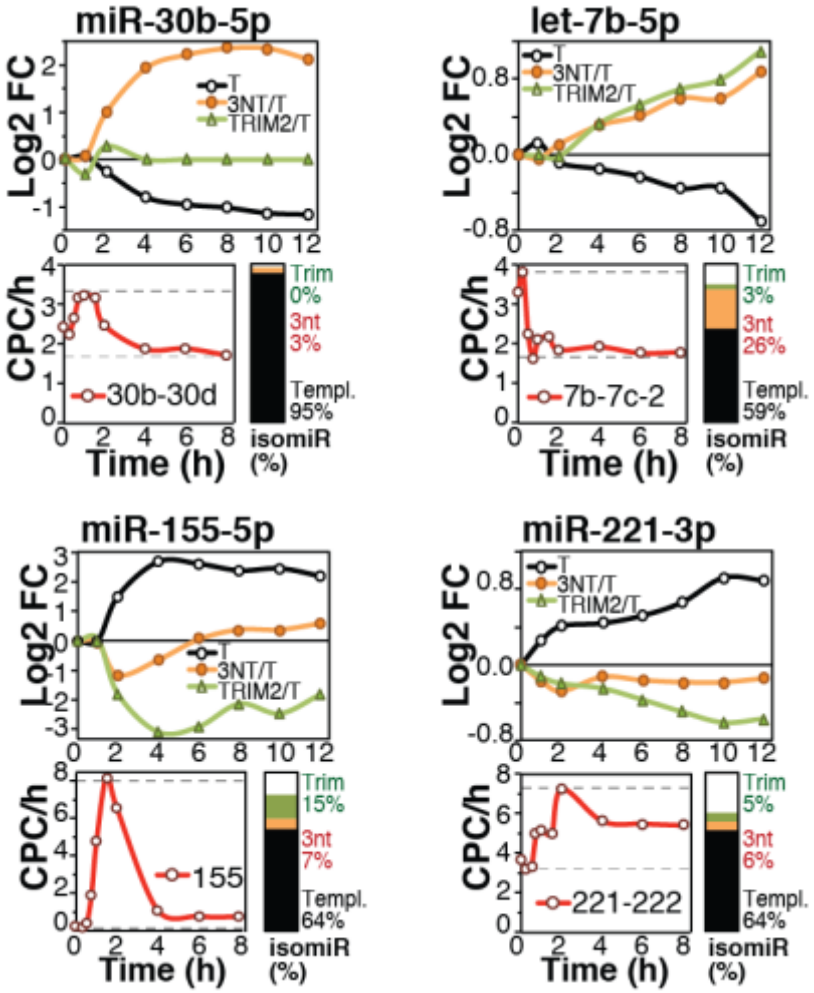

Figure 79. Examples of miRNA regulation in serum stimulation. Representative examples of 'Down' (miR-30b-5p andlet-7b-5p, **UPPER PANEL**) and 'Up' (miR-155-5' and miR-221-3p, **LOWER PANEL**) serum-regulated miRNAs are shown. For each miRNA is reported the regulation of templated (T), tailed (3'-NT/TOT) and trimmed (TRIM-2/TOT) forms, along with the changes of the primary transcript (below, in red and measured as CPC/h). A bar plot summarizes the frequency of each miRNA isoform.

A couple of observation could be also made. In case of miR-30b, the downregulation of the miRNA is not accompanied by a clear shut-off of transcription, suggesting that active degradation mechanisms might be in place, something we will discuss more deeply later. In case of miR-155, instead, we observed a strong peak of transcriptional activation at 2hrs post stimulation (**Figure 79-LOWER PANEL**) immediately quenched, similar to the transcriptional activation of immediate early serum response gene (i.e. jun and fos). This is translated into a rapid increase of miRNA total levels, with a time shift of few hours (compatible with the maturation process), afterwards miR-155 levels declined by decay. This situation reminds the stage C described in the model (**Figure 43**), when transcription is off and just miRNA degradation occurs. Hence, we modeled endogenous miR-155 decay using absolute expression values obtained from the time course (from 4 to 12 hrs). The half-life of miR-155 turned to be of 10.5 hours, in very good agreement with what has been

measured by the 4sU pulse-chase (12.3 hours, Table 1), further confirming the significance of the decay rate we identified.

4.6.3. Targets accumulation and miRNA downregulation significantly associate in serum response

We also followed miRNA targets along the time course of cell cycle re-entry, looking if it was somehow related to miRNA regulation and decay behavior. As previously, we exploited RNA-seq data and retrieved the expression of miRNA target genes (TG). We took advantage of the pipeline showed in (**Figure 51**) to retrieve either seed, 3C.03 and 3C.05 targets, expressed as absolute copies.

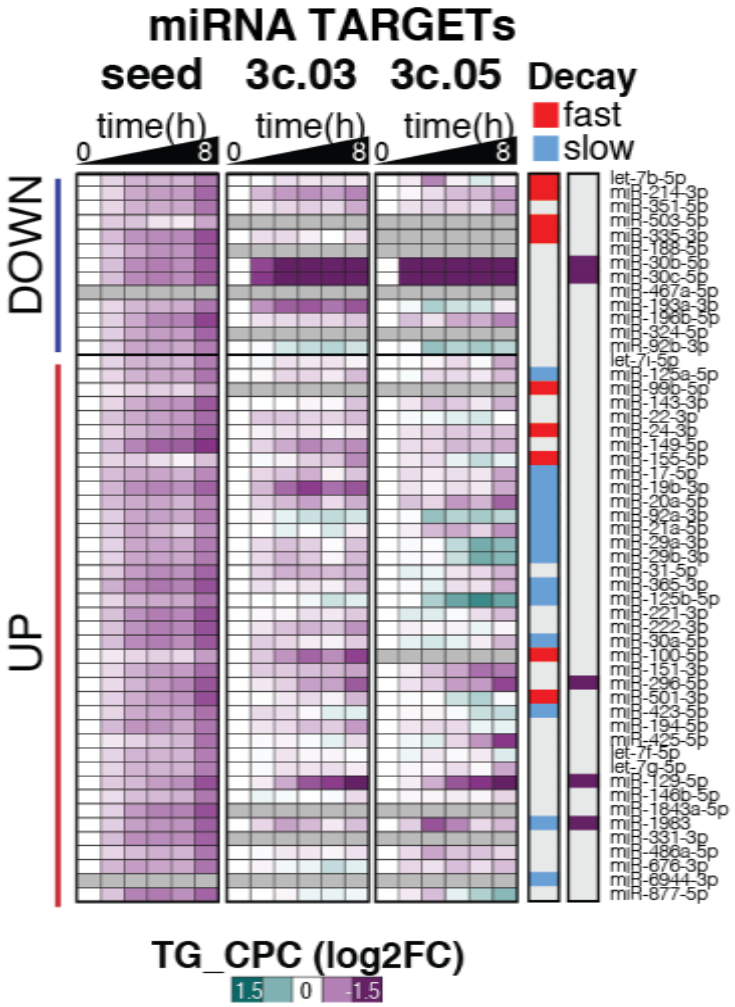

Figure 80. Targets expression in serum stimulation. The heat-maps show the fluctuations of miRNA targets along the time-course of serum stimulation, as in panel D. Targets were further distinguished according to the complementarity to the miRNA 3' end: TG_seed, seed interaction; TG_3C, seed plus 3' compensatory site with partial (3C.03) or extensive (3C.05) interaction

As shown in the heat-map (**Figure 80**), we observed a trend of increase in the expression of seed targets, which is common for all miRNAs and independent from their regulation. This effect is due

to the amplification of RNA content, which typically occurs while cells move from G0 to G1. However, when considering targets with 3' compensatory binding, we lost such general trend of accumulation as we were considering fewer and more specific targets. By plotting the distribution of targets by classes of regulation (down, up and all miRNAs), we observed a specific increase just for targets of 'Down' miRNAs that became more significant when considering "3C.05" target (**Figure 81**).

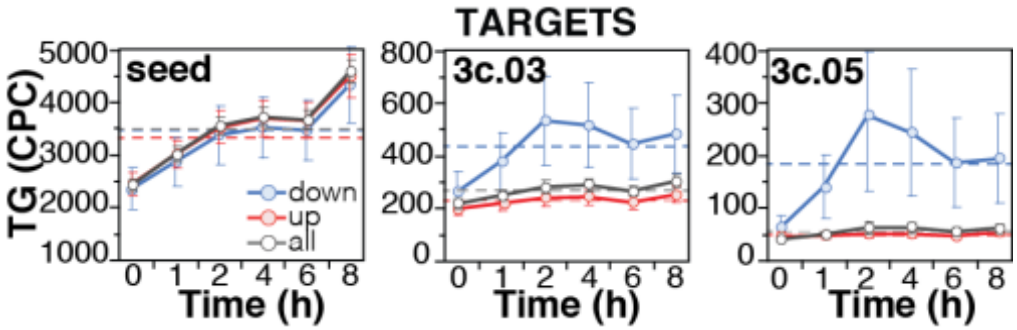

Figure 81. Targets and serum signature in serum stimulation. Mean target abundance (with s.e.m.) of downregulated (in blue), upregulated (in red) or all miRNAs (in black) along the time course of serum stimulation. Different types of complementarity are shown.

We, then, related target expression to miRNA expression by measuring Target:miRNA ratio (TPM) along the time-course (1-2-4-6-8 hrs), still distinguishing different types of complementarity. We could than appreciate that in some cases there was a change in TPM during the time course, suggesting an active mechanisms of miRNA regulation by target expression. This appears the case of miR-30b and -30c (two 'down' miRNAs), which showed a sudden increase in TPM_3C (both 3C.03 and 3C.05) soon after serum stimulation, to indicate that targets are increasing much and before miRNA downregulation. Conversely, miR-155 and miR-149 TPM_3C decreased upon serum **(Figure 82**). We noticed before that the transcription of miR-30b/30c gene locus is not much affected along the time course (see **Figure 79**), which supports the intriguing hypothesis of the induction by serum stimulation of highly complementary targets that might promote the miRNA clearance through target-induced miRNA decay (TIMD).

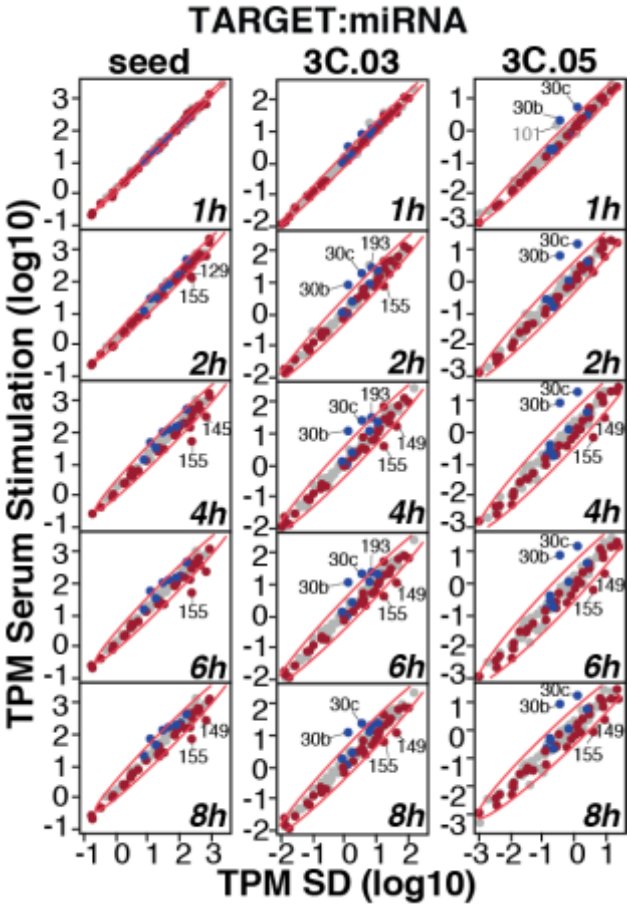

Figure 82. TPM calculation in serum stimulation. Correlation between target:miRNA ratio (TPM) in growing vs. serum depleted fibroblasts. Straight lines with shaded confidence intervals highlight the linear correlation. Targets were further distinguished according to the complementarity to the miRNA 3' end.

In conclusion, these data revealed the importance of decay mechanisms in the regulation of miRNA expression upon a physiological stimulus (serum stimulation) and highlighted the interplay between transcription, target expression, miRNA isoforms and decay in the dynamics of miRNA regulation.

4.7. CRISPR/Cas9 based approach to study miRNA:target interaction in decay mechanisms

4.7.1. Serpine1 is a candidate endogenous target for miR-30 regulation by TIMD mechanism

We showed that miRNA targets have the potential to impact on miRNA decay by a TIMD mechanism. Importantly, such mechanism has been described based on in vitro observation, on overexpression of synthetic targets or viral RNAs (Ameres et al. 2010; De et al. 2013; de la Mata et al. 2015; Haas et al. 2016). To our knowledge, no endogenous target has been shown to promote miRNA degradation in vivo. In the previous chapter, we have suggested that the regulation of miR-30b and miR-30c during serum-stimulation could be mediated by a decay mechanisms and in particular by target:miRNA interactions. In fact, upon serum stimulation levels of miR-30b and -30c were strongly down regulated during G0-G1 transition, although their transcription appeared as much unaltered. In addition, we observed a strong accumulation of decay-associated isoform and a concomitant induction of high-affinity target, in particular those with extensive 3'end complementarity. A closer inspection of such targets, revealed that one of them, Serpine1 (PAI1) was dramatically induced and very highly expressed at early time points in G0-G1 transition (**Figure 83-LEFT PANEL**). Indeed, Serpine1 accounts for up to 20% of total target pool of miR-30 family, which comes to 60-80% for 3C targets (**Figure 83-MIDDLE PANEL**). TPM values of miR-30c change accordingly during serum induction, from a nearly equimolar ratio in serum-depleted (SD) cells to a ten-times excess of targets at 4-6 hrs from stimulation (**Figure 83-RIGHT PANEL**). Based on these data, we sought to determine the impact of Serpine1 on miR-30bc regulation.

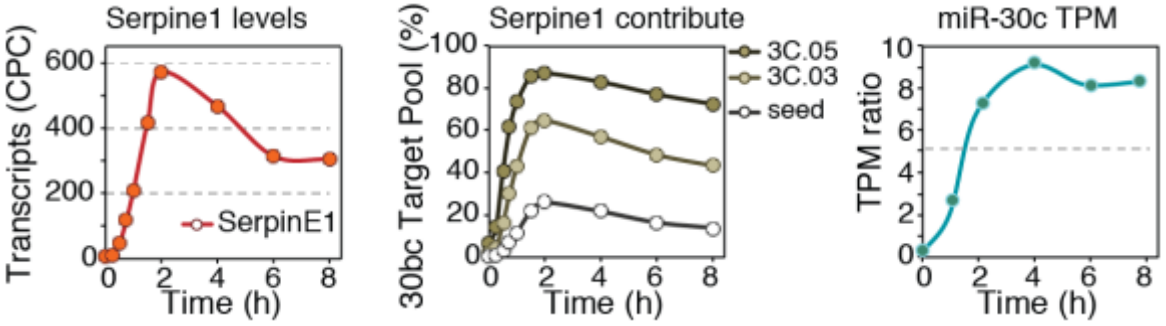

Figure 83. Serpine1 expression during serum stimulation. **LEFT PANEL**- Shown are Serpine1 levels expressed as copies per cell (CPC) upon serum induction. **MIDDLE PANEL**-Serpine1 contributes differently to total target pool of miR-30c-5p depending on the types of complementarity. Serpine1 contribution is expressed as fraction on total miR-30c target during the time course. **RIGHT PANEL**- Shown are target:miRNA ratio (TPM) for miR-30c measured at each time points of the G0-G1 transition. TPM were calculated taking into account copies of total miR-30c targets. Dashed line shows calculated TPM threshold for impacting on miR-30c degradation dynamic.

4.7.2. Generation of Serpine1-MRE30c deletion mutant exploiting CRISPR/Cas9 system

We decided to specifically interfere with Serpine1:miR-30c interaction. One possible approach is the use of shRNA-based technology, which leads to degradation of the Serpine1 transcript and lets miR-30b/c free from the binding. However, shRNAs down-regulate the entire transcript meaning that we would also interfere with Serpine1 functions, causing effects that are not specific of the miRNA:target interaction. We, hence, devised an alternative approach, based on the specific deletion of the miRNA responsive element (MRE) for miR-30bc located within the 3'-UTR of Serpine1. In such way we will not affect global levels of the endogenous transcript. To perform such specific deletion, we took advantage of CRISPR/Cas9 technology (Ran et al. 2013) (**Figure 84**).

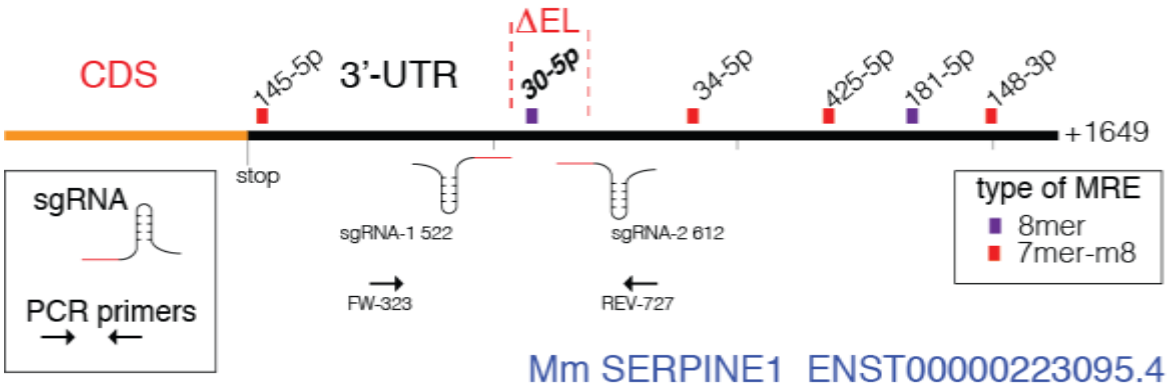

Figure 84. MRE manipulation exploiting CRISPR/Cas9 technology. Shown is the genomic context of CRISP/Cas9 editing and the binding site with affinity information of miRNAs on 3-UTR of Serpine1. sgRNA-1 and -2 have been generated for chopping position 522 and 612 of Serpine1 gene. A primer pair has been designed for detection of deletion (FW-323 and REV-727).

We set up the protocol starting from the guidelines provided by Zhang Lab: CRISPR Design Tool (http://crispr.mit.edu) (Ran et al. 2013) is used for sgRNAs selection (at least two sgRNA pairs for each MRE), which were subsequently cloned in the pSpCas9(BB)-2A-GFP (px458) vector harboring GFP marker. A detailed map is shown in **Figure 85**. We transfected 3T9 cells with Lipofectamine 3000 reagent and we FACS-sorted GFP expressing cells (top 2-3%, at 24h-48h post tfx) as single cell in several 96-well plates (for a total of 500 wells). After two weeks, growing clones (around 15%) were analyzed for microdeletions by PCR and positive clones (i.e. bearing MRE deletion) were further confirmed by DNA sequencing.

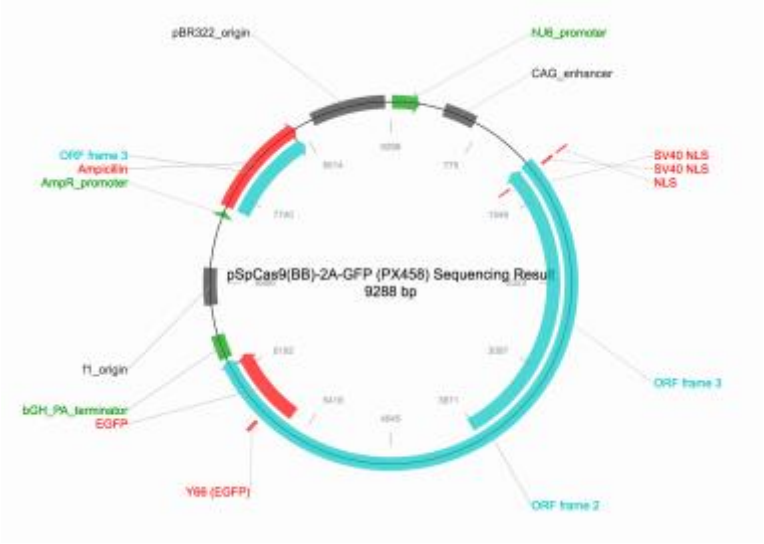

Figure 85. Vector map of pSpCas9(BB)-2A-GFP. Adapted from addgene.com

We screened more than 50 colonies and we generated both bi-allelic and mono-allelic deletions for miR-30c MRE, as showed by PCR screening (**Figure 86-UPPER PANEL**). The protocol efficiency was about 10% for mono-allelic and 2% for bi-allelic deletions. We finally isolated four clonal cell lines harboring mono-allelic (#6 and #22) and bi-allelic (#1 and #6) deletion of miR-30c MRE in Serpine1 3'UTR. We performed qPCR on extracted RNA to check the expression of Serpine1 total transcript and MRE sequence. We designed specific primers that allow monitoring the expression of normal and mutant transcripts. As expected, we found no difference in the level of Serpine1 mRNA among WT cells or the different clones, while 30c-MRE sequence expression was reduced by 50% and 100% in mono- and bi-allelic deletions, respectively, confirming that we modified MRE availability (**Figure 86-LOWER PANEL**). Thus, this strategy allows changing the TPM ratio without manipulating the expression level of the target.

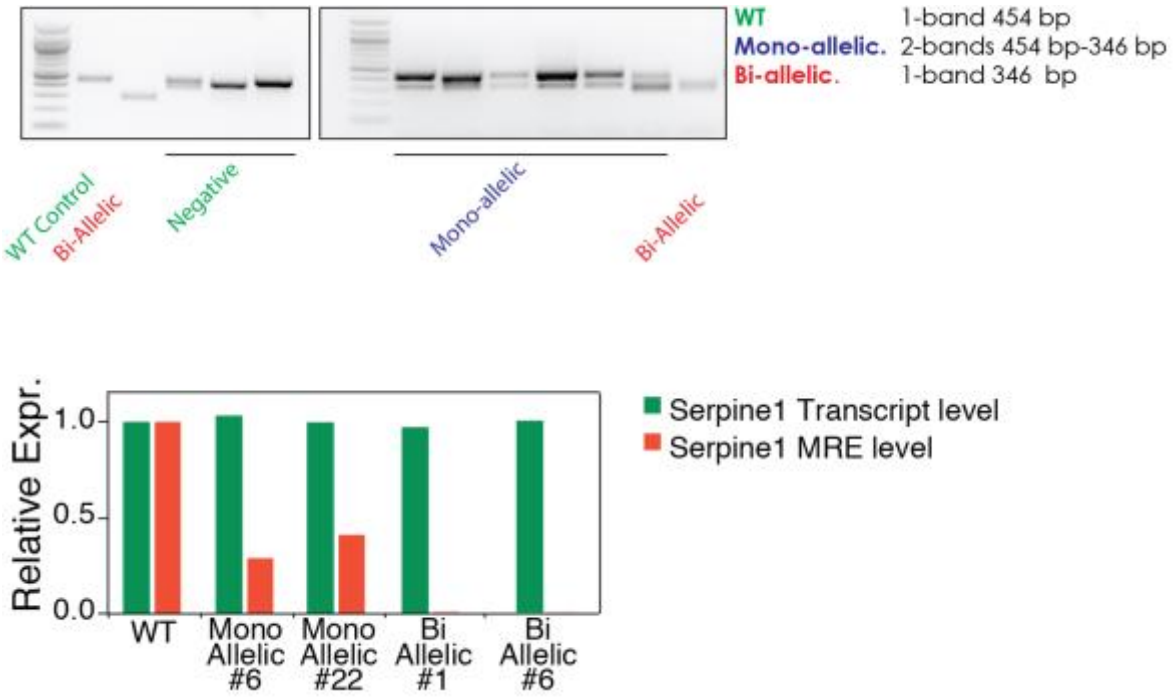

Figure 86. Mono-allelic and Bi-allelic deletion impaired level of MRE sequence. **UPPER PANEL**-Clones were checked through PCR on genomic DNA to reveal microdeletion of miR-30c MRE. Shown are single bands either for control and negative sample (454 bp) or bi-allelic clones (346 bp). Double bands for mono-allelic clones (454 and 346 bp). Agarose gel was performed at 1.5% and a PCR marker for microdeletions detection was used. **LOWER PANEL**- Total and mutant transcript levels were detected through qPCR. Primers were specifically design for distinguish Serpine1 transcript and MRE sequence respectively. Data were normalized on Rplp0 and displayed as log2 relative expression on WT sample.

We estimated the TPM values of miR-30c in serum stimulation in case of mono-allelic or bi-allelic MRE deletion. As expected, we found huge changes in Target:miRNA ratio after Serpine 1 manipulation, suggesting that TIMD might be impaired even by removing just one copy of miR-30c MRE (**Figure 87**).

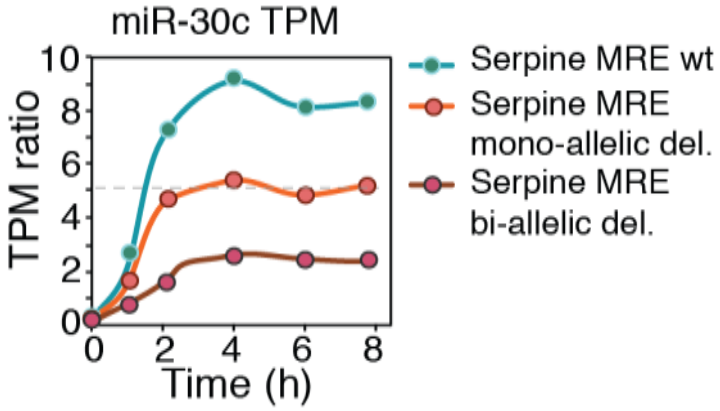

Figure 87. TPM variation during serum stimulation. Shown are target:miRNAs ratio for miR-30c measured at each time points of the G0-G1 transition. TPM were calculated taking into account copies of total miR-30c targets in three different situations when Serpine1 present: no MRE deletion, mono-allelic MRE deletion, bi-allelic MRE deletion. Dashed line shows calculated TPM threshold for impacting on miR-30c degradation dynamic.

4.7.3. Mono-allelic deletion of 30c-MRE reveals different dynamics in miR-30c regulation during serum stimulation

We performed a preliminary experiment to dissect the effect of TPM value variation on miRNA levels using the mono-allelic clones that were obtained in the initial round of screening. We analyzed miR-30c levels in steady-state conditions (growing and serum-depleted cells) and along the serum-induced cell cycle re-entry. Importantly, we focused particularly on G0-G1 transition, because it is a condition characterized by a massive up-regulation of Serpine1, which at 4hrs after stimulation reaches an expression level which might be compatible with miR-30c down regulation by TIMD, as previously showed **(Figure 87**).

We performed the experiment using two independent mono-allelic clones (#6 and #22) and the parental WT cells, in parallel. At first, we controlled the efficiency of serum stimulation by checking *Jun* and *c-Myc*, whose induction was similar among the different samples (**Figure 88**). Then, we measured the expression of Serpine1-total and Serpine1-MRE sequence levels (**Figure 89**). We found that the whole transcript was equally regulated in all samples (**Figure 89-LEFT PANEL)**, while the amount of MRE-containing transcripts was reduced, as predicted, by 50% in mono-allelic clones (**Figure 89-RIGHT PANEL**).

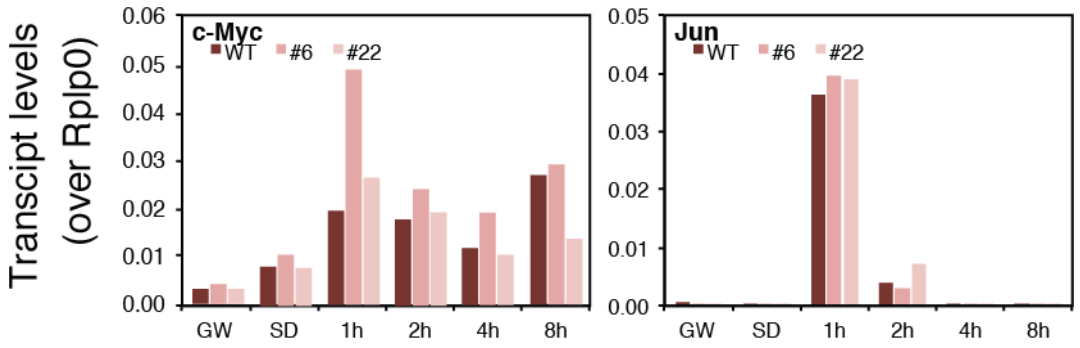

Figure 88. Early response genes to serum induction. C-Myc and Jun were analyzed as early response induced genes upon serum stimulation in normal cell population (WT) and mono-allelic clones (#6 and #22). The magnitude and and shape of the serum response is in line with previous analysis. Shown are the level of the genes in growing condition (GW) and during the time course (Serum depleted, SD to 8h post induction). Data were normalized on Rplp0 and displayed as log2 fold relative

expression.

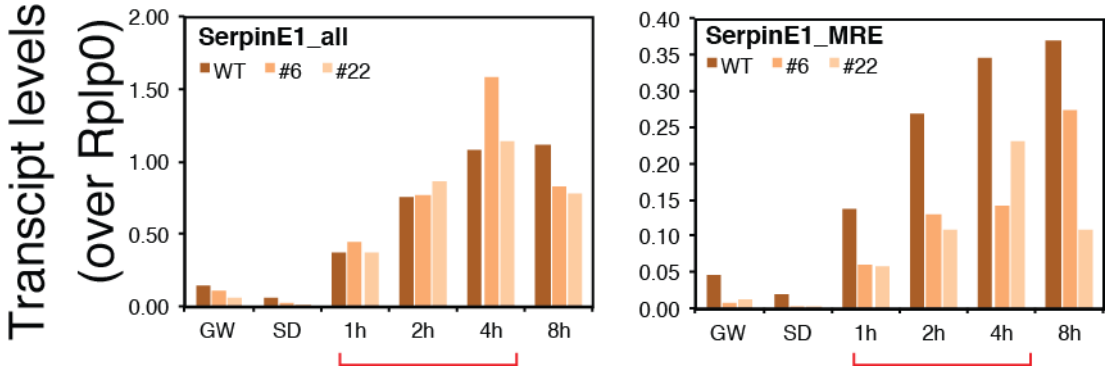

Figure 89. Serpine1 expression levels of normal cells and deletion clones. Serpine1 transcripts were analyzed with primers which specifically distinguish total (**LEFT PANEL**) and mutant (**RIGHT PANEL)** levels in normal cell population (WT) and mono-allelic clones (#6 and #22). Shown are the level of the genes in growing condition (GW) and during the time course (Serum depleted, SD to 8h post induction). Data were normalized on Rplp0 and displayed as log2 fold relative expression.

Next, we measured miRNA levels. As internal controls, we chose two unrelated miRNAs, miR-503 and miR-155, which were found to be repressed and induced by serum respectively (**Figure 73**), but whose expression should not be dependent on Serpine1 manipulation. We did not score any significant differences for both miR-503 and miR-155 in clones as compared to control cells (**Figure 90-RIGHT PANEL**). We finally assessed miR-30c levels. We observed that miRNA down regulation was slightly impaired in cells presenting the MRE deletion (**Figure 90-LEFT PANEL**). In particular, we observed an effect only in the time window 2-4 hours, which is exactly when Serpine1 reaches the maximum expression level. Of note, another miRNA of the 30 family, namely miR-30e, was profoundly affected by Serpine1-MRE deletion, suggesting that its role could be extended on other components of miR-30 family.

Other validation experiments are ongoing. We are going to use the bi-allelic deletion clones and multiple miRNAs by QPCR or Sequencing, which follows also decay-associated form to understand whether Serpine1 could specifically regulate miR-30 levels and validate the role of endogenous targets in promoting TIMD.

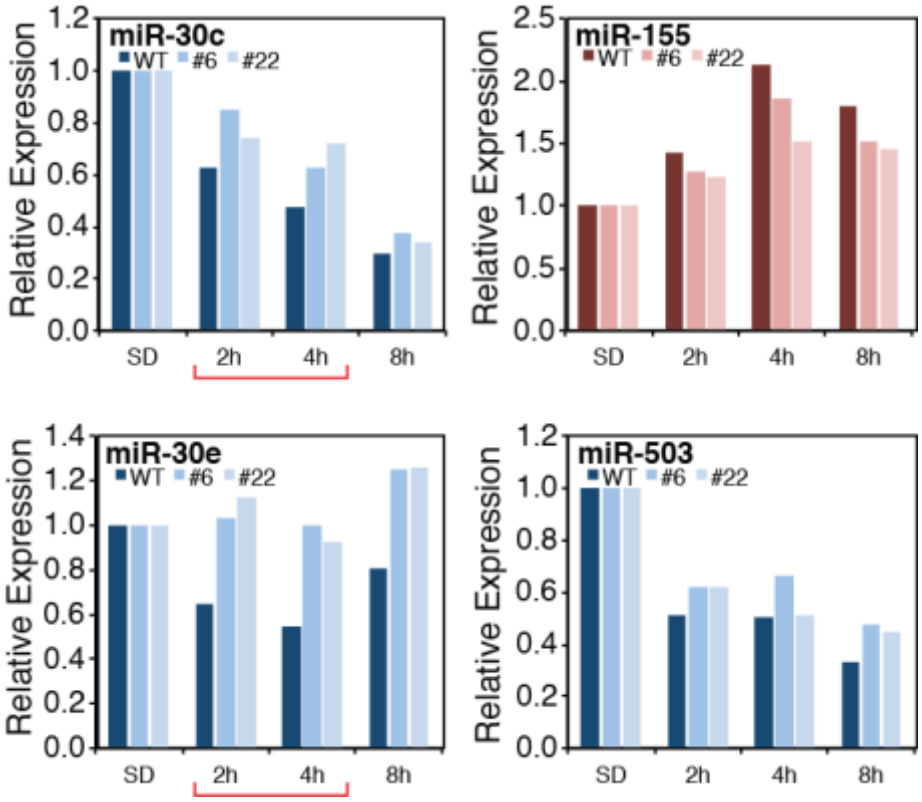

Figure 90. miRNAs response to serum induction upon MRE deletion. MiRNAs were analyzed by performing qPCR at each time points of serum stimulation in normal cell population (WT) and mono-allelic clones (#6 and #22). Data were normalized on Snord72 transcripts and are displayed as relative expression to SD. Red bars underlines the time window in which Serpine1 reaches maximum expression levels.

5. DISCUSSION

5.1 The regulation of miRNA pool is critical for cell identity

The regulation of the miRNA pool is essential for cell identity due to the important role that miRNAs exert in both physiological and pathological processes. Indeed, miRNAs have been associated to a huge number of cellular pathways such as cell cycle (Bueno et al. 2010), epithelial to mesenchymal transition (Ha and Kim 2014), differentiation (Shenoy and Blelloch 2014) and many others.

So far, the scientific community has been mainly focused on understanding how miRNAs exert their activity (i.e. repression of target mRNAs), starting from the basic view that one miRNA acts on one main target, which is related to a specific miRNA function. On the other hand, as typically miRNAs target multiple genes at the same time, alternative theories have been also proposed by which miRNAs work in a cooperative manner by co-targeting several genes involved in a given biological function (e.g. multiple genes of the same pathway). In addition, cooperation could also involve multiple miRNAs, with finely controlled regulation as a result of their common functions (Marzi et al. 2012; Han et al. 2015). To this end, to really understand miRNA functions, is critical to achieve a global view on miRNA pool and how it is regulated, including the dynamics that control their biogenesis and turnover. Many efforts have been put on characterizing the biosynthetic processes, from transcription of miRNA precursors to the mechanisms in control of the processing into mature forms and their activity on the miRISC (Ha and Kim 2014). Unfortunately, turnover mechanisms have been only poorly addressed and, thus, very little is known on how miRNAs are degraded in cells. Previous attempts to measure globally the degradation rates of miRNAs in mammalian cells relied on the use of inhibitors of miRNA transcription or processing to block the generation of new miRNAs. However, they represent non-physiological conditions which introduces profound side effects and under which the assessment of both ‘fast’ and ‘slow’ turnover rates is arduous. More specifically, the block/loss of miRNA processing enzymes (i.e. Dicer) requires up to three days to be effective, a time frame in which ‘fast’ decaying miRNAs are cleared and only the ‘slow’ species are retained (Gantier et al. 2011). In addition, Dicer ablation induces most mammalian cells to enter into a senescence/arrested state

which is far from physiology. Conversely, the block of transcription by the use of Polymerase II inhibitors can be maintained for few hours before inducing toxic effects (i.e. apoptosis), and, thus, identifies just those miRNAs that are quickly disappearing [the 'passenger' miRNAs, (Guo et al. 2015)]. Moreover, Polymerase II inhibition affects transcription of miRNA targets resulting in an artificial unbalance of target:miRNA ratios, with a possible aspecific effect on miRNA degradation pathway, as previously reported (Baccarini et al. 2011; Powers et al. 2016).

5.2 RNA labeling by 4sU revealed that half-lives of miRNA are heterogeneous

To address these issues, we developed an alternative approach for the determination of miRNA turnover in a close to physiological condition, without affecting transcription or processing of miRNAs, by exploiting the metabolic labeling of RNA in a pulse-chase experiment. This method is based on the incorporation of 4sU, a natural occurring analogue of uridine, which is safe for mammalian cells at limited concentrations. A prolonged treatment or a very high dose of 4sU could unbalance the nucleotide metabolism, interfering with the transcription of RNA and inducing metabolic stress.

Hence, the choices of 4sU concentration and time of treatment are critical to maintain cells in a close to physiological state. For instance, 3T9 cells tolerate high levels of 4sU (up to 300 uM) with no sign of transcriptional stress; HeLa and BJ human fibroblasts tolerate lower concentration (100uM) but still incorporate nicely 4sU into nascent RNA, while HEK293T showed high metabolic stress even at very low 4sU concentration and short treatment, with very poor incorporation. Differences in 4sU sensibility likely depend on the metabolic status of cells and pyrimidine metabolism, while differences in efficiency of incorporation could be ascribed to the activity of the kinases (UCK1/2) that convert 4sU into 4sUTP, whose expression is very different in human cells.

By combining 4sU RNA labeling (pulse-chase) with high throughput RNA sequencing we could determine miRNA decay rates at genome-wide level. We got precise measurement of about two hundreds of canonical miRNAs, almost all miRNAs that are expressed in fibroblasts. We found that most miRNAs are, indeed, stable molecules, with half-lives greater than 24hrs, as previously reported (Krol et al. 2010b; Ruegger and Grosshans 2012). However, a consistent number of

miRNAs displayed shorter decay times (<12h; N=61). We concluded that miRNA decay is rather heterogeneous, with at least two type of behaviors, a 'fast' and a 'slow' decay type. Importantly, 'fast' turnover does not appear as an exception anymore, restricted to few miRNAs and to specific contexts (i.e. retinal cells), but rather a feature of the miRNA pool. 'Fast' species include not only 'passenger' miRNAs, which are poorly loaded on Ago and, thus, quickly degraded (Guo et al. 2015), but also many 'guide' miRNAs (N=25), including the few (i.e. miR-503 and miR-182) that were previously described with a rapid turnover (Krol et al. 2010a; Rissland et al. 2011). Importantly, the rapid turnover of fast miRNAs is not due to a poor loading efficiency on Ago (as for passenger miRNAs), neither is linked to a particular genomic or transcriptional organization, but it rather appears as an intrinsic feature..

Recently, a different group has exploited a diverse chemistry for 4sU labeling and isolation (MST-Biotin XX) to analyze RNA stability (including miRNAs) by pulse labeling HEK293T cells (Duffy et al. 2015). In agreement with our results, those authors distinguished two groups of decay behavior, which resemble the 'fast' and 'slow' groups. Importantly, they also claimed about the low yield and weak pull-down efficiency in the isolation of 4sU labeled RNAs with low uridine content by HDPD-Biotin (the chemistry of commonly used and we exploited), which highlighted the requirement of a more efficient chemistry (namely the MST-Biotin XX). While the new chemistry is clearly more efficient in the recovery of long RNAs, it has not been tested in purifying miRNAs. When directly compared in a parallel extraction, we found no significant differences in 4sU incorporation of miRNAs by uridine content in MST-Biotin XX vs. HDPD-Biotin. Overall, higher yield was obtained by MST-Biotin XX but this increased recovery was at the expense of specificity, with much higher background level compared to HPDP-biotin. Based on these data we argued that the two chemistries could be equally applied to miRNAs with specific advantages and drawbacks that should be taken into account considering the context.

5.3 Effects of cell context on miRNA decay

A more general question is whether miRNA half-lives are an intrinsic feature or can be regulated according to the cell context. We observed limited variations in the half-life in human fibroblasts compared to mouse. In addition, our decay rates were similar to the few ones measured by others in

different systems (Krol et al. 2010a; Rissland et al. 2011). Nonetheless, we cannot exclude significant changes in miRNA stability in specific physio-pathological contexts, as observed for maternal miRNAs during embryogenesis (Lee et al. 2014). In this latter case, a specific enzyme, named Wispy, whose expression is modulated during embryogenesis, has been identified. Wispy is a terminal-transferase, which adds adenine at miRNA 3'end sequence, leading to global destabilization of miRNAs.

On the other hand, studies on mir-503 and miR-182 in mammals, suggested that they have an intrinsic fast decay, which is manifested upon dark adaptation (Krol et al. 2010a) or G0-G1 transition (Rissland et al. 2011).

Together, these data suggest that both active degradation and intrinsic fast miRNA behavior might exist and equally contribute to miRNAs turnover. Of note, in all cases, mechanisms that execute decay still remain unclear and more efforts have to be put in the discovering of enzymes that mediate these processes.

5.4 Impact of different biogenetic steps in the miRNA pool: the role of transcription and decay

To study the interplay between miRNA biogenesis and decay, we decided to quantitatively measure the transcription rate at miRNA loci. A relevant issue is that miRNA transcriptional units are not precisely defined, as the transcription start site (TSS) could be many kilobases far from miRNA gene and the promoter could be tissue specific. We devised a way to carefully define the genomic boundaries of miRNA transcriptional units by combining 4sU RNA sequencing, with short pulse of 4sU to enrich for primary transcripts, histone marks and Pol2 occupancy by Chromatin Immunoprecipitation (ChIP-seq) on putative miRNA genes; a method that could be extended to other cells and conditions. We focused on about one hundred of miRNA genes, for which we could then calculate the synthesis rate by coupling 4sU (short pulse) and total RNA sequencing with ad hoc bioinformatics tool. It is worth mentioning that our transcriptional units were largely overlapping with those identified by another study recently published by Mendell's lab, where a thorough identification of miRNA transcriptional units in multiple cell lines has been obtained

exploiting RNA sequencing upon Drosha inhibition, which accumulates pri-miRNAs, and the analysis on histone marks by ChIP-seq (Chang et al. 2015).

The dynamic range of transcription rates was wide (up to 500-fold) and correlated nicely with miRNA levels, supporting the hypothesis that miRNA expression is primarily controlled at the transcription step. Interestingly, we observed that low transcribed miRNAs are significantly associated with a fast decay behavior. It is tempting to speculate that fast miRNAs are preferentially low transcribed in order to avoid their accumulation in cells and allow a rapid control of their levels. As these pieces of evidence are based only on correlation studies, validation on specific candidates is needed to definitely link transcription and decay.

By considering the synthesis and decay rates we could reliably predict the abundance of miRNAs in steady state conditions. Our theoretical calculation assumes that such prediction is verified when processing is much faster than cell division ($k_2 >> \alpha$), a simplification that did not hold for complex miRNA clusters, where processing efficiency plays an important role in dictating the levels of each miRNAs contained in a cluster. A paradigmatic example is the 17-92 cluster, comprising six individual miRNAs which are differently processed: the loop region harboring miR-92a is immediately cut to form the pre-miR-92a which is loaded directly on DICER; the other five miRNAs are processed through the formation of a progenitor miRNA (pro-miRNA) which mediates their maturation (Du et al. 2015). This means that, despite being co-transcribed, miRNAs of cluster 17-92 accumulate differently in cells and, thus, their abundance cannot be described by only transcription and decay rate. We have to pinpoint that low efficiency maturation also impact on half-life calculation by metabolic labeling. Indeed, we supposed a negligible production of mature miRNAs from labeled precursors during the chase period, an assumption that might not be true for miRNAs with very low processing rate. In such case, the 'apparent' half-life increases and, hence, miRNA decay is faster than measured. We, thus, reasoned that it would be absolutely critical to approach also miRNA processing quantitatively. We are developing an approach based on a time course of 4sU pulse at increasing times to calculate maturation rate values (k_2) by interpolating the values of 4sU incorporation at each time-point. Once known such values, we could finally integrate all the measurements together (transcription, processing and decay) to get a

global view of miRNA regulation and clarify which are the impact and the interplay of each biogenetic step in the regulation of miRNA pool.

We used the mathematical model to infer the impact of transcription and decay on miRNA regulation in a dynamic condition, when miRNAs are transcriptionally regulated. We modeled kinetic parameters (k_1, k_2, k_3 and α) in a range compatible with experimental observations made by others and us. Hence, we concluded that while transcription primarily regulates the magnitude of miRNA expression, the decay is influencing the dynamics of miRNA regulation. An implication of such model is that 'slow' decaying miRNAs can accumulate to high levels and are subjected to fewer fluctuations. Conversely, miRNAs with 'fast' decay can give rise to sharp and quick changes in miRNA pool. Indeed, various fast miRNAs in our dataset are involved in dynamic conditions requiring rapid change in miRNAs expression. Relevant examples are the control of developmental transitions [Let-7b/c, miR-99, miR-100, (Thornton et al. 2014)], specialized functions of differentiated cells like neurons [miR-182, (Krol et al. 2010a)], growth factor response [miR-320, miR-155; (Avraham et al. 2010)] and epithelial-mesenchymal transition [miR-335, miR-205, (Pencheva and Tavazoie 2013)]. We tested serum-stimulation of quiescent fibroblasts as a condition in which cells undergo a relatively rapid (12h) physiological transition. In this context, we experimentally confirmed that miRNA repression could occur only for miRNAs with 'short' (fast) half-life. Of note, some miRNAs displayed a concomitant reduction in transcription rates. Conversely, we noticed other miRNAs whose expression level decrease without any modification in transcription rate, confirming the existence of active processes for miRNA degradation.

5.5 High complementary targets are determinants of miRNA decay

A relevant issue is to clarify the mechanisms in control of miRNA decay behavior. Others and we hypothesized that degradation occurs while miRNAs are exerting their function on the miRISC, meaning that RNA targets might be involved. One such mechanism is called target-induced (or –mediated) miRNA decay (TIMD, (Ruegger and Grosshans 2012; de la Mata et al. 2015)) and implies miRNA:target interaction as a bidirectional control mechanism, by which it is not just the miRNA that affects target RNAs by silencing, but also the targets could affect miRNA functions by promoting their degradation. TIMD mechanism has been only recently proposed by the Grosshans

lab, based on the evidence that in primary neuronal cells the rapid degradation of some miRNAs is induced by highly complementary targets (de la Mata et al. 2015). However, this mechanism is supported by multiple observations based on i) in vitro biochemical approaches, where highly complementary targets promotes either the release of miRNAs from Argonaute 2 (De et al. 2013) or their degradation by tailing and trimming (Ameres et al. 2010); ii) in vivo approaches using synhtetic targets (Baccarini et al. 2011; de la Mata et al. 2015; Haas et al. 2016), which promote downregulation and destabilization of miRNAs; iii) viral RNAs, which could induce potent degradation of specific miRNAs upon infection (Cazalla et al. 2010) (Marcinowski et al. 2012).

Our analyses at genomic level on murine fibroblasts (3T9) also support such model in the control of miRNA decay behavior. In particular, we observed that the ratio between high affinity targets and miRNA abundance (target per miRNA ratio – TPM) remarkably correlate with the type of miRNA decay. A main feature of TIMD is that extended target complementary does matter: highly-complementary targets with 3' end pairing efficiently promoted both miRNA unloading from Ago2 (De et al. 2013) and degradation of the miRNA in vitro and in vivo (Ameres et al. 2010; Baccarini et al. 2011; de la Mata et al. 2015). Indeed, we observed an increased significance in the correlation between high TPM and fast decaying miRNAs when we focused on targets with extensive complementary site at 3'end (3C targets, either 3C.03 and 3C.05). Of note, in our analyses 'fast' and 'slow' miRNAs displayed similar number of targets (and target copies) when considering just targets with seed matching, but these values became much different when focusing on targets with 3' complementarity. It is worth mentioning here that, besides the viral RNA HSURs (Cazalla et al. 2010) no endogenous target has been directly linked to TIMD mechanism so far.

Our analyses provided a list of potential targets involved in TIMD, which could be critical in clarifying the role played by such mechanism in physiology. Besides target expression levels, TPM values also depend on miRNA levels, which are primarily regulated by transcription. Thus, as mentioned above, transcription rate also plays a role in determining miRNA decay behavior, reinforcing the interplay between transcription and decay in controlling miRNA dynamics.

It remains unclear whether target degradation also occurs during TIMD. In the study by Grosshan's lab, authors somehow claimed that miRNA and target degradation are mutually exclusive (de la Mata et al. 2015). Using synthetic constructs, they showed that TIMD occurred with exogenous

targets harboring a single highly complementary site (1x MRE), while target degradation occurred with multiple sites (4x seed matches) in the sequence. We have to point out that four highly complementary sites represent an extremely rare situation (we did not find any endogenous targets with such characteristics in our dataset based on 3T9 cells), where the affinity between miRNA and target is so high to reasonably lead mainly to target degradation.

We also analyzed the activity of miRNAs on highly complementary targets. The repression was weakened at TPM_3C ratios greater than 10. This is in very good agreement with similar observations made by others (Mukherji et al. 2011) (Bosson et al. 2014) pointing out the existence of a threshold in target repression that depends on miRNA expression and target abundance. It would be definitively critical to perform in depth studies into this issue by using endogenous targets. We found interesting cases in our 3T9 datasets, with promising candidate RNA targets, with high affinity MRE, extensive complementarity (3C target) and high expression, suitable for TIMD. By exploiting these specific cases, we could clarify the mechanisms underlying miRNA degradation and target repression.

5.6 Tailing and trimming forms are intermediates of miRNA degradation

A target-mediated effect related to miRNA degradation is the accumulation of 3'-end non-templated miRNA modifications, which has been frequently observed under the same conditions of TIMD, namely the expression of synthetic highly complementary targets (Ameres et al. 2010; Baccarini et al. 2011; de la Mata et al. 2015). A significant correlation between miRNA modifications and decay behavior also emerged in our study. We observed that 'fast' miRNAs were enriched both in trimming, as consequence of shortening by exonucleases activity, and tailing variants, in particular adenylation and uridylation, due to terminal transferase activity. Together, these modifications appear as degradation intermediates and, thus, we refer to them as 'decay-associated' isoforms. An interesting point is the definition, in terms of time and place of occurrence, of target interaction for miRNA degradation and the generation of tailed and trimmed forms. Tangible clues came from the analysis of miRNA variants distribution on the Ago2. We found 'decay-associated' isomiRs loaded on Ago2, suggesting that active tailing and trimming

occur when miRNAs are functional. Something that has been observed also by others, including Grosshan's lab (de la Mata et al. 2015) and Narry Kim's lab (Lee et al. 2014).

As previously mentioned, the generation of decay-associated isoforms requires specific enzymatic activities (exonucleases and terminal transferases), generally called miRNases. Biochemical approaches to isolate miRNases are now on the way and could potentially lead to the identification of key regulatory enzymes involved in miRNA turnover. One such study comes from the Pfeffer's lab; indeed, they exploited biotinylated anti-miRs (synthetic perfect target) to mimic TIMD and purified catalytic activities on Ago2 complexes. In this way, a terminal-uridyl-transferase (TUT1) and 3'-5' exoribonuclease (DIS3L2) were isolated and shown to be potentially involved in TIMD mechanism (Haas et al. 2016).

5.7 Modulating miRNA decay by exogenous and endogenous targets

Previously, TIMD mechanism has been hypothesized based on experiments performed on hippocampal neurons (de la Mata et al. 2015). Using exogenous target expression, authors provide evidence that such mechanism occurs for miR-132, though endogenous targets have not been identified. A relevant issue is the context dependency. TIMD appeared more efficient in primary neurons as compared to HEK293T and MEF cell lines, even if expression levels of exogenous target and miR-132 were much similar, suggesting that tissue-specific factors (either enzymatic activities or competing RNAs) are involved.

A significant implication is the theoretical possibility to switch from 'high' to 'low' TPM and, thus, modify the activity and the decay of miRNAs. However, the number of miRNA targets is typically very high, and only few of them are expressed at enough high levels (hundreds of copies per cell) to influence by themself the total target pool. As mentioned before, we produced a catalogue of high affinity and 3'end complementary targets in fibroblasts, from which select potential candidates for TIMD mechanism. One such candidate is the Serpine1 (PAI1) transcript, which is highly complementary for miR-30b/c and much expressed upon serum stimulation of quiescent fibroblatsts. Indeed, these miRNAs undergo a quick down-regulation in the total levels upon serum-stimulation, without any major decrease in transcription of precursors and with a sudden increase of decay-associated isoforms, suggesting that active degradation is on place. Through

CRISP/Cas9 technology we specifically deleted the complementarity region for miR-30bc (MRE) on the 3'UTR of Serpine1 on one allele in preliminary experiments. We observed a corresponding effect on miR-30c regulation (loss of downregulation upon serum stimulation), which fully supports Serpine1 as an endogenous target involved in TIMD. Intriguingly, we did not see much effect on miR-30b regulation as we see for miR-30c, suggesting that the target pool of miR-30c and miR-30b might be different or, alternatively, other mechanisms might be in place. It is worth mentioning that genome engineering by CRISPR/cas9 technology allowed us to modify target sequence with such precision (only the MRE was deleted) that specifically interferes with miRNA:target interaction, keeping transcript level and protein functionality unaltered. This approach would be extremely valuable to dissect miRNA functions by manipulating endogenous targets, such as to validate miRNA phenotypes or test the competing endogenous RNA (ceRNA) hypothesis, though to our knowledge has never been used in such way.

5.8 miRNA degradation may also occur in pathological (cancer) contexts

Intriguingly, a TIMD mechanism may also occur in neurons under pathological conditions, such as in neuroblastoma. A recent publication from Daley's group showed that MYCN transcript, which is frequently genetically amplified and overexpressed in neuroblastoma, exerts a negative control on let-7 miRNAs by multiple mechanisms, which also include interaction of the RNA target with miRNAs (Powers et al. 2016). Authors claimed for a mechanism by which high levels of MYCN transcript are sufficient to sponge let-7, inhibiting its function, ensuing in a competing endogenous RNA (ceRNA) mechanism. However, given the high affinity of interaction, the exceptional high level of expression and extended 3' complementarity between let-7 miRNAs and MYCN transcript, it is tempting to speculate that a TIMD mechanism is on place. Indeed, high levels of MYCN induced downregulation of let-7 miRNAs, while silencing of the target restored let-7 expression (Powers et al. 2016). In the ceRNA hypothesis, miRNA downregulation by target is not contemplated (only competition between targets is foreseen). Hence a target-mediated degradation mechanism is plausible.

Undoubtedly, overexpression in cancer and/or genetic amplification represent a condition which is ideal for the induction of target-dependent degradation of miRNAs, since a sudden increase in

TPM is predicted. Signs of TIMD mechanism in cancer could rise from the exploitation of cancer dataset with matched miRNA and mRNA expression data (such as those provided by The Cancer Genome Atlas, TCGA). To this end, we explored TCGA to investigate Serpine1:miR-30c interaction in breast invasive carcinoma. A preliminary analysis revealed that samples with low vs. high expression of Serpine1 (10^{th} and 90^{th} percentile, respectively) significantly anti-correlate with miR-30c levels, which also showed a coherent regulation of decay-associated variants (trimmed forms), suggesting that a TIMD mechanism may also occur in breast cancer (**Figure 91**).

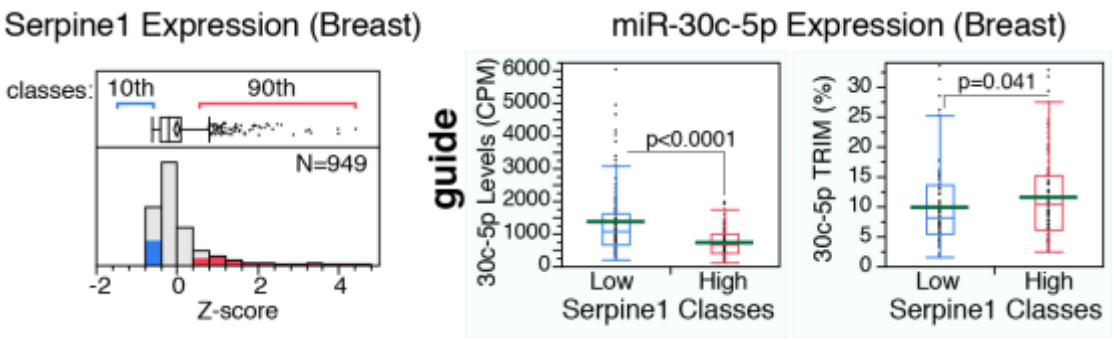

Figure 91 Serpine1 expression in TCGA dataset. **LEFT PANEL**. 949 tumors from TCGA dataset were analyzed for Serpine1 expression. Top and bottom decile were used to isolate the "low" and "high" Serpine1 classes shown in right panel. **RIGHT PANEL** One-way analysis of miR-30c-5p expression (copies-per-million, CPM, left panels) or trimming (as % of total reads, right panels) within Serpine1 "high" and "low" classes, as defined in left panel. P values by Wilcoxon test

Nevertheless, ceRNA and TIMD appear as two different mechanisms, which are closely connected. In both cases, targets exert an inhibitory function on miRNAs, ensuing in target derepression. In one case (ceRNA hypothesis), the effect is produced just by competition for the same miRNA between different target, provided the ceRNA has high affinity for miRNA and constitute a significant fraction of the target pool (Bosson et al. 2014). In the other case (TIMD), the effect is produced by high-affinity targets with extended complementarity, which still have to be expressed at enough high levels to significantly impact on target pool (and reach a threshold in TPM) to induce miRNA degradation. To this regard, we see the urgency for a deeper understanding of the balance between ceRNAs and TIMD in regulating miRNAs pool dynamics, both in physiological and pathological systems, which still remain unclear by in-depth studies on endogenous targets.

5.9 Concluding remarks and future plans

With this study, we aimed at providing an integrated framework for the quantitative analysis of miRNA biology, which highlighted novel functions and mechanisms in control of miRNA dynamics in transcriptome shaping and definition of cell identity. Pivotal for such analysis are the development of *ad hoc* tools and approach for the quantitative assessment of miRNA related features, including transcription rate of miRNA precursors, turnover of mature molecules, structural heterogeneity (IsomiRs) and activity on targets (TPM). Other features are still missing and we are going towards the development of other tools and complementary approach to get a global and comprehensive view of the regulation of miRNA pool. Through such integrated and quantitative framework, we will certainly achieve a deeper understanding of the regulatory circuitries controlling miRNA concentration and, more importantly, activity.

In parallel, we will apply our tools and models to clarify the role of miRNA degradation dynamics both in physiological and pathological systems, with particular respect to the identification of endogenous targets able to elicit a TIMD mechanism and the definition of biochemical activities that mediate miRNA decay. To this regard, a clarification of the interplay of ceRNA and TIMD mechanisms is also urgently needed and might be provided by exploiting precision genome engineering by CRISPR/cas9 technology.

Appendix

Data table 1

Table 1. miRNA half-life values

miRNA NAME	Half Life (FINAL)	Half Life (min)	Half Life (max)	R square	Decay class
mmu-miR-214-3p	4,55	3,14	8,26	0,897	FAST
mmu-miR-466b-3p	5,07	3,52	9,06	0,891	FAST
mmu-miR-574-3p	7,35	5,89	9,76	0,961	FAST
mmu-miR-501-3p	7,93	6,66	9,79	0,977	FAST
mmu-miR-669c-5p	7,48	6,00	9,92	0,961	FAST
mmu-miR-205-5p	7,83	5,89	11,70	0,932	FAST
mmu-miR-652-3p	7,25	5,18	12,10	0,904	FAST
mmu-miR-99b-5p	10,90	9,65	12,70	0,987	FAST
mmu-miR-24-3p	10,10	8,28	12,80	0,969	FAST
mmu-let-7b-5p	8,69	6,50	13,10	0,927	FAST
mmu-miR-328-3p	9,95	7,62	14,30	0,937	FAST
mmu-miR-320-3p	9,94	7,41	15,10	0,921	FAST
mmu-miR-1249-3p	10,60	7,77	16,50	0,920	FAST
mmu-miR-155-5p	12,30	9,41	17,60	0,939	FAST
mmu-let-7c-5p	11,70	8,66	18,00	0,918	FAST
mmu-miR-335-5p	4,66	3,53	6,85	0,947	FAST
mmu-miR-100-5p	7,93	6,53	10,10	0,971	FAST
mmu-miR-140-3p	7,78	5,61	12,60	0,906	FAST
mmu-miR-182-5p	9,05	6,66	14,10	0,918	FAST
mmu-miR-298-5p	8,76	5,98	16,30	0,864	FAST
mmu-miR-103-3p	13,40	11,20	16,60	0,974	FAST
mmu-miR-152-3p	6,34	3,91	16,80	0,798	FAST
mmu-miR-532-5p	12,30	9,32	18,00	0,931	FAST
mmu-miR-199a-3p	9,59	6,50	18,30	0,859	FAST
mmu-miR-224-5p	9,23	6,36	16,80	0,872	FAST
mmu-miR-221-3p	16,30	13,40	20,90	0,966	OTHER
mmu-let-7a-5p	13,00	9,13	22,60	0,880	OTHER
mmu-miR-132-3p	13,50	9,60	22,70	0,895	OTHER
mmu-miR-1839-5p	11,90	7,96	23,60	0,847	OTHER
mmu-miR-98-5p	12,20	8,06	24,70	0,837	OTHER
mmu-miR-26b-5p	9,43	5,79	25,40	0,772	OTHER
mmu-miR-31-5p	13,50	8,96	27,00	0,841	OTHER
mmu-let-7g-5p	12,30	7,84	28,70	0,802	OTHER
mmu-miR-196b-5p	10,80	6,66	29,00	0,768	OTHER
mmu-let-7d-5p	14,60	9,31	34,30	0,796	OTHER
mmu-miR-877-5p	14,00	8,78	34,90	0,805	OTHER

mmu-miR-676-3p	18,70	11,80	44,40	0,792	OTHER
mmu-let-7e-5p	22,70	10,40	>48	0,464	OTHER
mmu-let-7f-5p	19,10	11,10	>48	0,708	OTHER
mmu-miR-146b-5p	24,00	8,84	>48	0,302	OTHER
mmu-miR-149-5p	22,60	7,19	>48	0,255	OTHER
mmu-miR-7a-5p	18,30	8,01	>48	0,472	OTHER
mmu-miR-222-3p	14,10	10,70	20,80	0,931	OTHER
mmu-miR-6539	8,38	5,24	20,90	0,821	OTHER
mmu-miR-664-5p	13,80	9,89	22,70	0,902	OTHER
mmu-miR-143-3p	11,80	7,90	23,20	0,850	OTHER
mmu-miR-744-5p	13,90	9,91	23,50	0,895	OTHER
mmu-miR-23b-3p	13,00	8,92	23,80	0,865	OTHER
mmu-miR-145a-5p	13,00	8,63	26,30	0,851	OTHER
mmu-miR-129-5p	16,10	10,50	34,80	0,819	OTHER
mmu-miR-342-3p	17,50	11,20	39,80	0,805	OTHER
mmu-miR-128-3p	21,10	14,10	42,00	0,842	OTHER
mmu-miR-1843b-5p	11,70	6,70	45,30	0,722	OTHER
mmu-miR-26a-5p	12,20	7,04	45,30	0,704	OTHER
mmu-let-7i-5p	25,40	13,50	>48	0,621	OTHER
mmu-miR-107-3p	27,80	10,50	>48	0,322	OTHER
mmu-miR-1198-5p	17,10	9,69	>48	0,687	OTHER
mmu-miR-181d-5p	17,90	10,60	>48	0,729	OTHER
mmu-miR-183-5p	17,30	10,10	>48	0,718	OTHER
mmu-miR-486a-5p	26,10	12,50	>48	0,535	OTHER
mmu-miR-296-5p	14,90	10,90	23,50	0,910	OTHER
mmu-miR-378a-3p	15,50	11,10	25,40	0,896	OTHER
mmu-miR-148a-3p	10,70	6,61	27,70	0,780	OTHER
mmu-miR-138-5p	11,80	7,50	28,00	0,808	OTHER
mmu-miR-28a-5p	14,90	9,75	31,60	0,826	OTHER
mmu-miR-3057-5p	21,10	14,40	39,80	0,861	OTHER
mmu-miR-30d-5p	15,70	9,74	40,90	0,772	OTHER
mmu-miR-1191b-5p	29,10	6,64	>48	0,096	OTHER
mmu-miR-148b-3p	>48	13,60	>48	0,081	OTHER
mmu-miR-151-3p	27,90	14,60	>48	0,605	OTHER
mmu-miR-191-5p	>48	14,70	>48	0,062	OTHER
mmu-miR-23a-3p	22,70	12,70	>48	0,669	OTHER
mmu-miR-27b-3p	21,90	9,34	>48	0,405	OTHER
mmu-miR-30c-5p	16,20	8,99	>48	0,668	OTHER
mmu-miR-344d-3p	15,90	9,37	>48	0,739	OTHER
mmu-miR-361-5p	20,70	12,30	>48	0,742	OTHER
mmu-miR-421-3p	28,10	14,70	>48	0,603	OTHER
mmu-miR-466h-5p	8,76	4,71	>48	0,627	OTHER
mmu-miR-467c-5p	11,70	6,47	>48	0,653	OTHER
mmu-miR-484	21,10	11,00	>48	0,603	OTHER

mmu-miR-92b-3p	35,40	7,99	>48	0,085	OTHER
mmu-miR-425-5p	9,48	5,68	28,60	0,750	OTHER
mmu-miR-322-5p	10,60	6,37	31,90	0,747	OTHER
mmu-miR-30b-5p	12,50	7,29	42,90	0,730	OTHER
mmu-miR-101b-3p	20,00	9,72	>48	0,538	OTHER
mmu-miR-15a-5p	28,40	11,20	>48	0,363	OTHER
mmu-miR-181c-5p	45,00	12,30	>48	0,150	OTHER
mmu-miR-193a-3p	13,10	5,41	>48	0,435	OTHER
mmu-miR-194-5p	33,50	10,50	>48	0,223	OTHER
mmu-miR-22-3p	28,00	14,20	>48	0,577	OTHER
mmu-miR-27a-3p	>48	14,40	>48	0,068	OTHER
mmu-miR-344b-3p	10,90	5,72	>48	0,611	OTHER
mmu-miR-34c-5p	29,90	9,59	>48	0,213	OTHER
mmu-miR-351-5p	12,70	5,63	>48	0,421	OTHER
mmu-miR-450b-5p	>48	14,20	>48	-0,011	OTHER
mmu-miR-872-5p	23,90	10,60	>48	0,458	OTHER
mmu-miR-96-5p	17,70	6,79	>48	0,307	OTHER
mmu-miR-181b-5p	28,80	18,20	>48	0,794	SLOW
mmu-miR-1964-3p	>48	36,80	>48	0,070	SLOW
mmu-miR-25-3p	>48	28,70	>48	0,371	SLOW
mmu-miR-6540-5p	>48	>48	>48	0,000	SLOW
mmu-miR-6944-3p	>48	21,70	>48	0,043	SLOW
mmu-miR-92a-3p	>48	>48	>48	0,489	SLOW
mmu-miR-125a-5p	26,80	18,40	>48	0,860	SLOW
mmu-miR-125b-5p	41,30	28,00	>48	0,853	SLOW
mmu-miR-15b-5p	37,50	20,10	>48	0,638	SLOW
mmu-miR-16-5p	>48	15,70	>48	0,086	SLOW
mmu-miR-181a-5p	26,30	16,50	>48	0,789	SLOW
mmu-miR-1983	43,80	28,40	>48	0,821	SLOW
mmu-miR-218-5p	>48	17,60	>48	0,104	SLOW
mmu-miR-365-3p	>48	20,60	>48	0,141	SLOW
mmu-miR-423-5p	35,50	19,70	>48	0,668	SLOW
mmu-miR-93-5p	28,00	18,60	>48	0,838	SLOW
mmu-miR-99a-5p	>48	>48	>48	0,000	SLOW
mmu-miR-130a-3p	42,00	15,20	>48	0,300	SLOW
mmu-miR-130b-3p	40,40	16,20	>48	0,381	SLOW
mmu-miR-17-5p	38,20	15,50	>48	0,384	SLOW
mmu-miR-186-5p	>48	>48	>48	0,000	SLOW
mmu-miR-192-5p	>48	16,40	>48	0,063	SLOW
mmu-miR-19b-3p	>48	>48	>48	0,000	SLOW
mmu-miR-20a-5p	42,20	18,60	>48	0,461	SLOW
mmu-miR-21a-5p	>48	35,90	>48	-0,002	SLOW
mmu-miR-29a-3p	31,30	16,20	>48	0,596	SLOW
mmu-miR-29b-3p	>48	>48	>48	0,000	SLOW

mmu-miR-301a-3p	>48	>48	>48	0,000	SLOW
mmu-miR-301b-3p	>48	>48	>48	0,000	SLOW
mmu-miR-30a-5p	27,60	15,90	>48	0,708	SLOW
mmu-miR-30e-5p	>48	>48	>48	0,000	SLOW
mmu-miR-34a-5p	>48	18,40	>48	0,264	SLOW

Data table 2

Table 2 miRNA loci definition and synthesis rate

miRNA NAME	pri-miRNA region	pre-miRNA region	Average synthesis rate (RPKM/h)
mmu-let-7a-1	chr13:48,625,924-48,641,947	chr13:48,633,548-48,633,641	**56,72**
mmu-let-7a-2	chr9:41,335,847-41,347,232	chr9:41344799-41344894	**7,65**
mmu-let-7b-5p	chr15:85,531,339-85,538,026	chr15:85537749-85537833	**20,30**
mmu-let-7c-1-5p	chr16:77,598,016-77,601,268	chr16:77599902-77599995	**1,75**
mmu-let-7c-2-5p	chr15:85,531,339-85,538,026	chr15:85537749-85537833	**20,30**
mmu-let-7d-5p	chr13:48,625,924-48,641,947		**56,72**
mmu-let-7e	chr17:17,964,516-17,980,285	chr17:17967316-17967408	**46,82**
mmu-let-7i	chr10:122,416,951-122,422,812	chr10:122422696-122422780	**18,36**
mmu-miR-100-5p	chr9:41,335,847-41,347,232	chr9:41339508-41339587	**7,70**
mmu-miR-103-1-3p	chr11:35,595,249-35,596,934	chr11:35595898-35595983	**17,19**
mmu-miR-103-2-3p	chr2:131,113,466-131,117,939	chr2:131113788-131113873	**4,58**
mmu-miR-106b-3p	chr5:138,606,439-138,607,121		**18,40**
mmu-miR-1249-3p	chr15:84,781,388-84,783,468	chr15:84781956-84782053	**4,24**
mmu-miR-125a-5p	chr17:17,964,516-17,980,285	chr17:17967776-17967843	**46,81**
mmu-miR-125b-1-5p	chr9:41,389,499-41,401,108	chr9:41390009-41390085	**219,22**
mmu-miR-125b-2-5p	chr16:77,644,837-77,652,946	chr16:77646518-77646588	**1,88**
mmu-miR-130a-3p	chr2:84,579,589-84,583,890	chr2:84581272-84581335	**11,60**
mmu-miR-130b-3p	chr16:17,121,721-17,125,215	chr16:17124154-17124235	**9,31**
mmu-miR-140-3p	chr8:110,074,092-110,076,142	chr8:110,075,144-110,075,213	**14,97**
mmu-miR-143	chr18:61,805,240-61,812,027	chr18:61808850-61808912	**15,37**
mmu-miR-145	chr18:61,805,240-61,812,027		**15,37**
mmu-miR-149	chr1:94,728,790-94,749,806	chr1:94,746,955-94,747,020	**2,45**
mmu-miR-151	chr15:73,073,258-73,087,275	chr15:73,085,245-73,085,312	**14,42**
mmu-miR-152-3p	chr11:96,711,402-96,711,970	chr11:96711707-96711779	**2,67**
mmu-miR-155-5p	chr16:84,703,710-84,719,727	chr16:84714385-84714449	**8,76**
mmu-miR-15a-5p	chr14:62,244,265-62,251,250		**26,82**
mmu-miR-15b-5p	chr3:68,813,632-68,820,002	chr3:68,813,694-68,813,757	**54,22**
mmu-miR-16-1-5p	chr14:62,244,265-62,251,250	chr14:62250717-62250809	**26,82**
mmu-miR-16-2-5p	chr3:68,813,632-68,820,002	chr3:68813824-68813918	**54,34**
mmu-miR-17-5p	chr14:115,441,507-115,446,111	chr14:115442893-115442976	**52,64**
mmu-miR-181a-1-5p	chr1:139,859,788-139,866,074	chr1:139863032-139863118	**4,53**
mmu-miR-181a-2-5p	chr2:38,707,091-38,711,257	chr2:38708255-38708330	**11,18**
mmu-miR-181b-1-5p	chr1:139,859,788-139,866,074	chr1:139863216-139863295	**4,53**
mmu-miR-181b-2-5p	chr2:38,707,091-38,711,257		**11,18**
mmu-miR-182-5p	chr6:30,115,777-30,124,226	chr6:30115918-30115992	**3,93**
mmu-miR-183-5p	chr6:30,115,777-30,124,226		**3,93**
mmu-miR-186-5p	chr3:157,206,290-157,207,891	chr3:157207243-157207313	**40,92**
mmu-miR-191-5p	chr9:108,469,867-108,472,159	chr9:108470650-108470723	**2,46**
mmu-miR-192-5p	chr19:6,263,562-6,265,931	chr19:6264844-6264932	**0,26**

mmu-miR-194-5p	chr19:6,263,562-6,265,931		**0,26**
mmu-miR-1964-3p	chr7:30,556,560-30,560,300	chr7:30558313-30558395	**5,47**
mmu-miR-1983	chr13:21,982,875-21,994,505	chr13:21,988,787-21,988,918	**0,05**
mmu-miR-199a-1-3p	chr9:21,299,241-21,303,566		**5,03**
mmu-miR-199a-2-3p	chr1:164,147,835-164,155,141	chr1:164147945-164148054	**64,03**
mmu-miR-19a	chr14:115,441,507-115,446,111		**53,02**
mmu-miR-19b-1-3p	chr14:115,441,507-115,446,111	chr14:115443527-115443613	**52,64**
mmu-miR-19b-2-3p	chrX:50,094,541-50,098,178	chrX:50,095,160-50,095,243	**0,02**
mmu-miR-205-5p	chr1:195,333,484-195,335,975	chr1:195333657-195333724	**0,03**
mmu-miR-20a-5p	chr14:115,441,507-115,446,111	chr14:115,443,379-115,443,485	**52,95**
mmu-miR-214-3p	chr1:164,147,835-164,155,141	chr1:164153499-164153608	**64,06**
mmu-miR-218-1-5p	chr5:48,611,420-48,615,839	chr5:48615181-48615290	**8,47**
mmu-miR-218-2-5p	chr11:35,426,233-35,435,462	chr11:35430318-35430427	**0,01**
mmu-miR-21a-5p	chr11:86,390,826-86,398,796	chr11:86397569-86397660	**86,22**
mmu-miR-22	chr11:75,275,206-75,279,977	chr11:75277218-75277312	**45,28**
mmu-miR-221	chrX:18,719,567-18,724,242	chrX:18723420-18723514	**28,34**
mmu-miR-222	chrX:18,719,567-18,724,242	chrX:18,724,019-18,724,097	**28,05**
mmu-miR-224-5p	chrX:69,503,958-69,507,750	chrX:69506370-69506451	**1,97**
mmu-miR-23a-3p	chr8:86,730,722-86,733,993		**22,39**
mmu-miR-23b-3p	chr13:63,401,071-63,403,087		**32,52**
mmu-miR-24-1-3p	chr13:63,401,071-63,403,087	chr13:63402516-63402583	**32,30**
mmu-miR-24-2-3p	chr8:86,730,722-86,733,993	chr8:86732714-86732820	**22,39**
mmu-miR-25-3p	chr5:138,606,439-138,607,121	chr5:138606549-138606632	**18,42**
mmu-miR-26a-1-5p	chr9:118,939,430-118,942,619	chr9:118940914-118941003	**4,76**
mmu-miR-26a-2-5p	chr10:126,431,102-126,432,873	chr10:126432586-126432669	**4,92**
mmu-miR-27a-3p	chr8:86,730,722-86,733,993		**22,39**
mmu-miR-27b-3p	chr13:63,401,071-63,403,087	chr13:63,402,020-63,402,092	**32,52**
mmu-miR-296-5p	chr2:174,092,647-174,093,036		**6,60**
mmu-miR-298-5p	chr2:174,092,647-174,093,036	chr2:174093005-174093086	**6,60**
mmu-miR-29a-3p	chr6:31,004,720-31,022,331	chr6:31012660-31012747	**54,57**
mmu-miR-29b-1-3p	chr6:31,004,720-31,022,331	chr6:31013023-31013093	**54,38**
mmu-miR-29b-2-3p	chr1:196,844,061-196,864,459	chr1:196863741-196863828	**1,65**
mmu-miR-29c-3p	chr1:196,844,061-196,864,459		**1,65**
mmu-miR-301a-3p	chr11:86,922,923-86,929,562	chr11:86926506-86926591	**40,39**
mmu-miR-301b-3p	chr16:17,121,721-17,125,215	chr16:17124493-17124589	**9,36**
mmu-miR-30a	chr1:23,263,039-23,302,826	chr1:23,279,108-23,279,178	**17,54**
mmu-miR-30b	chr15:68,162,962-68,194,043	chr15:68168977-68169072	**15,30**
mmu-miR-30c-1	chr4:120,441,660-120,446,226		**10,27**
mmu-miR-30c-2	chr1:23,263,039-23,302,826		**17,54**
mmu-miR-30d	chr15:68,162,962-68,194,043		**15,30**
mmu-miR-30e-5p	chr4:120,441,660-120,446,226	chr4:120445211-120445302	**10,27**
mmu-miR-31	chr4:88,545,318-88,584,210	chr4:88,556,461-88,556,566	**116,98**
mmu-miR-320-3p	chr14:70,843,374-70,844,589	chr14:70843317-70843398	**0,82**
mmu-miR-322	chrX:50,406,385-50,410,299		**8,96**

mmu-miR-335-5p	chr6:30,690,947-30,692,071	chr6:30,691,299-30,691,396	**0,58**
mmu-miR-34a-5p	chr4:149,442,180-149,445,107	chr4:149442563-149442664	**5,75**
mmu-miR-351	chrX:50,406,385-50,410,299	chrX:50,406,432-50,406,530	**9,07**
mmu-miR-365-1-3p	chr16:13,448,205-13,458,599	chr16:13,453,933-13,454,019	**0,12**
mmu-miR-365-2-3p	chr11:79,525,612-79,551,845	chr11:79539902-79540013	**33,75**
mmu-miR-374	chrX:100,765,399-100,772,577		**15,69**
mmu-miR-421	chrX:100,765,399-100,772,577	chrX:100768399-100768493	**15,69**
mmu-miR-423-5p	chr11:76,890,303-76,891,873	chr11:76891566-76891674	**9,61**
mmu-miR-425	chr9:108,469,867-108,472,159		**2,46**
mmu-miR-466b-3p	chr2:10,394,148-10,426,070	chr2:10420312-10420393	**0,49**
mmu-miR-501-3p	chrX:6,810,379-6,827,376	chrX:6818369-6818477	**2,79**
mmu-miR-503	chrX:50,406,385-50,410,299	chrX:50,407,161-50,407,231	**8,96**
mmu-miR-532-5p	chrX:6,810,379-6,827,376	chrX:6825528-6825623	**2,78**
mmu-miR-574-3p	chr5:65,361,596-65,367,788	chr5:65,361,557-65,361,634	**6,80**
mmu-miR-652-3p	chrX:139,159,387-139,186,419	chrX:139,173,543-139,173,640	**4,76**
mmu-miR-669c-5p	chr2:10,394,148-10,426,070	chr2:10420312-10420393	**0,49**
mmu-miR-92a-1-3p	chr14:115,441,507-115,446,111	chr14:115443649-115443728	**53,02**
mmu-miR-92a-2-3p	chrX:50,094,541-50,098,178	chrX:50095015-50095105	**0,02**
mmu-miR-93-5p	chr5:138,606,439-138,607,121	chr5:138606751-138606838	**18,40**
mmu-miR-96-5p	chr6:30,115,777-30,124,226		**3,93**
mmu-miR-99a-5p	chr16:77,598,016-77,601,268	chr16:77599181-77599245	**1,76**
mmu-miR-99b-5p	chr17:17,964,516-17,980,285	chr17:17967152-17967221	**46,74**

Data table 3

Table 3. Values from the mathematical modelling of the impact of transcription and decay on miRNAs regulation

T1/2	Transcription Rate (K1)	alpha	miR at plateau (100h limit)	PRI at plateau (100h limit)	CPC at plateau	Time to 90% of plateau (hours)
SLOW (T1/2=24h)	K1= 1 Low Transcr.	a=0	33	1	34	75
		a=1/48	20	1	20	46
		a=1/24	14	1	14	33
	K1= 6 High Transcr.	a=0	196	6	205	75
		a=1/48	112	6	120	46
		a=1/24	84	6	84	33
FAST (T1/2=4h)	K1= 1 Low Transcr.	a=0	5,8	1	6	14
		a=1/48	5,1	1	5	13
		a=1/24	4,6	1	5	12
	K1= 6 High Transcr.	a=0	34	6	35	14
		a=1/48	31	6	31	13
		a=1/24	28	6	28	12
SLOW (T1/2=24h)	K1= 1 Low Transcr.	a=0	33	3	34	78
		a=1/48	20	3	20	48
		a=1/24	14	3	14	35
	K1= 6 High Transcr.	a=0	195	18	205	79
		a=1/48	120	17	120	48
		a=1/24	84	16	84	35
FAST (T1/2=4h)	K1= 1 Low Transcr.	a=0	6	3	6	17
		a=1/48	5	3	5	15
		a=1/24	5	3	5	14
	K1= 6 High Transcr.	a=0	35	18	35	17
		a=1/48	31	17	31	16
		a=1/24	28	16	28	14
SLOW (T1/2=24h)	K1= 1 Low Transcr.	a=0	32	10	34	85
		a=1/48	20	8	20	54
		a=1/24	14	7	14	41
	K1= 6 High Transcr.	a=0	191	60	204	87
		a=1/48	119	50	120	56
		a=1/24	84	42	84	41
FAST (T1/2=4h)	K1= 1 Low Transcr.	a=0	6	10	6	30
		a=1/48	5	8	5	26
		a=1/24	5	7	5	23
	K1= 6 High Transcr.	a=0	34	60	34	30
		a=1/48	31	50	31	26
		a=1/24	28	42	28	23

Data table 4

Table 4. IsomiRs expression in 3T9 cells

miRNA	5prime	trimmed	3prime NT	can+templ	SUM
mmu-let-7a-5p	0,05%	8,93%	9,06%	81,96%	100,00%
mmu-let-7b-5p	0,00%	13,64%	33,89%	52,47%	100,00%
mmu-let-7c-5p	0,00%	7,16%	7,79%	85,05%	100,00%
mmu-let-7d-5p	0,95%	12,60%	7,49%	78,96%	100,00%
mmu-let-7e-5p	0,00%	18,48%	19,69%	61,83%	100,00%
mmu-let-7f-5p	0,00%	8,49%	6,96%	84,55%	100,00%
mmu-let-7g-5p	0,84%	8,46%	11,82%	78,89%	100,00%
mmu-let-7i-5p	0,00%	5,58%	17,87%	76,55%	100,00%
mmu-miR-100-5p	0,00%	16,10%	9,50%	74,40%	100,00%
mmu-miR-101b-3p	0,00%	0,00%	0,00%	100,00%	100,00%
mmu-miR-103-3p	0,00%	19,12%	5,94%	74,95%	100,00%
mmu-miR-107-3p	0,00%	90,12%	0,00%	9,88%	100,00%
mmu-miR-1191b-5p	0,00%	0,00%	0,00%	100,00%	100,00%
mmu-miR-1198-5p	0,00%	20,21%	7,95%	71,84%	100,00%
mmu-miR-1249-3p	0,00%	25,67%	0,00%	74,33%	100,00%
mmu-miR-125a-5p	0,00%	30,79%	4,50%	64,72%	100,00%
mmu-miR-125b-5p	0,00%	7,38%	16,11%	76,52%	100,00%
mmu-miR-128-3p	0,00%	12,03%	23,39%	64,58%	100,00%
mmu-miR-129-5p	0,00%	0,00%	18,25%	81,75%	100,00%
mmu-miR-130a-3p	0,00%	61,64%	15,98%	22,38%	100,00%
mmu-miR-130b-3p	0,00%	26,29%	53,37%	20,34%	100,00%
mmu-miR-132-3p	0,00%	0,00%	0,00%	100,00%	100,00%
mmu-miR-138-5p	0,00%	0,00%	0,00%	100,00%	100,00%
mmu-miR-140-3p	0,00%	0,93%	34,32%	64,75%	100,00%
mmu-miR-143-3p	0,49%	31,24%	13,56%	54,71%	100,00%
mmu-miR-145a-5p	0,00%	6,61%	9,67%	83,72%	100,00%
mmu-miR-146b-5p	0,00%	0,00%	3,15%	96,85%	100,00%
mmu-miR-148a-3p	0,00%	0,00%	6,15%	93,85%	100,00%
mmu-miR-148b-3p	0,00%	0,00%	90,33%	9,67%	100,00%
mmu-miR-149-5p	0,00%	43,06%	13,88%	43,07%	100,00%
mmu-miR-151-3p	1,76%	13,14%	25,31%	59,80%	100,00%
mmu-miR-152-3p	0,00%	0,00%	81,39%	18,61%	100,00%
mmu-miR-155-5p	0,00%	14,17%	11,89%	73,94%	100,00%
mmu-miR-15a-5p	0,00%	64,45%	0,00%	35,55%	100,00%
mmu-miR-15b-5p	0,00%	16,24%	0,00%	83,76%	100,00%
mmu-miR-16-5p	0,00%	2,96%	0,50%	96,54%	100,00%
mmu-miR-17-5p	0,00%	0,00%	10,18%	89,82%	100,00%
mmu-miR-181a-5p	0,00%	32,85%	0,70%	66,46%	100,00%
mmu-miR-181b-5p	0,00%	46,34%	3,41%	50,25%	100,00%

mmu-miR-181c-5p	0,00%	9,74%	0,00%	90,26%	100,00%
mmu-miR-181d-5p	0,00%	36,12%	0,00%	63,88%	100,00%
mmu-miR-182-5p	0,00%	56,22%	10,91%	32,88%	100,00%
mmu-miR-183-5p	0,00%	5,70%	11,05%	83,26%	100,00%
mmu-miR-1839-5p	0,00%	0,00%	0,00%	100,00%	100,00%
mmu-miR-1843b-5p	0,00%	0,00%	0,00%	100,00%	100,00%
mmu-miR-186-5p	0,00%	11,44%	3,70%	84,85%	100,00%
mmu-miR-191-5p	0,00%	1,93%	5,65%	92,42%	100,00%
mmu-miR-192-5p	0,00%	0,00%	5,79%	94,21%	100,00%
mmu-miR-193a-3p	0,00%	0,00%	0,00%	100,00%	100,00%
mmu-miR-194-5p	0,00%	0,00%	0,00%	100,00%	100,00%
mmu-miR-1964-3p	0,00%	0,00%	0,00%	100,00%	100,00%
mmu-miR-196b-5p	0,00%	0,00%	9,12%	90,88%	100,00%
mmu-miR-1983	0,00%	0,00%	0,00%	100,00%	100,00%
mmu-miR-199a-3p	1,67%	60,43%	14,12%	23,78%	100,00%
mmu-miR-19b-3p	0,00%	0,00%	0,00%	100,00%	100,00%
mmu-miR-205-5p	0,00%	5,97%	43,64%	50,39%	100,00%
mmu-miR-20a-5p	0,00%	0,00%	0,00%	100,00%	100,00%
mmu-miR-214-3p	15,45%	29,36%	5,33%	49,86%	100,00%
mmu-miR-218-5p	0,00%	0,00%	0,00%	100,00%	100,00%
mmu-miR-21a-5p	0,58%	1,69%	14,10%	83,63%	100,00%
mmu-miR-22-3p	0,00%	2,73%	0,62%	96,65%	100,00%
mmu-miR-221-3p	0,00%	41,67%	13,19%	45,14%	100,00%
mmu-miR-222-3p	0,24%	0,00%	1,01%	98,75%	100,00%
mmu-miR-224-5p	0,00%	0,00%	0,00%	100,00%	100,00%
mmu-miR-23a-3p	0,00%	7,85%	13,55%	78,60%	100,00%
mmu-miR-23b-3p	0,00%	4,87%	38,01%	57,12%	100,00%
mmu-miR-24-3p	0,00%	31,43%	29,33%	39,24%	100,00%
mmu-miR-25-3p	0,00%	17,16%	10,99%	71,85%	100,00%
mmu-miR-26a-5p	0,00%	7,38%	6,47%	86,15%	100,00%
mmu-miR-26b-5p	0,00%	3,69%	15,54%	80,76%	100,00%
mmu-miR-27a-3p	0,00%	87,46%	0,00%	12,54%	100,00%
mmu-miR-27b-3p	0,10%	47,60%	14,28%	38,03%	100,00%
mmu-miR-28a-5p	0,00%	10,73%	17,14%	72,13%	100,00%
mmu-miR-296-5p	0,00%	0,00%	0,00%	100,00%	100,00%
mmu-miR-298-5p	0,00%	45,25%	0,49%	54,26%	100,00%
mmu-miR-29a-3p	6,03%	21,89%	11,66%	60,42%	100,00%
mmu-miR-29b-3p	0,00%	0,00%	0,00%	100,00%	100,00%
mmu-miR-301a-3p	0,00%	0,00%	0,00%	100,00%	100,00%
mmu-miR-301b-3p	0,00%	0,00%	0,00%	100,00%	100,00%
mmu-miR-3057-5p	0,00%	24,83%	12,95%	62,22%	100,00%
mmu-miR-30a-5p	0,00%	3,93%	2,08%	93,99%	100,00%
mmu-miR-30b-5p	0,00%	0,00%	0,00%	100,00%	100,00%
mmu-miR-30c-5p	0,00%	0,00%	1,67%	98,33%	100,00%

mmu-miR-30d-5p	0,00%	3,43%	3,33%	93,24%	100,00%
mmu-miR-30e-5p	0,00%	0,00%	2,71%	97,29%	100,00%
mmu-miR-31-5p	0,00%	6,05%	2,23%	91,72%	100,00%
mmu-miR-320-3p	0,00%	9,48%	25,78%	64,74%	100,00%
mmu-miR-322-5p	0,00%	0,00%	24,53%	75,47%	100,00%
mmu-miR-328-3p	0,00%	8,61%	58,01%	33,38%	100,00%
mmu-miR-335-5p	0,00%	54,60%	0,00%	45,40%	100,00%
mmu-miR-342-3p	0,00%	0,00%	15,57%	84,43%	100,00%
mmu-miR-344b-3p	0,00%	0,00%	0,00%	100,00%	100,00%
mmu-miR-344d-3p	0,00%	0,00%	0,00%	100,00%	100,00%
mmu-miR-34a-5p	0,00%	0,00%	0,00%	100,00%	100,00%
mmu-miR-34c-5p	0,00%	0,00%	0,00%	100,00%	100,00%
mmu-miR-351-5p	0,00%	56,56%	24,48%	18,96%	100,00%
mmu-miR-361-5p	0,00%	47,37%	0,00%	52,63%	100,00%
mmu-miR-365-3p	0,00%	0,00%	0,00%	100,00%	100,00%
mmu-miR-378a-3p	0,00%	0,00%	13,50%	86,50%	100,00%
mmu-miR-421-3p	0,00%	26,02%	3,11%	70,87%	100,00%
mmu-miR-423-5p	0,00%	19,01%	8,39%	72,60%	100,00%
mmu-miR-425-5p	0,00%	60,09%	0,00%	39,91%	100,00%
mmu-miR-450b-5p	0,00%	0,00%	0,00%	100,00%	100,00%
mmu-miR-466b-3p	0,00%	0,00%	0,00%	100,00%	100,00%
mmu-miR-466h-5p	0,00%	0,00%	0,00%	100,00%	100,00%
mmu-miR-467c-5p	0,00%	0,00%	0,00%	100,00%	100,00%
mmu-miR-484	0,00%	27,65%	8,40%	63,95%	100,00%
mmu-miR-486a-5p	0,00%	8,36%	49,67%	41,97%	100,00%
mmu-miR-501-3p	0,00%	12,78%	12,50%	74,73%	100,00%
mmu-miR-532-5p	0,00%	19,60%	26,88%	53,51%	100,00%
mmu-miR-574-3p	0,00%	33,38%	6,71%	59,90%	100,00%
mmu-miR-652-3p	0,00%	30,62%	55,35%	14,03%	100,00%
mmu-miR-6539	0,00%	87,09%	0,00%	12,91%	100,00%
mmu-miR-6540-5p	0,00%	0,00%	71,40%	28,60%	100,00%
mmu-miR-664-5p	0,00%	0,00%	0,00%	100,00%	100,00%
mmu-miR-669c-5p	0,00%	0,00%	0,00%	100,00%	100,00%
mmu-miR-676-3p	0,00%	11,64%	0,00%	88,36%	100,00%
mmu-miR-6944-3p	0,00%	0,00%	81,13%	18,87%	100,00%
mmu-miR-744-5p	0,00%	60,10%	3,24%	36,65%	100,00%
mmu-miR-7a-5p	0,00%	0,00%	0,00%	100,00%	100,00%
mmu-miR-872-5p	0,00%	0,00%	0,00%	100,00%	100,00%
mmu-miR-877-5p	0,00%	0,00%	38,16%	61,84%	100,00%
mmu-miR-92a-3p	0,00%	0,40%	54,11%	45,49%	100,00%
mmu-miR-92b-3p	0,00%	31,52%	32,69%	35,78%	100,00%
mmu-miR-93-5p	0,00%	51,41%	8,03%	40,56%	100,00%
mmu-miR-96-5p	0,00%	0,00%	0,00%	100,00%	100,00%
mmu-miR-98-5p	0,00%	8,07%	7,88%	84,05%	100,00%

mmu-miR-99a-5p	0,00%	0,00%	0,00%	100,00%	100,00%
mmu-miR-99b-5p	0,00%	28,42%	16,62%	54,96%	100,00%

Data table 5

Table 5. miRNAs transcription rate in serum stimulation

miRNA name	SERUM REG (final)	0h (CPC/hr)	15' (CPC/hr)	30' (CPC/hr)	45' (CPC/hr)	60' (CPC/hr)	90' (CPC/hr)	120' (CPC/hr)	240' (CPC/hr)	360' (CPC/hr)	480' (CPC/hr)
mmu-let-7b-5p	DOWN	3,298	3,824	2,222	1,632	2,09	2,175	1,849	1,924	1,768	1,79
mmu-miR-214-3p	DOWN	17,084	27,035	16,851	11,165	8,201	10,335	10,898	4,302	4,275	4,306
mmu-miR-351-5p	DOWN	6,879	4,716	1,978	0,838	0,871	0,743	0,673	0,968	0,572	0,57
mmu-miR-503-5p	DOWN	6,879	4,716	1,978	0,838	0,871	0,743	0,673	0,968	0,572	0,57
mmu-miR-335-3p	DOWN	33,262	43,695	16,876	14,251	12,73	8,747	7,034	6,574	5,993	5,642
mmu-miR-188-5p	DOWN	0,282	0,312	0,398	0,355	0,239	0,264	0,276	0,359	0,352	0,325
mmu-miR-30b-5p	DOWN	2,434	2,252	2,665	3,165	3,22	3,171	2,475	1,876	1,889	1,723
mmu-miR-30c-5p	DOWN	3,045	3,197	3,865	3,273	2,412	2,277	2,344	3,665	4,074	3,969
mmu-miR-467a-5p	DOWN	0,125	0,132	0,204	0,135	0,066	0,095	0,101	0,093	0,121	0,106
mmu-miR-193a-3p	DOWN	2,399	2,85	3,117	4,96	6,116	5,637	4,888	5,598	4,873	4,301
mmu-miR-196b-5p	DOWN	NA	NA	NA	NA	NA	NA	NA	NA	NA	NA
mmu-miR-324-5p	DOWN	NA	NA	NA	NA	NA	NA	NA	NA	NA	NA
mmu-miR-92b-3p	DOWN	NA	NA	NA	NA	NA	NA	NA	NA	NA	NA
mmu-let-7i-5p	UP	3,802	4,579	7,402	7,675	5,837	6,074	6,221	5,655	5,152	5,134
mmu-miR-125a-5p	UP	5,423	5,513	6,335	8,751	9,852	8,217	7,967	6,142	5,894	5,606
mmu-miR-99b-5p	UP	5,423	5,513	6,335	8,751	9,852	8,217	7,967	6,142	5,894	5,606
mmu-miR-143-3p	UP	3,945	21,08	34,213	11,638	7,358	6,395	6,264	5,339	3,985	2,874
mmu-miR-22-3p	UP	10,272	26,798	30,064	24,737	22,678	19,818	17,969	16,333	12,977	11,217
mmu-miR-24-3p	UP	13,478	18,997	27,501	28,615	34,495	22,667	12,022	12,545	12,122	11,046
mmu-miR-149-5p	UP	0,173	0,231	0,404	1,289	2,087	1,959	2,054	1,044	0,44	0,277
mmu-miR-155-5p	UP	0,213	0,19	0,329	1,894	4,756	8,289	6,559	1,121	0,771	0,741
mmu-miR-17-5p	UP	2,473	2,47	1,635	3,001	5,405	5,676	4,73	4,687	4,885	6,201
mmu-miR-19b-3p	UP	2,473	2,47	1,635	3,001	5,405	5,676	4,73	4,687	4,885	6,201
mmu-miR-20a-5p	UP	2,473	2,47	1,635	3,001	5,405	5,676	4,73	4,687	4,885	6,201
mmu-miR-92a-3p	UP	2,473	2,47	1,635	3,001	5,405	5,676	4,73	4,687	4,885	6,201
mmu-miR-21a-5p	UP	13,202	45,622	43,74	40,048	38,559	43,917	39,949	27,703	21,747	19,385
mmu-miR-29a-3p	UP	3,51	4,006	2,828	5,68	14,08	24,142	16,768	12,906	9,251	8,963
mmu-miR-29b-3p	UP	3,87	4,425	3,242	5,883	14,266	24,498	17,059	13,29	9,562	9,179
mmu-miR-31-5p	UP	11,065	9,659	6,951	16,94	24,198	24,571	21,084	19,452	16,521	16,026
mmu-miR-365-3p	UP	2,675	3,1	3,224	5,257	6,639	6,152	5,297	5,833	4,982	4,36
mmu-miR-125b-5p	UP	22,884	18,916	21,255	35,976	33,4	34,669	33,84	35,003	35,504	39,18
mmu-miR-221-3p	UP	3,723	3,221	3,313	4,996	5,161	4,983	7,246	5,617	5,487	5,405
mmu-miR-222-3p	UP	3,723	3,221	3,313	4,996	5,161	4,983	7,246	5,617	5,487	5,405
mmu-miR-30a-5p	UP	1,648	1,746	2,005	1,71	1,154	1,1	1,098	2,509	3,087	2,995
mmu-miR-100-5p	UP	1,132	1,188	1,124	0,809	1,001	0,947	0,984	1	0,877	0,799
mmu-miR-151-3p	UP	1,912	1,919	2,004	1,895	1,514	1,894	2,919	2,402	2,053	1,989
mmu-miR-296-5p	UP	0,932	1,014	0,39	0,597	1,024	1,026	1,024	0,899	0,79	0,734
mmu-miR-501-3p	UP	0,282	0,312	0,398	0,355	0,239	0,264	0,276	0,359	0,352	0,325
mmu-miR-423-5p	UP	1,759	1,46	1,48	1,495	1,277	1,322	1,11	1,126	1,05	1,378

mmu-miR-194-5p	UP	0,125	0,182	0,195	0,054	0,057	0,054	0,041	0,058	0,065	0,05
mmu-miR-425-5p	UP	0,488	0,547	0,499	0,233	0,236	0,173	0,225	0,343	0,3	0,41
mmu-let-7f-5p	UP	13,311	16,895	19,325	13,681	11,87	10,122	10,123	10,021	9,514	8,837
mmu-let-7g-5p	UP	NA	NA	NA	NA	NA	NA	NA	NA	NA	NA
mmu-miR-129-5p	UP	NA	NA	NA	NA	NA	NA	NA	NA	NA	NA
mmu-miR-146b-5p	UP	NA	NA	NA	NA	NA	NA	NA	NA	NA	NA
mmu-miR-1843a-5p	UP	NA	NA	NA	NA	NA	NA	NA	NA	NA	NA
mmu-miR-1983	UP	NA	NA	NA	NA	NA	NA	NA	NA	NA	NA
mmu-miR-331-3p	UP	NA	NA	NA	NA	NA	NA	NA	NA	NA	NA
mmu-miR-486a-5p	UP	NA	NA	NA	NA	NA	NA	NA	NA	NA	NA
mmu-miR-676-3p	UP	NA	NA	NA	NA	NA	NA	NA	NA	NA	NA
mmu-miR-6944-3p	UP	NA	NA	NA	NA	NA	NA	NA	NA	NA	NA
mmu-miR-877-5p	UP	NA	NA	NA	NA	NA	NA	NA	NA	NA	NA

REFERENCES

Ameres SL, Horwich MD, Hung JH, Xu J, Ghildiyal M, Weng Z, Zamore PD. 2010. Target RNA-directed trimming and tailing of small silencing RNAs. *Science* **328**: 1534-1539.

Avraham R, Sas-Chen A, Manor O, Steinfeld I, Shalgi R, Tarcic G, Bossel N, Zeisel A, Amit I, Zwang Y et al. 2010. EGF decreases the abundance of microRNAs that restrain oncogenic transcription factors. *Sci Signal* **3**: ra43.

Azuma-Mukai A, Oguri H, Mituyama T, Qian ZR, Asai K, Siomi H, Siomi MC. 2008. Characterization of endogenous human Argonautes and their miRNA partners in RNA silencing. *Proc Natl Acad Sci U S A* **105**: 7964-7969.

Babiarz JE, Ruby JG, Wang Y, Bartel DP, Blelloch R. 2008. Mouse ES cells express endogenous shRNAs, siRNAs, and other Microprocessor-independent, Dicer-dependent small RNAs. *Genes & development* **22**: 2773-2785.

Baccarini A, Chauhan H, Gardner TJ, Jayaprakash AD, Sachidanandam R, Brown BD. 2011. Kinetic analysis reveals the fate of a microRNA following target regulation in mammalian cells. *Curr Biol* **21**: 369-376.

Bail S, Swerdel M, Liu H, Jiao X, Goff LA, Hart RP, Kiledjian M. 2010. Differential regulation of microRNA stability. *RNA* **16**: 1032-1039.

Bartel DP. 2009. MicroRNAs: target recognition and regulatory functions. *Cell* **136**: 215-233.

Bosson AD, Zamudio JR, Sharp PA. 2014. Endogenous miRNA and target concentrations determine susceptibility to potential ceRNA competition. *Mol Cell* **56**: 347-359.

Brown BD, Venneri MA, Zingale A, Sergi Sergi L, Naldini L. 2006. Endogenous microRNA regulation suppresses transgene expression in hematopoietic lineages and enables stable gene transfer. *Nature medicine* **12**: 585-591.

Bueno MJ, Gomez de Cedron M, Laresgoiti U, Fernandez-Piqueras J, Zubiaga AM, Malumbres M. 2010. Multiple E2F-induced microRNAs prevent replicative stress in response to mitogenic signaling. *Mol Cell Biol* **30**: 2983-2995.

Burger K, Muhl B, Kellner M, Rohrmoser M, Gruber-Eber A, Windhager L, Friedel CC, Dolken L, Eick D. 2013. 4-thiouridine inhibits rRNA synthesis and causes a nucleolar stress response. *RNA Biol* **10**: 1623-1630.

Burroughs AM, Ando Y, de Hoon MJ, Tomaru Y, Suzuki H, Hayashizaki Y, Daub CO. 2011. Deep-sequencing of human Argonaute-associated small RNAs provides insight into miRNA sorting and reveals Argonaute association with RNA fragments of diverse origin. *RNA Biol* **8**: 158-177.

Calin GA, Dumitru CD, Shimizu M, Bichi R, Zupo S, Noch E, Aldler H, Rattan S, Keating M, Rai K et al. 2002. Frequent deletions and down-regulation of micro- RNA genes miR15 and miR16 at 13q14 in chronic lymphocytic leukemia. *Proc Natl Acad Sci U S A* **99**: 15524-15529.

Carthew RW, Sontheimer EJ. 2009. Origins and Mechanisms of miRNAs and siRNAs. *Cell* **136**: 642-655.

Cazalla D, Yario T, Steitz JA. 2010. Down-regulation of a host microRNA by a Herpesvirus saimiri noncoding RNA. *Science* **328**: 1563-1566.

Cech TR, Steitz JA. 2014. The noncoding RNA revolution-trashing old rules to forge new ones. *Cell* **157**: 77-94.

Cesana M, Cacchiarelli D, Legnini I, Santini T, Sthandier O, Chinappi M, Tramontano A, Bozzoni I. 2011. A long noncoding RNA controls muscle differentiation by functioning as a competing endogenous RNA. *Cell* **147**: 358-369.

Chang HM, Triboulet R, Thornton JE, Gregory RI. 2013. A role for the Perlman syndrome exonuclease Dis3l2 in the Lin28-let-7 pathway. *Nature* **497**: 244-248.

Chang TC, Pertea M, Lee S, Salzberg SL, Mendell JT. 2015. Genome-wide annotation of microRNA primary transcript structures reveals novel regulatory mechanisms. *Genome Res* **25**: 1401-1409.

Chang TC, Yu D, Lee YS, Wentzel EA, Arking DE, West KM, Dang CV, Thomas-Tikhonenko A, Mendell JT. 2008. Widespread microRNA repression by Myc contributes to tumorigenesis. *Nature genetics* **40**: 43-50.

Chatterjee S, Grosshans H. 2009. Active turnover modulates mature microRNA activity in Caenorhabditis elegans. *Nature* **461**: 546-549.

Chiang HR, Schoenfeld LW, Ruby JG, Auyeung VC, Spies N, Baek D, Johnston WK, Russ C, Luo S, Babiarz JE et al. 2010. Mammalian microRNAs: experimental evaluation of novel and previously annotated genes. *Genes & development* **24**: 992-1009.

Chong MM, Zhang G, Cheloufi S, Neubert TA, Hannon GJ, Littman DR. 2010. Canonical and alternate functions of the microRNA biogenesis machinery. *Genes & development* **24**: 1951-1960.

Cleary MD, Meiering CD, Jan E, Guymon R, Boothroyd JC. 2005. Biosynthetic labeling of RNA with uracil phosphoribosyltransferase allows cell-specific microarray analysis of mRNA synthesis and decay. *Nat Biotechnol* **23**: 232-237.

Cloonan N, Wani S, Xu Q, Gu J, Lea K, Heater S, Barbacioru C, Steptoe AL, Martin HC, Nourbakhsh E et al. 2011. MicroRNAs and their isomiRs function cooperatively to target common biological pathways. *Genome biology* **12**: R126.

D'Ambrogio A, Gu W, Udagawa T, Mello CC, Richter JD. 2012. Specific miRNA stabilization by Gld2-catalyzed monoadenylation. *Cell reports* **2**: 1537-1545.

Das SK, Sokhi UK, Bhutia SK, Azab B, Su ZZ, Sarkar D, Fisher PB. 2010. Human polynucleotide phosphorylase selectively and preferentially degrades microRNA-221 in human melanoma cells. *Proc Natl Acad Sci U S A* **107**: 11948-11953.

Davis-Dusenbery BN, Hata A. 2010. Mechanisms of control of microRNA biogenesis. *Journal of biochemistry* **148**: 381-392.

de la Mata M, Gaidatzis D, Vitanescu M, Stadler MB, Wentzel C, Scheiffele P, Filipowicz W, Grosshans H. 2015. Potent degradation of neuronal miRNAs induced by highly complementary targets. *EMBO Rep* **16**: 500-511.

De N, Young L, Lau PW, Meisner NC, Morrissey DV, MacRae IJ. 2013. Highly complementary target RNAs promote release of guide RNAs from human Argonaute2. *Mol Cell* **50**: 344-355.

de Pretis S, Kress T, Morelli MJ, Melloni GE, Riva L, Amati B, Pelizzola M. 2015. INSPEcT: a computational tool to infer mRNA synthesis, processing and degradation dynamics from RNA- and 4sU-seq time course experiments. *Bioinformatics* doi:10.1093/bioinformatics/btv288.

Denzler R, Agarwal V, Stefano J, Bartel DP, Stoffel M. 2014. Assessing the ceRNA hypothesis with quantitative measurements of miRNA and target abundance. *Mol Cell* **54**: 766-776.

Dolken L, Ruzsics Z, Radle B, Friedel CC, Zimmer R, Mages J, Hoffmann R, Dickinson P, Forster T, Ghazal P et al. 2008. High-resolution gene expression profiling for simultaneous kinetic parameter analysis of RNA synthesis and decay. *RNA* **14**: 1959-1972.

Du P, Wang L, Sliz P, Gregory RI. 2015. A Biogenesis Step Upstream of Microprocessor Controls miR-17 approximately 92 Expression. *Cell* **162**: 885-899.

Dueck A, Ziegler C, Eichner A, Berezikov E, Meister G. 2012. microRNAs associated with the different human Argonaute proteins. *Nucleic Acids Res* **40**: 9850-9862.

Duffy EE, Rutenberg-Schoenberg M, Stark CD, Kitchen RR, Gerstein MB, Simon MD. 2015. Tracking Distinct RNA Populations Using Efficient and Reversible Covalent Chemistry. *Mol Cell* **59**: 858-866.

Elkayam E, Kuhn CD, Tocilj A, Haase AD, Greene EM, Hannon GJ, Joshua-Tor L. 2012. The structure of human argonaute-2 in complex with miR-20a. *Cell* **150**: 100-110.

Ender C, Krek A, Friedlander MR, Beitzinger M, Weinmann L, Chen W, Pfeffer S, Rajewsky N, Meister G. 2008. A human snoRNA with microRNA-like functions. *Mol Cell* **32**: 519-528.

Eulalio A, Huntzinger E, Izaurralde E. 2008. Getting to the root of miRNA-mediated gene silencing. *Cell* **132**: 9-14.

Follenzi A, Naldini L. 2002. Generation of HIV-1 derived lentiviral vectors. *Methods in enzymology* **346**: 454-465.

Fukunaga R, Han BW, Hung JH, Xu J, Weng Z, Zamore PD. 2012. Dicer partner proteins tune the length of mature miRNAs in flies and mammals. *Cell* **151**: 533-546.

Gantier MP, McCoy CE, Rusinova I, Saulep D, Wang D, Xu D, Irving AT, Behlke MA, Hertzog PJ, Mackay F et al. 2011. Analysis of microRNA turnover in mammalian cells following Dicer1 ablation. *Nucleic Acids Res* **39**: 5692-5703.

Griffiths-Jones S, Saini HK, van Dongen S, Enright AJ. 2008. miRBase: tools for microRNA genomics. *Nucleic Acids Res* **36**: D154-158.

Guil S, Caceres JF. 2007. The multifunctional RNA-binding protein hnRNP A1 is required for processing of miR-18a. *Nature structural & molecular biology* **14**: 591-596.
Guil S, Esteller M. 2009. DNA methylomes, histone codes and miRNAs: tying it all together. *The international journal of biochemistry & cell biology* **41**: 87-95.
Guo L, Yang Q, Lu J, Li H, Ge Q, Gu W, Bai Y, Lu Z. 2011. A comprehensive survey of miRNA repertoire and 3' addition events in the placentas of patients with pre-eclampsia from high-throughput sequencing. *PloS one* **6**: e21072.
Guo Y, Liu J, Elfenbein SJ, Ma Y, Zhong M, Qiu C, Ding Y, Lu J. 2015. Characterization of the mammalian miRNA turnover landscape. *Nucleic Acids Res* **43**: 2326-2341.
Ha M, Kim VN. 2014. Regulation of microRNA biogenesis. *Nature reviews Molecular cell biology* **15**: 509-524.
Haas G, Cetin S, Messmer M, Chane-Woon-Ming B, Terenzi O, Chicher J, Kuhn L, Hammann P, Pfeffer S. 2016. Identification of factors involved in target RNA-directed microRNA degradation. *Nucleic Acids Res* **44**: 2873-2887.
Han YC, Vidigal JA, Mu P, Yao E, Singh I, Gonzalez AJ, Concepcion CP, Bonetti C, Ogrodowski P, Carver B et al. 2015. An allelic series of miR-17 approximately 92-mutant mice uncovers functional specialization and cooperation among members of a microRNA polycistron. *Nature genetics* **47**: 766-775.
Hu HY, Yan Z, Xu Y, Hu H, Menzel C, Zhou YH, Chen W, Khaitovich P. 2009. Sequence features associated with microRNA strand selection in humans and flies. *BMC genomics* **10**: 413.
Huntzinger E, Izaurralde E. 2011. Gene silencing by microRNAs: contributions of translational repression and mRNA decay. *Nature reviews Genetics* **12**: 99-110.
Hwang HW, Wentzel EA, Mendell JT. 2007. A hexanucleotide element directs microRNA nuclear import. *Science* **315**: 97-100.
Iwasaki S, Kobayashi M, Yoda M, Sakaguchi Y, Katsuma S, Suzuki T, Tomari Y. 2010. Hsc70/Hsp90 chaperone machinery mediates ATP-dependent RISC loading of small RNA duplexes. *Mol Cell* **39**: 292-299.
Jeyapalan Z, Deng Z, Shatseva T, Fang L, He C, Yang BB. 2011. Expression of CD44 3'-untranslated region regulates endogenous microRNA functions in tumorigenesis and angiogenesis. *Nucleic Acids Res* **39**: 3026-3041.
Jonas S, Izaurralde E. 2015. Towards a molecular understanding of microRNA-mediated gene silencing. *Nature reviews Genetics* **16**: 421-433.
Karle JM, Anderson LW, Cysyk RL. 1984. Effect of plasma concentrations of uridine on pyrimidine biosynthesis in cultured L1210 cells. *The Journal of biological chemistry* **259**: 67-72.
Karreth FA, Reschke M, Ruocco A, Ng C, Chapuy B, Leopold V, Sjoberg M, Keane TM, Verma A, Ala U et al. 2015. The BRAF pseudogene functions as a competitive endogenous RNA and induces lymphoma in vivo. *Cell* **161**: 319-332.
Kim GW, Lee SH, Cho H, Kim M, Shin EC, Oh JW. 2016. Hepatitis C Virus Core Protein Promotes miR-122 Destabilization by Inhibiting GLD-2. *PLoS pathogens* **12**: e1005714.
Kim VN, Han J, Siomi MC. 2009. Biogenesis of small RNAs in animals. *Nature reviews Molecular cell biology* **10**: 126-139.
Kim YK, Heo I, Kim VN. 2010. Modifications of small RNAs and their associated proteins. *Cell* **143**: 703-709.
Kim YK, Wee G, Park J, Kim J, Baek D, Kim JS, Kim VN. 2013. TALEN-based knockout library for human microRNAs. *Nature structural & molecular biology* **20**: 1458-1464.
Kotani A, Ha D, Schotte D, den Boer ML, Armstrong SA, Lodish HF. 2010. A novel mutation in the miR-128b gene reduces miRNA processing and leads to glucocorticoid resistance of MLL-AF4 acute lymphocytic leukemia cells. *Cell cycle* **9**: 1037-1042.
Krol J, Busskamp V, Markiewicz I, Stadler MB, Ribi S, Richter J, Duebel J, Bicker S, Fehling HJ, Schubeler D et al. 2010a. Characterizing light-regulated retinal microRNAs reveals rapid turnover as a common property of neuronal microRNAs. *Cell* **141**: 618-631.
Krol J, Loedige I, Filipowicz W. 2010b. The widespread regulation of microRNA biogenesis, function and decay. *Nature reviews Genetics* **11**: 597-610.
Kumar MS, Lu J, Mercer KL, Golub TR, Jacks T. 2007. Impaired microRNA processing enhances cellular transformation and tumorigenesis. *Nature genetics* **39**: 673-677.
Lagos-Quintana M, Rauhut R, Lendeckel W, Tuschl T. 2001. Identification of novel genes coding for small expressed RNAs. *Science* **294**: 853-858.

Lau NC, Lim LP, Weinstein EG, Bartel DP. 2001. An abundant class of tiny RNAs with probable regulatory roles in Caenorhabditis elegans. *Science* **294**: 858-862.
Lee M, Choi Y, Kim K, Jin H, Lim J, Nguyen TA, Yang J, Jeong M, Giraldez AJ, Yang H et al. 2014. Adenylation of maternally inherited microRNAs by Wispy. *Mol Cell* **56**: 696-707.
Lee RC, Ambros V. 2001. An extensive class of small RNAs in Caenorhabditis elegans. *Science* **294**: 862-864.
Lee RC, Feinbaum RL, Ambros V. 1993. The C. elegans heterochronic gene lin-4 encodes small RNAs with antisense complementarity to lin-14. *Cell* **75**: 843-854.
Lewis BP, Burge CB, Bartel DP. 2005. Conserved seed pairing, often flanked by adenosines, indicates that thousands of human genes are microRNA targets. *Cell* **120**: 15-20.
Li Y, Kowdley KV. 2012. MicroRNAs in common human diseases. *Genomics, proteomics & bioinformatics* **10**: 246-253.
Lin S, Gregory RI. 2015. MicroRNA biogenesis pathways in cancer. *Nature reviews Cancer* **15**: 321-333.
Lund E, Guttinger S, Calado A, Dahlberg JE, Kutay U. 2004. Nuclear export of microRNA precursors. *Science* **303**: 95-98.
Marcinowski L, Tanguy M, Krmpotic A, Radle B, Lisnic VJ, Tuddenham L, Chane-Woon-Ming B, Ruzsics Z, Erhard F, Benkartek C et al. 2012. Degradation of cellular mir-27 by a novel, highly abundant viral transcript is important for efficient virus replication in vivo. *PLoS pathogens* **8**: e1002510.
Marzi MJ, Ghini F, Cerruti B, de Pretis S, Bonetti P, Giacomelli C, Gorski MM, Kress T, Pelizzola M, Muller H et al. 2016. Degradation dynamics of microRNAs revealed by a novel pulse-chase approach. *Genome Res* **26**: 554-565.
Marzi MJ, Puggioni EM, Dall'Olio V, Bucci G, Bernard L, Bianchi F, Crescenzi M, Di Fiore PP, Nicassio F. 2012. Differentiation-associated microRNAs antagonize the Rb-E2F pathway to restrict proliferation. *The Journal of cell biology* **199**: 77-95.
Melvin WT, Milne HB, Slater AA, Allen HJ, Keir HM. 1978. Incorporation of 6-thioguanosine and 4-thiouridine into RNA. Application to isolation of newly synthesised RNA by affinity chromatography. *Eur J Biochem* **92**: 373-379.
Mori M, Triboulet R, Mohseni M, Schlegelmilch K, Shrestha K, Camargo FD, Gregory RI. 2014. Hippo signaling regulates microprocessor and links cell-density-dependent miRNA biogenesis to cancer. *Cell* **156**: 893-906.
Mukherji S, Ebert MS, Zheng GX, Tsang JS, Sharp PA, van Oudenaarden A. 2011. MicroRNAs can generate thresholds in target gene expression. *Nature genetics* **43**: 854-859.
Muller H, Marzi MJ, Nicassio F. 2014. IsomiRage: From Functional Classification to Differential Expression of miRNA Isoforms. *Front Bioeng Biotechnol* **2**: 38.
Mullokandov G, Baccarini A, Ruzo A, Jayaprakash AD, Tung N, Israelow B, Evans MJ, Sachidanandam R, Brown BD. 2012. High-throughput assessment of microRNA activity and function using microRNA sensor and decoy libraries. *Nature methods* **9**: 840-846.
Neilsen CT, Goodall GJ, Bracken CP. 2012. IsomiRs--the overlooked repertoire in the dynamic microRNAome. *Trends Genet* **28**: 544-549.
Nguyen TA, Jo MH, Choi YG, Park J, Kwon SC, Hohng S, Kim VN, Woo JS. 2015. Functional Anatomy of the Human Microprocessor. *Cell* **161**: 1374-1387.
Okada N, Lin CP, Ribeiro MC, Biton A, Lai G, He X, Bu P, Vogel H, Jablons DM, Keller AC et al. 2014. A positive feedback between p53 and miR-34 miRNAs mediates tumor suppression. *Genes & development* **28**: 438-450.
Ozsolak F, Poling LL, Wang Z, Liu H, Liu XS, Roeder RG, Zhang X, Song JS, Fisher DE. 2008. Chromatin structure analyses identify miRNA promoters. *Genes & development* **22**: 3172-3183.
Paroo Z, Ye X, Chen S, Liu Q. 2009. Phosphorylation of the human microRNA-generating complex mediates MAPK/Erk signaling. *Cell* **139**: 112-122.
Pasquinelli AE, Reinhart BJ, Slack F, Martindale MQ, Kuroda MI, Maller B, Hayward DC, Ball EE, Degnan B, Muller P et al. 2000. Conservation of the sequence and temporal expression of let-7 heterochronic regulatory RNA. *Nature* **408**: 86-89.
Pencheva N, Tavazoie SF. 2013. Control of metastatic progression by microRNA regulatory networks. *Nature cell biology* **15**: 546-554.

Poliseno L, Salmena L, Zhang J, Carver B, Haveman WJ, Pandolfi PP. 2010. A coding-independent function of gene and pseudogene mRNAs regulates tumour biology. *Nature* **465**: 1033-1038.

Powers JT, Tsanov KM, Pearson DS, Roels F, Spina CS, Ebright R, Seligson M, de Soysa Y, Cahan P, Theissen J et al. 2016. Multiple mechanisms disrupt the let-7 microRNA family in neuroblastoma. *Nature* **535**: 246-251.

Rabani M, Levin JZ, Fan L, Adiconis X, Raychowdhury R, Garber M, Gnirke A, Nusbaum C, Hacohen N, Friedman N et al. 2011. Metabolic labeling of RNA uncovers principles of RNA production and degradation dynamics in mammalian cells. *Nat Biotechnol* **29**: 436-442.

Ramachandran V, Chen X. 2008. Degradation of microRNAs by a family of exoribonucleases in Arabidopsis. *Science* **321**: 1490-1492.

Ran FA, Hsu PD, Wright J, Agarwala V, Scott DA, Zhang F. 2013. Genome engineering using the CRISPR-Cas9 system. *Nature protocols* **8**: 2281-2308.

Rissland OS, Hong SJ, Bartel DP. 2011. MicroRNA destabilization enables dynamic regulation of the miR-16 family in response to cell-cycle changes. *Mol Cell* **43**: 993-1004.

Ruegger S, Grosshans H. 2012. MicroRNA turnover: when, how, and why. *Trends Biochem Sci* **37**: 436-446.

Sabo A, Kress TR, Pelizzola M, de Pretis S, Gorski MM, Tesi A, Morelli MJ, Bora P, Doni M, Verrecchia A et al. 2014. Selective transcriptional regulation by Myc in cellular growth control and lymphomagenesis. *Nature* **511**: 488-492.

Salmena L, Poliseno L, Tay Y, Kats L, Pandolfi PP. 2011. A ceRNA hypothesis: the Rosetta Stone of a hidden RNA language? *Cell* **146**: 353-358.

Schwarz DS, Hutvagner G, Du T, Xu Z, Aronin N, Zamore PD. 2003. Asymmetry in the assembly of the RNAi enzyme complex. *Cell* **115**: 199-208.

Shenoy A, Blelloch RH. 2014. Regulation of microRNA function in somatic stem cell proliferation and differentiation. *Nature reviews Molecular cell biology* **15**: 565-576.

Slade I, Bacchelli C, Davies H, Murray A, Abbaszadeh F, Hanks S, Barfoot R, Burke A, Chisholm J, Hewitt M et al. 2011. DICER1 syndrome: clarifying the diagnosis, clinical features and management implications of a pleiotropic tumour predisposition syndrome. *Journal of medical genetics* **48**: 273-278.

Sobell HM. 1985. Actinomycin and DNA transcription. *Proc Natl Acad Sci U S A* **82**: 5328-5331.

Sumazin P, Yang X, Chiu HS, Chung WJ, Iyer A, Llobet-Navas D, Rajbhandari P, Bansal M, Guarnieri P, Silva J et al. 2011. An extensive microRNA-mediated network of RNA-RNA interactions regulates established oncogenic pathways in glioblastoma. *Cell* **147**: 370-381.

Thomson DW, Dinger ME. 2016. Endogenous microRNA sponges: evidence and controversy. *Nature reviews Genetics* **17**: 272-283.

Thornton JE, Du P, Jing L, Sjekloca L, Lin S, Grossi E, Sliz P, Zon LI, Gregory RI. 2014. Selective microRNA uridylation by Zcchc6 (TUT7) and Zcchc11 (TUT4). *Nucleic Acids Res* **42**: 11777-11791.

Trabucchi M, Briata P, Garcia-Mayoral M, Haase AD, Filipowicz W, Ramos A, Gherzi R, Rosenfeld MG. 2009. The RNA-binding protein KSRP promotes the biogenesis of a subset of microRNAs. *Nature* **459**: 1010-1014.

van Kuilenburg AB, Meinsma R. 2016. The pivotal role of uridine-cytidine kinases in pyrimidine metabolism and activation of cytotoxic nucleoside analogues in neuroblastoma. *Biochimica et biophysica acta* **1862**: 1504-1512.

Viswanathan SR, Daley GQ, Gregory RI. 2008. Selective blockade of microRNA processing by Lin28. *Science* **320**: 97-100.

Yang E, van Nimwegen E, Zavolan M, Rajewsky N, Schroeder M, Magnasco M, Darnell JE, Jr. 2003. Decay rates of human mRNAs: correlation with functional characteristics and sequence attributes. *Genome Res* **13**: 1863-1872.